NASA Technical Paper 3557

Improved Method for Prediction of Attainable Wing Leading-Edge Thrust

Harry W. Carlson, Marcus O. McElroy, Wendy B. Lessard, and L. Arnold McCullers

April 1996

NASA Technical Paper 3557

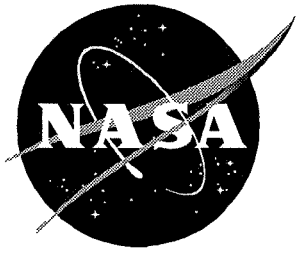

Improved Method for Prediction of Attainable Wing Leading-Edge Thrust

Harry W. Carlson
Lockheed Engineering & Sciences Company • Hampton, Virginia

Marcus O. McElroy and Wendy B. Lessard
Langley Research Center • Hampton, Virginia

L. Arnold McCullers
ViGYAN, Inc. • Hampton, Virginia

National Aeronautics and Space Administration
Langley Research Center • Hampton, Virginia 23681-0001

April 1996

Available electronically at the following URL address: http://techreports.larc.nasa.gov/ltrs/ltrs.html

Printed copies available from the following:

NASA Center for AeroSpace Information
800 Elkridge Landing Road
Linthicum Heights, MD 21090-2934
(301) 621-0390

National Technical Information Service (NTIS)
5285 Port Royal Road
Springfield, VA 22161-2171
(703) 487-4650

Contents

Abstract

Prediction of the loss of wing leading-edge thrust and the accompanying increase in drag due to lift, when flow is not completely attached, presents a difficult but commonly encountered problem. A method (now called the previous method) for the prediction of attainable leading-edge thrust and the resultant effect on airplane aerodynamic performance has been in use for more than a decade. Recently, the method has been revised to enhance its applicability to current airplane design and evaluation problems. The improved method (called the present method) provides for a greater range of airfoil shapes from very sharp to very blunt leading edges. It is also based on a wider range of Reynolds numbers than was available for the previous method. The present method, when employed in computer codes for aerodynamic analysis, generally results in improved correlation with experimental wing-body axial-force data and provides reasonable estimates of the measured drag.

Introduction

The loss of wing leading-edge thrust and the accompanying increase in drag due to lift, when flow is not completely attached, is a commonly encountered problem. Such problems are particularly severe for airplanes that employ the thin highly swept wings required to provide some degree of supersonic flight capability. Development of a generalized system for the prediction of airplane lifting efficiency is dependent on a means of evaluating the amount of wing leading-edge thrust that can actually be attained.

Leading-edge thrust results from the high velocities and the accompanying low pressures that occur as air flows from a stagnation point on the under surface of the wing around the leading edge to the upper surface. This thrust can be developed at supersonic speeds as well as at subsonic speeds provided that the component of the free-stream Mach number normal to the wing leading edge is less than 1.0. The loss of leading-edge thrust resulting from flow separation is dependent on flight conditions (i.e., Mach number and Reynolds number), on wing section geometry (i.e., maximum thickness, location of maximum thickness, and leading-edge radius), and on the incidence of the wing section leading-edge mean camber surface relative to the local flow. Flow separation characteristics of highly swept wings can be especially complex because the upwash ahead of the leading edge increases dramatically from the wing centerline to regions near the wingtip.

A first step in the development of a practical system for the analysis of separated flow problems was provided by the theoretical-empirical attainable leading-edge thrust prediction method advanced in reference 1. This method is based on the following:

1. Use of simple sweep theory to permit a two-dimensional analysis
2. Employment of theoretical airfoil computer codes to define thrust dependence on section geometric characteristics with pressures limited to a vacuum
3. Generalization of the thrust dependence on limiting pressures to include the more severe limitations of realistically achievable pressures
4. Examination of experimental two-dimensional airfoil data to define the more realistic limiting pressure dependence on local Mach and Reynolds numbers

The attainable thrust prediction method was employed in computer codes for the estimation of drag due to lift (AERO2S, refs. 2 and 3) and the design of wing surfaces for minimization of drag (WINGDES, ref. 4). The aerodynamic analysis computer code (AERO2S) provides estimates of the aerodynamic characteristics of a wing and body in combination with either a canard or a horizontal tail surface. It includes provisions for convenient handling of deflected wing leading- and trailing-edge flaps. This computer code is applicable only for subsonic speeds. The wing design computer code (WINGDES) provides both a design and an analysis capability and is applicable to both subsonic and supersonic speeds. However, it cannot accommodate a second surface and is not arranged for convenient handling of flaps. References 5–8 provide an updated description of these computer codes and examples of their application to practical problems.

Although computer codes employing the attainable thrust method have been successfully applied to a variety of problems, a need for certain improvements to the basic attainable thrust prediction procedures has been recognized. One deficiency of the method described in reference 1 is a poor representation of the thrust-producing capabilities of airfoil sections with sharp or nearly sharp leading edges. The method, as originally formulated, dictated that airfoils with a leading-edge radius of zero could produce no thrust. As shown by theoretical

two-dimensional airfoil data, which is discussed later, and by experimental investigations (e.g., ref. 9), sharp and nearly sharp airfoil sections do in fact provide appreciable levels of attainable thrust. In the application of the method described in reference 1, the problem was overcome in part by substitution of a radius other than zero for nominally sharp leading edges; however, this process depends on the skill and experience of the computer code user. The present method described in this paper provides a better solution in which the theoretical two-dimensional airfoil matrix is expanded to include a leading-edge radius of zero. With this change the method is applicable to a continuous range of leading-edge radii from zero through the standard values to very large values approaching half of the wing maximum thickness.

Expansion of the two-dimensional airfoil matrix to include variations in location of maximum thickness was accomplished by a revised relationship between streamwise airfoil sections of the wing and the derived two-dimensional sections, a relationship that results in much closer representation of the real flow over a lifting surface. Revision of the attainable thrust prediction method also provided an opportunity to take advantage of information relating to the effect of Reynolds number on attainable thrust that was not available before publication of reference 1. In reference 1, the two-dimensional experimental data used to define limiting pressures were restricted to $R \leq 8 \times 10^6$ (based on the chord). The present method discussed herein makes use of data obtained up to $R = 30 \times 10^6$.

Because revisions to the previous method are quite extensive, the development of the present method is covered in detail, even at the expense of some repetition. Some examples of the application of the present method to data for wings and wing-body configurations are given. Correlations are included for data previously used in references 6 and 8 and for new data as well. In addition, instructions are given for the evolution of the system to accommodate new two-dimensional airfoil data, as it becomes available, so as to provide a more exact and more complete formulation of attainable thrust dependence on Mach and Reynolds numbers.

Symbols

b wing span, in.

C_A axial- or chord-force coefficient

C_D drag coefficient

ΔC_D drag coefficient due to lift, $C_D - C_{D,0}$

$C_{D,0}$ drag coefficient at $\alpha = 0°$ for configuration with no wing camber or twist

C_L lift coefficient

C_m pitching-moment coefficient

C_N normal-force coefficient

C_p pressure coefficient

$C_{p,\mathrm{lim}}$ limiting pressure coefficient used in definition of attainable thrust

$C_{p,\mathrm{vac}}$ vacuum pressure coefficient, $-\dfrac{2}{\gamma M^2}$

c local wing chord, in.

c_{av} average wing chord, $\dfrac{S}{b}$, in.

c_A section axial- or chord-force coefficient

Δc_A change in section axial- or chord-force coefficient relative to $\alpha = 0°$

c_t section theoretical thrust coefficient (from linearized theory for zero-thickness airfoils)

c_t^* section attainable thrust coefficient

$\bar{c}$ mean aerodynamic chord, in.

e_1, e_2, e_3 exponents used in curve-fit equation for attainable thrust factor

e_4 exponent used in curve-fit equation for limiting pressure coefficient

K parameter used in curve-fit equation for limiting pressure coefficient

K_t attainable thrust factor, fraction of theoretical thrust actually attainable, $\dfrac{c_t^*}{c_t} = \dfrac{c_{t,n}^*}{c_{t,n}}$

k parameter used in curve-fit equation for attainable thrust factor

k_1, k_2, k_3, k_4 constants used in airfoil section definition

M free-stream Mach number

M_e equivalent Mach number replacing M_n to account for $C_{p,\mathrm{lim}} \neq C_{p,\mathrm{vac}}$

M_n normal Mach number (fig. 2)

P_{at} attainable thrust parameter, $\dfrac{K_t}{1 + \left(\dfrac{\tau}{c}\right)_n^{1.2}}$

P_{tt} theoretical thrust parameter, $c_{t,n}\beta_n\left[\dfrac{\left(\dfrac{\tau}{c}\right)_n\left(\dfrac{\eta}{0.5}\right)^{e_1}}{0.09}\right]^{e_2}$

q dynamic pressure

R	Reynolds number based on mean aerodynamic chord
r	leading-edge radius, in.
r_i	leading-edge radius index, $\frac{\frac{r}{c}\eta}{\left(\frac{\tau}{c}\right)^2}$
S	wing area, in.^{2}
s	spanwise distance, in.
t	section theoretical leading-edge thrust
t^*	section attainable leading-edge thrust
X,Y,Z	Cartesian coordinates, positive aft, left, and up, respectively (fig. 2)
x'	distance behind wing leading edge
α	angle of attack, deg
β_n	$= \sqrt{1 - M_n^2}$
γ	ratio of specific heats, 1.4
$\delta_{L,n}$	leading-edge flap deflection angle measured normal to hinge line, positive with leading edge down, deg
$\delta_{T,n}$	trailing-edge flap deflection angle measured normal to hinge line, positive with trailing edge down, deg
η	location of maximum thickness as fraction of chord
Λ_{le}	wing leading-edge sweep angle, deg
τ	section maximum thickness, in.
Subscript:	
n	quantities pertaining to wing section normal to leading edge

Present Method Development

Development of the present method for the prediction of attainable leading-edge thrust is based on the fundamental principle that this force results from pressures acting on a surface, and thus, the amount of theoretical thrust that can actually be realized is dependent on constraints imposed by wing geometry and achievable pressure levels. The goal of the present method is to provide a means of quantifying that portion of this theoretical thrust that can be attained through empirically derived mathematical relationships involving wing flow conditions and wing geometry. The present method, when incorporated into existing linearized theory lifting surface computer codes, estimates attainable leading-edge thrust by providing multiplication factors that are applied to the calculated theoretical thrust.

The process used in generation of the prediction method is rather complex. Figure 1 provides a visual guide to aid in an understanding of the general plan of development described in the following paragraphs.

First, the relationships between wing streamwise airfoil sections and sections normal to the leading edge are established, and the use of a two-dimensional analysis to solve a three-dimensional problem is justified. Simple sweep theory is applied to streamwise section flow conditions, geometry characteristics, and thrust coefficients to obtain the corresponding two-dimensional values.

Second, a computer code for subsonic two-dimensional airfoils is employed to define limitations on the theoretical thrust imposed by airfoil geometry constraints and by a limiting pressure equal to the vacuum pressure. A variety of airfoil sections are treated, and the computer code results are collected and represented by a relationship expressing the dependence of an attainable thrust parameter P_{at} on a theoretical thrust parameter P_{tt}.

Third, theoretical considerations are employed for the general case that enables the vacuum limit thrust parameters to be applied to pressure limitations other than the vacuum limit. As shown later, this is accomplished by replacement of the normal Mach number with an appropriately defined equivalent Mach number.

Fourth, the actual value of the limiting pressure, which reflects the more severe limitations of the real flow, is obtained through the use of theoretical and experimental two-dimensional airfoil data. For a collection of test data, the estimated attainable thrust with thrust factors evaluated from the foregoing relationships and a trial value of the limiting pressure are compared with the experimental thrust data. The calculation is repeated with successive trial values of the limiting pressure until a sufficiently close match of estimated and measured thrusts is achieved. Collected data are then empirically represented to establish the variation of the limiting pressure with Mach number and Reynolds number.

The complete present method, when applied to lifting surface aerodynamic computer codes, modifies the computed results and replaces the theoretical leading-edge thrust with an estimated attainable thrust value. The procedure calls for the treatment of a number of span stations from the wing root chord to the wingtip. For each station, the theoretical thrust is multiplied by a factor dependent on the local flow conditions and the local airfoil geometry.

Normal Airfoil and Flow Parameter Derivation

The derivation of normal airfoil sections and appropriate flow parameters based on simple sweep theory is explained with the aid of figure 2 and sketch A. As shown in figure 2, a different sweep angle Λ_{le} may be required for each span station. Simple sweep theory is applicable to a constant-chord wing of infinite aspect ratio as shown in sketch A.

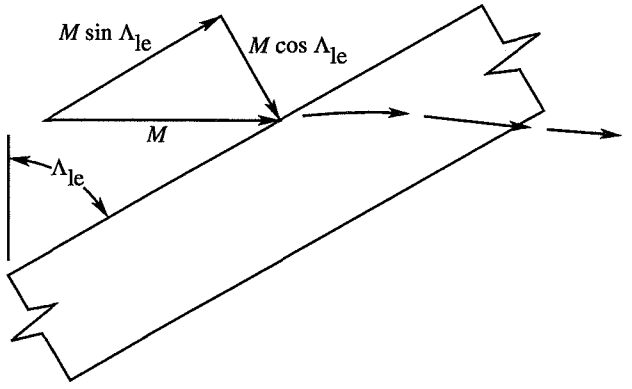

Sketch A

The fundamental concept is based on constant flow properties along lines parallel to the leading edge so that the addition of a velocity field with vectors parallel to the leading edge will not alter the flow. Thus, the free-stream flow, in terms of Mach number, can be divided into the following two components: a flow perpendicular to the leading edge, which determines the flow properties, and a flow parallel to the leading edge, which has no influence. This line of reasoning permits flow properties for the infinitely swept wing to be calculated from two-dimensional flow properties for a section perpendicular to the leading edge immersed in a uniform flow of velocity $M_n = M \cos \Lambda_{le}$.

Even for wings that depart dramatically from a constant-chord, constant-sweep condition, the concept is useful for the analysis of leading-edge thrust because it is dependent primarily on flow behavior in the vicinity of the leading edge. As shown by the vectors in figure 2 and sketch A, a constant velocity $M \sin \Lambda_{le}$ added to the normal velocity $M \cos \Lambda_{le}$ gives a resultant flow which approximates the actual flow over the wing upper surface as represented by the arrows.

The derivation of normal section geometric characteristics is explained with the aid of sketch B. In accordance with simple sweep theory principles, the normal section chord is defined as

$$c_n = c \cos \Lambda_{le}$$

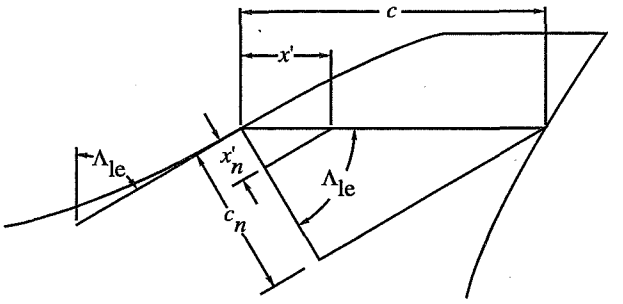

Sketch B

and the normal section thickness is the same as that of the streamwise section along lines parallel to the wing leading edge. Thus, the normal section thickness ratio is

$$\left(\frac{\tau}{c}\right)_n = \left(\frac{\tau}{c}\right)\frac{1}{\cos \Lambda_{le}}$$

By inspection, the nondimensionalized location of maximum thickness for the normal section is the same as that for the streamwise section, i.e., $\eta_n = \eta$. The leading-edge radius of the normal section is derived by an equation representing a generalized form of an airfoil thickness distribution given in reference 10. A modified form of that equation, which was adapted to the purposes of this study and which has the normal section symbols of this paper, is

$$\tau_n = k_{1,n}\sqrt{x'_n} + k_{2,n}x'_n + k_{3,n}x'^{3/2}_n + k_{4,n}x'^{2}_n$$

The first term dominates the shape near the leading edge, and the constant $k_{1,n}$ defines the leading-edge radius. For the normal section near the leading edge

$$\tau_n \approx k_{1,n}\sqrt{x'_n} = k_{1,n}\sqrt{x' \cos \Lambda_{le}}$$

For the streamwise section

$$\tau \approx k_1\sqrt{x'}$$

So that for $\tau_n = \tau$,

$$k_{1,n} = \frac{k_1}{\sqrt{\cos \Lambda_{le}}}$$

The leading-edge radius (ref. 10) for the normal section is given by

$$r_n = \frac{(k_{1,n})^2}{2}$$

and for the streamwise section by

$$r = \frac{(k_1)^2}{2}$$

Thus, for the normal section

$$\left(\frac{r}{c}\right)_n = \frac{r_n}{c_n} = \frac{r}{c}\frac{r_n}{r}\frac{c}{c_n} = \frac{r}{c}\frac{(k_{1,n})^2}{(k_1)^2}\frac{1}{\cos\Lambda_{le}}$$

$$= \frac{r}{c}\frac{1}{\cos^2\Lambda_{le}}$$

These transformations define a wing section that can be analyzed for the effect of geometry and pressure limitations on the attainable leading-edge thrust by use of theoretical and experimental two-dimensional wing data.[1]

The basic premise of the attainable thrust prediction method is that an attainable thrust factor K_t, which is derived from the two-dimensional analysis, can be applied to the calculated theoretical leading-edge thrust for the three-dimensional wing at the corresponding span station. Thus, an essential part of the present method is a connection between two-dimensional and three-dimensional thrust coefficients. The section thrust coefficient may be defined as the thrust force per unit dynamic pressure, per unit chord, and per unit spanwise distance. Thus for the streamwise section,

$$c_t = \frac{dt}{dy}\frac{1}{qc}$$

Sketch C aids in describing the derivation of the normal section thrust coefficient.

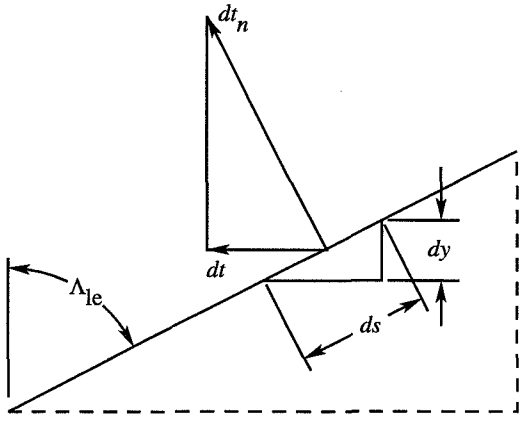

Sketch C

[1]In the original development of the attainable thrust prediction method (ref. 1), normal section dimensions were defined differently. That transformation, however, was applicable only to a normal section with maximum thickness at the 50-percent chord location. The normal airfoil section, as generated in this paper, is more consistent with simple sweep theory concepts and the actual flow over the wing surface.

The thrust vector in the normal direction is

$$dt_n = \frac{dt}{\cos\Lambda_{le}}$$

the dynamic pressure in the normal direction is

$$q_n = q\left(\frac{M_n}{M}\right)^2 = q\cos^2\Lambda_{le}$$

and the incremental distance in the spanwise direction for the normal section is

$$ds = \frac{dy}{\cos\Lambda_{le}}$$

The normal section thrust coefficient then becomes

$$c_{t,n} = \frac{dt_n}{ds}\frac{1}{q_n c_n}$$

$$= \frac{dt}{\cos\Lambda_{le}}\frac{\cos\Lambda_{le}}{dy}\frac{1}{qc_n\cos^2\Lambda_{le}}$$

$$= \frac{dt}{dy}\frac{1}{qc}\frac{c}{c_n}\frac{1}{\cos^2\Lambda_{le}}$$

$$= c_t\frac{c}{c_n}\frac{1}{\cos^2\Lambda_{le}}$$

In the WINGDES and AERO2S computer codes, the section thrust coefficient is referenced to an average chord c_{av}, which then results in

$$c_{t,n} = c_t\frac{c_{av}}{c_n}\frac{1}{\cos^2\Lambda_{le}}$$

The normal section Reynolds number differs from the streamwise Reynolds number because of changes in the velocity (Mach number) and in the local chord. Thus,

$$R_n = R\frac{c_n}{\bar{c}}\frac{M_n}{M}$$

Theoretical Two-Dimensional Airfoil Analysis ($C_{p,lim} = C_{p,vac}$)

For the series of symmetrical two-dimensional airfoil sections represented in figure 3, the subsonic airfoil program of reference 11 was employed to define inviscid flow pressure distributions and integrated thrust coefficients at a Mach number of 0. The airfoils were defined by the following equation:

$$\tau_n = k_{1,n}\sqrt{x'_n} + k_{2,n}x'_n + k_{3,n}x'^{3/2}_n + k_{4,n}x'^2_n$$

in which the coefficients were selected to produce the required section thickness, location of maximum

thickness, and leading-edge radius. Maximum airfoil thickness ranged from 3 to 15 percent of the chord. The location of maximum thickness varied from 10 to 50 percent of the chord. A leading-edge radius index

$$r_{i,n} = \frac{\left(\frac{r}{c}\right)_n \eta}{\left(\frac{\tau}{c}\right)_n^2}$$

could be defined as an appropriate measure of the relative bluntness of airfoil sections. For the majority of NACA airfoils, which span a wide range of thicknesses and maximum thickness locations (see ref. 10 for a representative collection), this index varies within a narrow range of 0.27 to 0.33. An index of 0.3 was chosen to represent a standard leading-edge radius. Other leading-edge radius indices of interest included values of 0, 0.15, 0.60, and 1.2. For a given airfoil, pressure distributions and thrust coefficients across a range of normal Mach numbers were calculated by application of the Prandtl-Glauert rule

$$C_p\sqrt{1 - M_n^2} = C_p\beta_n = \text{Constant}$$

to pressure distributions obtained at a Mach number of 0. This simple means of handling Mach number effects was employed for the sake of consistency with linearized theory methods used for estimating theoretical thrust. A typical pressure distribution for a wing section at lifting conditions is shown in sketch D.

Values of the integrated section thrust coefficient without pressure limitation were calculated from

$$c_t = \frac{1}{c}\oint C_p\, dz$$

The section thrust coefficients were relatively independent of the airfoil thickness and the leading-edge radius and were in reasonably good agreement with the two-dimensional theoretical value for a zero-thickness airfoil, $(2\pi \sin^2 \alpha)/\beta_n$, except for a small increase that tended to be linearly dependent on the airfoil thickness. The suction peak of the theoretical pressure distribution can be quite large, often exceeding the vacuum pressure limit for a given Mach number. Thus, the theoretical section thrust coefficient can be unrealistically high.

To determine the effect on the thrust coefficient of realistically attainable pressure distributions, the computer code integration was performed with the pressure coefficients limited to values greater than or equal to specified pressure coefficients $C_{p,\text{lim}}$, which truncates the suction peak as shown in sketch E. This pressure limitation is intended to account, in an approximate way, for two of the factors which limit attainable thrust: the real-world failure to attain theoretical peak suction pressures, and the tendency of experimental suction peaks to occur at a more rearward position on the airfoil. The specified limiting pressure coefficients were set equal to the vacuum pressure limit $-2/\gamma M_n^2$. As discussed in reference 1 and as explained later, repetition of the integration with

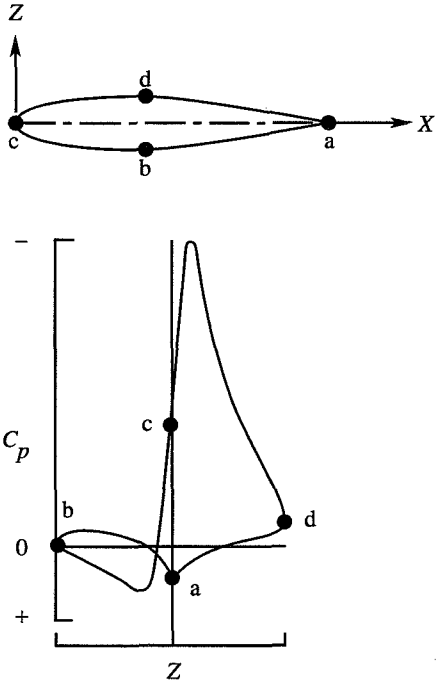

Sketch D

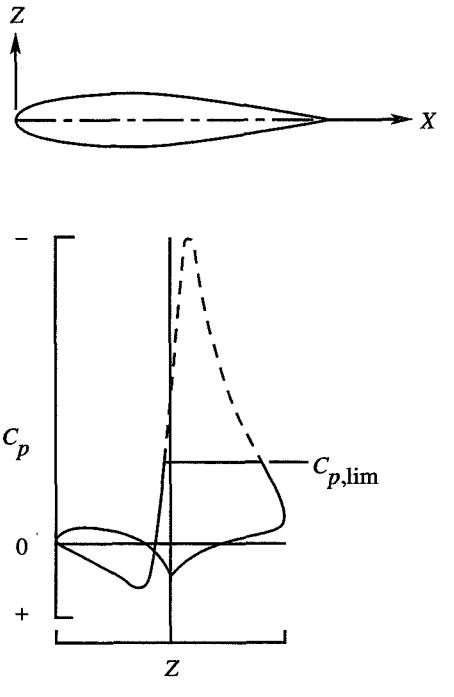

Sketch E

more severe real-world pressure limitations is not necessary. The one set of data with $C_{p,\lim} = C_{p,\text{vac}}$ is sufficient because results for other limiting pressures can be derived from that data with an appropriate substitution of an equivalent Mach number M_e for M_n. The integrated value of c_t associated with $C_{p,\lim}$ is designated c_t^* and the attainable thrust factor is simply $K_t = c_{t,n}^* / c_{t,n}$ with $c_{t,n} = (2\pi \sin^2 \alpha)/\beta_n$. A normal section thrust coefficient $c_{t,n}$ defined in this way is appropriate only for a zero-thickness two-dimensional airfoil. The zero-thickness reference is chosen because the thrust factor is eventually applied to three-dimensional wing code theoretical thrust coefficients for a surface that also has zero thickness.

Shown in figure 4 is an example of the variation of the attainable and theoretical thrusts with angle of attack for a given normal airfoil section at a given normal Mach number. Inset sketches show pressure distributions for 6°, 12°, 18°, and 24° angles of attack. As figure 4 shows, the limitation imposed by vacuum pressures can be quite severe for high angles. In figure 4, the attainable thrust factor K_t is shown as a function of angle of attack; however, as discussed previously, the connection between two-dimensional airfoil sections and the three-dimensional wing sections is made through theoretical leading-edge thrust coefficients and not angle of attack. To find an appropriate three-dimensional wing section angle of attack to match a two-dimensional section angle of attack would be difficult, if not impossible, because of the extreme variation of upwash just ahead of the wing leading edge. The theoretical thrust coefficients provide a better connection because of the dependence of these coefficients on linearized theory singularity strength, which is a measure of pressure levels in the vicinity of the section leading edges. When pressure limiting has only a small effect, as it does for low Mach numbers and low angles of attack, the subsonic airfoil computer code gave values of theoretical thrust greater than that for a zero-thickness airfoil. Thus, K_t can be greater than 1.0 with a maximum value that tends to increase with increasing airfoil thickness. Because experimental data show little or no evidence of the theoretical benefit of airfoil thickness on attainable thrust given by the two-dimensional airfoil computer code, the attainable thrust factor K_t, as shown in figure 4, is restricted to values of 1.0 or less.[2]

[2] In retrospect, an alternative procedure could have been applied. An attainable thrust factor defined as the ratio between thrust coefficients with and without pressure limiting ($(2\pi \sin^2 \alpha)/\beta_n$ replaced by c_t^* for $M_n = 0$) would automatically limit K_t to values less than 1.0. Although this alternative procedure has some attractive features, the resultant method would not be expected to give significantly different results. As shown later, experimental data are used to calibrate the method. A different calibration would compensate for changes in the K_t factor.

After the vacuum pressure-limited thrust coefficient data are determined for the wide range of airfoil sections depicted in figure 3, the next step is to represent the data by empirical equations for use in automated calculations. The representation process is quite involved and was developed after considerable trial and error. For the interested reader, a discussion of the strategy employed is given in appendix A. As discussed in appendix A, the use of a theoretical thrust parameter P_{tt} and an attainable thrust parameter P_{at} provided the means of incorporating a range of airfoil geometric properties in a simplified representation of the attainable thrust factor K_t. Results of the data representation are shown in figure 5 in the form of P_{at} given as a function of P_{tt}. Each of the five plots in figure 5 shows results for a given value of the radius index.

The curves shown in figure 5 represent a fairing of the data provided by a single equation derived in appendix A to cover Mach numbers ranging from 0 to nearly 1.0, maximum thickness ratios from $(\tau/c)_n = 0$ to 0.15, locations of maximum thickness from $\eta = 0.1$ to 0.5, and leading-edge radius indices from 0 to 1.2. The equation is

$$P_{at} = k(P_{tt})^{e_3}$$

or

$$\frac{K_t}{1 + \left(\frac{\tau}{c}\right)_n^{1.2}} = k\left\{c_{t,n}\beta_n\left[\frac{\left(\frac{\tau}{c}\right)_n\left(\frac{\eta}{0.5}\right)^{e_1 - e_2}}{0.09}\right]^{e_2}\right\}^{e_3} \qquad (1)$$

with K_t limited to values less than 1.0 where

$$k = \left\{0.14[1.0 - (1.0 - \sqrt{r_{i,n}})M_n^5] + 0.11\sqrt{r_{i,n}}\right\} \times \left(\frac{1 - M_n}{M_n}\right)^{0.48(1 + r_{i,n}^{0.3})}$$

$$e_1 = 0.4r_{i,n}^{0.16} - 0.7$$

$$e_2 = 1.6r_{i,n}^{0.10} - 3.0$$

$$e_3 = -0.32r_{i,n}^{0.10} - 0.3$$

The limitation of K_t to values no greater than 1.0 permits attainable thrust to equal, but not exceed, theoretical thrust values defined by lifting surface theory. In the curve-fitting exercise, primary attention was given to representation of factors near the middle of the P_{at} range. In addition, the greatest emphasis was placed on data

representing nominal airfoil parameters of $(\tau/c)_n = 0.09$ and $\eta = 0.5$. Thus, the system is less accurate for extreme airfoil shapes, particularly for thin airfoils with forward locations of maximum thickness and sharp or nearly sharp leading edges.

In figure 5, the decrease in P_{at} with increasing P_{tt} is clearly shown, as is the strong dependence on Mach number. A comparison of the plots in figure 5 shows the effect of increasing leading-edge radius. A sharp leading edge (fig. 5(a)) produces a substantial level of attainable thrust. Through an oversight, the previous attainable thrust method of reference 1 did not account for any of this thrust. For a leading-edge radius of zero, the previous method gave a thrust of zero. Sketch F is an example of the variation of attainable thrust with increasing leading-edge radius for a 9-percent thick airfoil with maximum thickness at the 50-percent chord station at an angle of attack of 12° at $M_n = 0.5$.

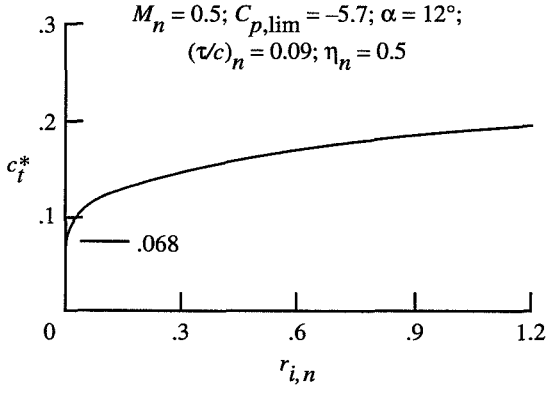

Sketch F

In figure 5 the considerable dependence of the attainable thrust parameter on maximum thickness and its location is not clearly evident. Sketch G shows the variation of attainable thrust with increasing thickness for an airfoil with a leading-edge radius index of 0.3 and maximum thickness at the 50-percent chord station at the same flow conditions. The nearly linear dependence of thrust on thickness clearly illustrates the importance of thickness and its frontal projected area in the development of thrust.

The effect of the location of maximum thickness on developed thrust is illustrated in sketch H for the same nominal conditions of maximum $(\tau/c)_n = 0.09$, $r_{i,n} = 0.3$, $\alpha = 12°$, and $M_n = 0.5$. Benefits of a more forward location of projected frontal areas on which thrust is developed are clearly shown. However, these thrust benefits are achieved at the expense of a tendency toward increased profile drag for such sections.

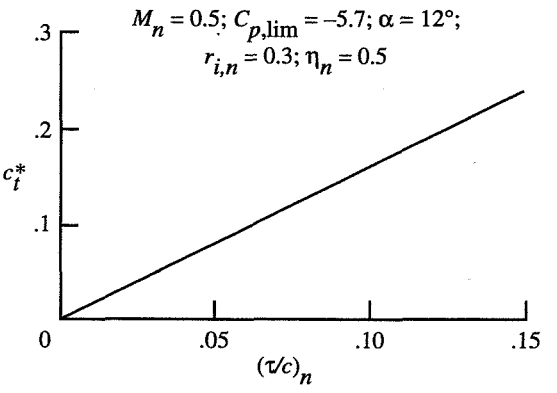

Sketch G

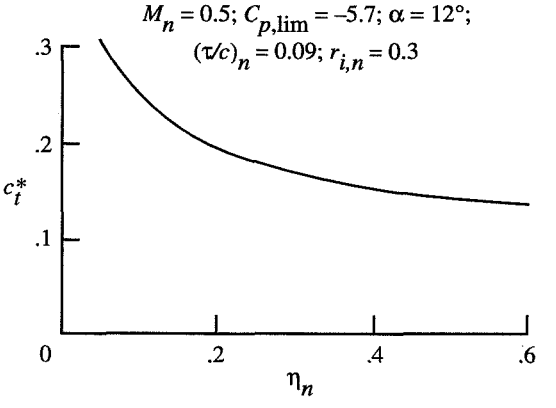

Sketch H

Equivalent Mach Number Concept ($C_{p,\lim} \neq C_{p,vac}$)

Equation (1) was developed to account for the reduction in attainable leading-edge thrust resulting from the application of realistic constraints on local pressure coefficients. A limiting pressure defined by the vacuum pressure coefficient has been shown to have a powerful effect on the amount of theoretical leading-edge thrust that can actually be realized. However, even more severe limits on achievable thrust are experienced in the real flow over airfoil sections when the local flow lacks sufficient energy to negotiate turns about the airfoil surface without becoming detached from that surface. Establishment of values for these more severe limitations is addressed in the following section of this paper. Before that, a means of application of equation (1) to the estimation of attainable thrust for values of limiting pressure other than the vacuum limit is developed. Equation (1) can be used for a full range of limiting pressures between 0 and $C_{p,vac}$ by substitution of a properly defined equivalent Mach number M_e for the normal Mach number M_n. The substitute Mach number is defined by the following logic. As

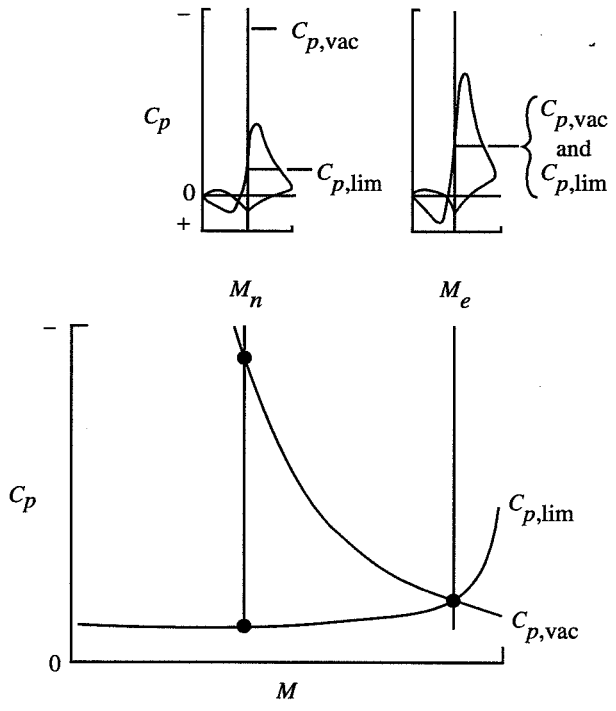

Sketch I

illustrated by the pressure distributions shown in sketch I for a given airfoil section at the same positive angle of attack, the pressure coefficient at any point on the airfoil will vary with Mach number according to the Prandtl-Glauert rule. Thus, if the limiting pressure $C_{p,\text{lim}}$ also changes in accordance with the Prandtl-Glauert rule

$$C_{p,\,\text{lim}}(M_e) = C_{p,\,\text{lim}}(M_n)\frac{\sqrt{1-M_n^2}}{\sqrt{1-M_e^2}}$$

the attainable thrust factor K_t will be the same at all Mach numbers because both $c^*_{t,\,n}$ and $c_{t,\,n}$ will have the same Mach number dependence. Then with M_e selected so that $C_{p,\text{lim}}(M_e) = C_{p,\text{vac}}(M_e)$, the appropriate value of K_t for the normal Mach number under consideration is calculated by substitution of M_e for M_n in equation (1). The required M_e is determined by setting $C_{p,\text{vac}}(M_e) = C_{p,\text{lim}}(M_e)$, the intersection point of the curves shown in sketch I, and by solving for M_e. Thus,

$$C_{p,\,\text{vac}}(M_e) = C_{p,\,\text{lim}}(M_e)$$

$$-\frac{2}{\gamma M_e^2} = C_{p,\,\text{lim}}(M_n)\frac{\sqrt{1-M_n^2}}{\sqrt{1-M_e^2}}$$

and after the solution for the equivalent normal Mach number,

$$M_e = -\frac{\sqrt{2}}{\gamma\, C_{p,\,\text{lim}}\sqrt{1-M_n^2}}\sqrt{\sqrt{1+\left(\gamma C_{p,\,\text{lim}}\sqrt{1-M_n^2}\right)^2}-1} \quad (2)$$

Experimental Two-Dimensional Airfoil Analysis ($C_{p,\text{lim}}$ Calibration)

To define practical values of the limiting pressure coefficient, an incomplete version of the present method was applied to experimental two-dimensional airfoil data for symmetrical sections. (See refs. 10–18.) Correlations of axial-force coefficients predicted by this incomplete present method with experimentally determined axial-force coefficients, as shown in the examples of figure 6, were used to determine, by trial, values of $C_{p,\text{lim}}$ that would match the experimental trends. For these symmetrical sections, Δc_A is simply the negative of $c^*_{t,\,n}$. The example correlations in figure 6 were chosen to represent the procedures that were applied to the large amount of data available in the references. These data had a range of airfoil maximum thicknesses from 4 to 15 percent of the chord and locations of maximum thickness from 10 to 42 percent of the chord. However, leading-edge radius indices had only a small range of 0.24 to 0.33. Mach numbers ranged from 0.03 to 0.90, and Reynolds numbers varied from less than 1×10^6 up to 30×10^6.

To evaluate limiting pressure coefficients, equations (1) and (2) were combined in a computational process in which K_t and $c^*_{t,\,n}$ were calculated for a series of trial $C_{p,\text{lim}}$ values to find the value that most closely matched the experimental data. In matching the trial curve fit to the experimental data, particular attention is given to breakaway of the experimental axial force from the theoretical leading-edge full-thrust curve. For most of the plots, this breakaway point can be established with reasonable certainty. For other plots a breakaway point of the experimental data is not readily obvious. The problem occurs because axial-force data were not presented directly for some of the experimental investigations; the axial force had to be derived from lift- and drag-coefficient data. For some of these data, as in the examples in figure 6(c), C_D data were omitted even though C_L versus α data were shown in the plots. Generally, this occurred for angles of attack in excess of the angle at which maximum lift was obtained. Presumably the authors wanted to avoid two values of drag at a given lift coefficient. Because of the absence of C_D data, axial force could not be calculated for all of the angles of attack listed in the reference data. However, extrapolation of the C_D curve subject to nearly maximum C_L or subject to C_D values greater than the maximum plot values would lead to C_A values on or above the curves

corresponding to the specified limiting pressure coefficients. Thus, when properly interpreted, these data also provide estimates of limiting pressures. For the lower plots in figure 6(c), complete data were provided for the highest angle of attack shown. These experimental data closely follow the theoretical full-thrust curve for the entire plot and show no breakaway tendencies. For this case, only the fact that limiting pressures are less than (i.e., greater negative value) those that would cause a breakaway at the highest angle of attack at which data are shown could be determined. The examples shown in figure 6 include curves of calculated ΔC_A for the selected value of $C_{p,\text{lim}}$ and for values of ±20 percent of $C_{p,\text{lim}}$. Obviously, establishment of precise values of limiting pressure coefficients is not possible; however, as shown in figure 6, attainable thrust and, especially, its breakaway point can be predicted with reasonable accuracy with only approximate limiting pressure estimates.

Data from figure 6 and from a large number of other plots of axial-force coefficient versus angle of attack (87 plots in all) were used in figure 7 to define the dependence of the limiting pressure coefficient on Mach number and Reynolds number. Although the $C_{p,\text{lim}}$ data showed some dependence on airfoil section geometric characteristics, this dependence was not systematic and was small compared to that of M_n and R_n. The limiting pressure is shown as a function of Mach number for a series of nominal Reynolds numbers. Nominal Reynolds number data were obtained by either interpolation or extrapolation of Reynolds number data such as that shown in sketch J. All of the data shown in figure 7 were obtained for relatively smooth airfoil sections with no attempt to establish turbulent flow through the use of artificial roughness. Thus, the Reynolds number effect

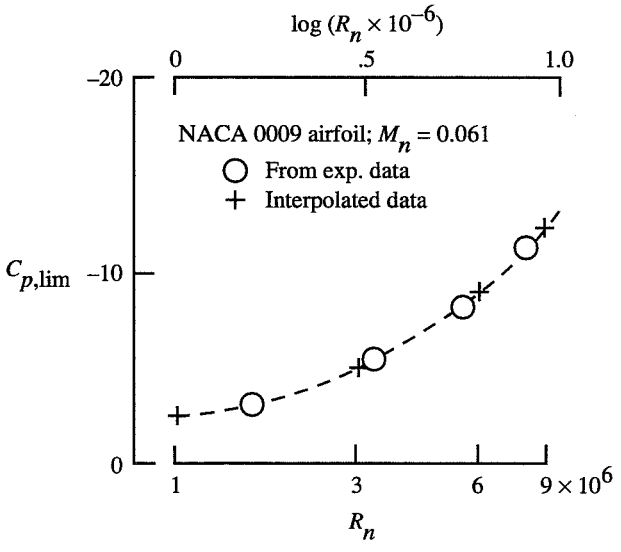

Sketch J

shown here includes the effect of transition from laminar to turbulent flow. A large amount of scatter is noted in the data, especially for the nominal Reynolds number of 3.0×10^6. At this Reynolds number, evidence of transitional flow can reasonably be expected. The solid curves shown in figure 7 represent an attempt to mathematically express the variation of the limiting pressure coefficient with Mach number and Reynolds number. The curve fit was chosen to closely represent the upper limit of the data. Thus, a system that uses this empirical relationship to predict attainable thrust tends to represent idealized conditions, i.e., smooth surfaces and stable uniform flow with little turbulence ahead of the airfoil or wing.

The curve-fit equation chosen to represent the data has the form

$$C_{p,\text{lim}} = -\frac{2}{\gamma M_n^2}\left(\frac{R_n \times 10^{-6}}{R_n \times 10^{-6} + K}\right)^{e_4} \tag{3}$$

which was chosen to give a limiting pressure approaching the vacuum limit for infinitely large Reynolds numbers and a limiting pressure approaching 0 for infinitely small Reynolds numbers. Values of K and the exponent e_4 were chosen by a trial-and-error process to closely match an upper bound of the empirically derived $C_{p,\text{lim}}$ distribution. These values are

$$K = 10^{8(1-M_n)}$$

$$e_4 = 0.028 M_n^{-0.75}$$

The data and the curve fits in figure 7 show a strong dependence of the limiting pressure on Mach number equal, at least, in importance to the dependence on Reynolds number. The tendency for the limiting pressure to decrease with increasing Mach number was expected because $C_{p,\text{vac}}$ decreases with increasing M_n. The existence of a limiting pressure peak and the drop-off for Mach numbers less than about 0.15 were not anticipated. To search for validation of this Mach number trend and to further explore Reynolds number effects, the Navier-Stokes computer code described in reference 19 was employed as described in appendix B. Basically, the computer code was used to create two-dimensional airfoil axial-force data, which was treated in the same fashion as the experimental data, to define another set of limiting pressures. Because of the time-consuming nature of the computer code, only a few representative cases were handled. The Navier-Stokes computer code was first used to provide data for a NACA 0009 airfoil at a Reynolds number of 9×10^6 for a series of Mach numbers. For these conditions shown in figure 7(d), $C_{p,\text{lim}}$, as defined by the Navier-Stokes computer code data, has a

variation with Mach number similar to that given by the data but at a slightly higher level. This is understandable because the airfoil model can be expected to have surface roughness not modeled in the theoretical airfoil shape, and the wind tunnel flow could have turbulence levels higher than anticipated. Even with this additional confirmation, some uncertainty remains about the evaluation of limiting pressure for normal Mach numbers below 0.1. Thus, results of the computer codes employing this attainable thrust estimation technique are questionable for Mach number and sweep angle combinations in which $M \cos \Lambda_{le} < 0.1$. For example, results for a 70° swept leading-edge wing could be somewhat suspect for free-stream Mach numbers less than about 0.3.

Navier-Stokes computer code data depicting the dependence of limiting pressures on Reynolds number are compared with results given by the curve fit in sketch K. The Navier-Stokes results are for an NACA 0009 airfoil at a Mach number of 0.16. For this Mach number, the Navier-Stokes results indicate a more beneficial effect of increasing Reynolds number than is given by equation (3) used in the present method. Further, more complete studies using Navier-Stokes computer codes in conjunction with appropriate experimental verification may eventually lead to a more accurate representation of limiting pressures. In particular, a need exists for better definition of limiting pressure coefficients at high Reynolds numbers and low Mach numbers. The use of such additional data in a revised calibration of the present attainable thrust prediction method is discussed in the section entitled "Future Limiting Pressure Redefinition With Use of AERO2S Computer Code."

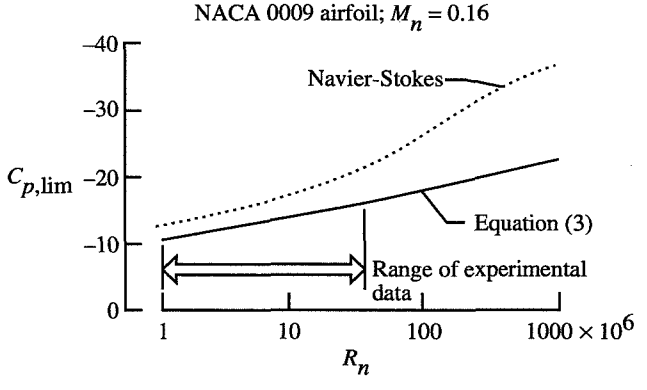

Sketch K

The variation of the limiting pressure coefficient with Reynolds number is depicted in figure 8. The curve-fit data shown here were obtained from equation (3). The experimental data used in generation of the curve fit are omitted. The purpose is to show in a single plot the influence of both Mach number and Reynolds number on limiting pressure trends. At high Mach numbers, the limiting pressure obviously is relatively insensitive to Reynolds number and is severely constrained by the vacuum pressure limit. However, at low Mach numbers, a strong sensitivity to Reynolds number exists. With the present curve fit, the greatest changes with Reynolds number occur for a Mach number of about 0.1. However, this strong sensitivity does not lead to correspondingly large changes in leading-edge thrust because $C_{p,\lim}$ acts only as a bound in the pressure integral for $c_{t,n}^*$.

These limiting pressure data from the analysis of two-dimensional airfoil experimental data (eq. (3)) are used to define an equivalent Mach number M_e (eq. (2)) for use in the theoretical two-dimensional airfoil analysis (eq. (1)) to estimate the dependence of attainable thrust for two-dimensional airfoils on airfoil geometric properties and flow conditions. In essence, the experimental two-dimensional airfoil data provide the calibration of the system. The product of this two-dimensional analysis is a factor K_t defined by equation (1) that relates the attainable two-dimensional thrust to the theoretical two-dimensional thrust by

$$c_{t,n}^* = K_t c_{t,n}$$

Guidelines for Present Method Application to Three-Dimensional Wing Computer Codes

The present method for the prediction of attainable leading-edge thrust described in this paper is intended to be incorporated into linearized theory lifting surface computer codes (e.g., AERO2S and WINGDES), which provide a calculation of theoretical leading-edge thrust. The first step in programming of the attainable leading-edge thrust method for inclusion in linearized theory lifting surface computer codes is implementation of the simple sweep analysis to define the equivalent normal or two-dimensional airfoil geometric characteristics and flow conditions for a series of streamwise sections from the wing root to the wingtip. For each of a large number of wingspan stations, the following terms define the normal section geometric characteristics:

$$c_n = c \cos \Lambda_{le}$$

$$\left(\frac{\tau}{c}\right)_n = \left(\frac{\tau}{c}\right)\frac{1}{\cos \Lambda_{le}}$$

$$\eta_n = \eta$$

$$\left(\frac{r}{c}\right)_n = \frac{r}{c}\frac{1}{\cos^2 \Lambda_{le}}$$

$$r_{i,n} = \frac{\left(\frac{r}{c}\right)_n \eta}{\left(\frac{\tau}{c}\right)_n^2}$$

In addition, for each span station, the normal Mach number, the normal Reynolds number, and the normal section thrust coefficient are defined as follows:

$$M_n = M \cos \Lambda_{le}$$

$$R_n = R\frac{c_n}{c} \cos \Lambda_{le}$$

$$c_{t,n} = c_t \frac{c}{c_n}\frac{1}{\cos^2 \Lambda_{le}}$$

or with c_t nondimensionalized as in AERO2S and WINGDES

$$c_{t,n} = c_t \frac{c_{av}}{c_n}\frac{1}{\cos^2 \Lambda_{le}}$$

The theoretical thrust coefficient c_t is supplied by the linearized theory lifting surface analysis. This coefficient accounts for variations of the theoretical leading-edge full-thrust coefficient with such factors as free-stream Mach number, wing planform, and wing twist and camber.

For each span station, the limiting pressure coefficient is then calculated from

$$C_{p,\lim} = -\frac{2}{\gamma M_n^2}\left(\frac{R_n \times 10^{-6}}{R_n \times 10^{-6} + K}\right)^{e_4}$$

where

$$K = 10^{8(1-M_n)}$$

$$e_4 = 0.028 M_n^{-0.75}$$

The limiting pressure coefficient is then used to calculate the equivalent Mach number

$$M_e = -\frac{\sqrt{2}}{\gamma C_{p,\lim}\sqrt{1-M_n^2}}\sqrt{\sqrt{1+(\gamma C_{p,\lim}\sqrt{1-M_n^2})^2}-1}$$

which accounts for differences between the more realistic limiting pressure coefficients and the vacuum pressure coefficient.

The attainable thrust factor K_t is calculated from

$$\frac{K_t}{1+\left(\frac{\tau}{c}\right)_n^{1.2}} = k\left\{c_{t,n}\beta_n\left[\frac{\left(\frac{\tau}{c}\right)_n\left(\frac{\eta}{0.5}\right)^{e_1-e_2}}{0.09}\right]\right\}^{e_3}$$

with K_t limited to values less than 1.0 where

$$k = \left\{0.14[1.0-(1.0-\sqrt{r_{i,n}})M_e^5]+0.11\sqrt{r_{i,n}}\right\} \times \left(\frac{1-M_e}{M_e}\right)^{0.48(1+r_{i,n}^{0.3})}$$

$$e_1 = 0.4 r_{i,n}^{0.16} - 0.7$$

$$e_2 = 1.6 r_{i,n}^{0.10} - 3.0$$

$$e_3 = -0.32 r_{i,n}^{0.10} - 0.3$$

The ratio of attainable theoretical thrust K_t for each normal airfoil section is then applied to the theoretical thrust for the wing at the wing spanwise station from which the normal section was derived to arrive at a spanwise distribution of attainable thrust. The attainable thrust section coefficient is then

$$c_t^* = K_t c_t$$

where c_t is the theoretical leading-edge full-thrust coefficient defined by the attached flow linearized theory lifting surface solution.

For a given wing and a given set of test or flight conditions, the theoretical leading-edge thrust c_t given by a linearized theory computer code will vary with span position and wing angle of attack. The attainable thrust factor K_t determined by the attainable thrust method will vary with those quantities and with other factors including local leading-edge sweep angle and wing section characteristics. The effect of wing twist and camber or flap deflection is accounted for in the calculated c_t value. Because the attainable thrust factor is dependent on the theoretical thrust, it is also influenced by wing twist, wing camber, or flap deflection. The same spanwise integration techniques used in the lifting surface computer code can be employed to calculate wing attainable thrust coefficients.

Present Method Validation

To illustrate the applicability of the present attainable thrust prediction method, a series of comparisons of theoretical and experimental data for wing-body configurations is presented in figures 9–18. The AERO2S computer code described in reference 7 and the WINGDES computer code described in reference 8 were modified to replace the previous attainable thrust prediction method with the present version. For some examples, results using both versions are shown. Computer code-estimated forces include attainable thrust and the effects of a separated vortex whose strength is determined by the Polhamus leading-edge suction analogy and whose location is given by delta wing empirical data (computer code vortex option (1)). Computer code results are designated by the solid line for the present method and by the long-dash–short-dash line for the previous method. Computer code results without the addition of either attainable leading-edge thrust or vortex forces are shown by the short-dash line. Because some amount of either of these forces is almost always present, this curve gives a conservative estimate of the drag upper limit. As an additional reference, a theoretical leading-edge full-thrust curve given by the computer code is shown on the axial-force coefficient plot and on the lift-drag plot. The purpose of the attainable thrust prediction is to provide an estimate of the portion of the theoretical thrust that can actually be achieved. These reference curves help in an assessment of the success of the prediction.

Because the purpose of this attainable thrust study is the development and assessment of methods for prediction of drag associated with the generation of lift, the zero-lift drag coefficient $C_{D,0}$ for a flat wing configuration (a wing with no twist or camber) used to construct the theoretical curves was obtained from experimental data. This was accomplished by setting $C_{D,0}$ equal to the limiting value of the axial-force coefficient for a flat wing configuration as α approaches 0 ($C_D = C_A$ at $\alpha = 0°$). Use of the C_A rather than the C_D curves gives a more accurate result because of the lesser sensitivity to angle of attack or C_L variation.

Figure 9 shows data at a Mach number of 0.4 and a Reynolds number of 2.5×10^6 for a 60° swept delta wing fighter with a rounded leading-edge NACA 64A00X airfoil. Correlations using this experimental data from reference 20 were originally shown in reference 6. For the undeflected flap or flat wing case in figure 9(a) and the 20° deflection case in figure 9(b), the present attainable thrust method predicts thrust that is slightly greater (i.e., more negative C_A) than the previous method but nearly equal to the experimental values.

For these data and for all of the theoretical-experimental correlations to be shown, little or no difference is noted in predicted normal-force coefficients and pitching-moment coefficients because of the change in the attainable thrust prediction. Differences between experimental and theoretical C_N and C_m curves shown in figure 9 are not addressed here. However, the C_N differences are responsible for the lack of improvement in C_D prediction for the present method in spite of the C_A improvement. Note that for the deflected flap case, the difference between no-thrust and full-thrust theoretical C_A curves is smaller at a given positive angle of attack. Thus, the deflected flap configuration is less sensitive to the attainable thrust prediction than is the undeflected flap or flat wing configuration.

Data for the same 60° swept delta wing fighter at a higher Mach number of 0.8 are shown in figure 10. Here, the newer attainable thrust prediction is slightly poorer at angles of attack above 10°. The prediction of drag does not change below lift coefficients of about 0.5 and changes by only a small amount up to $C_L = 0.8$. This poorer prediction of wing characteristics for high-lift coefficients as sonic speeds are approached is to be expected. The AERO2S and WINGDES computer codes are not applicable at transonic speeds.

Figure 11 shows data at a Mach number of 0.4 for a wing-body configuration identical in all respects to that in figure 9 except for the substitution of a sharp leading-edge airfoil. The leading edge of this airfoil, which can not practically have a sharp leading edge, was estimated to have a leading-edge radius of 0.002 in. With this radius, the present method gives a very good estimate of the thrust actually achieved. Sketch L illustrates an important point concerning the sensitivity of thrust to the leading-edge radius in the previous and present system. With the previous method, a wide variation between results with zero radius and the small estimated radius was obtained. For the present method, that range is reduced, and even if the radius were zero, a significant amount of thrust would remain. Thus, the present method is not nearly so dependent on the skill of the user in choosing an appropriate radius for a particular case.

Data for a 44° swept trapezoidal wing fighter at a Mach number of 0.4 and a Reynolds number of 1.9×10^6 are shown in figure 12. These data from reference 20 were also used in correlations presented in reference 6. Little difference between the predictions given by the two methods is seen up to an angle of attack of about 8° or a C_N of about 0.5, and both methods agree well with the experimental data. However, beyond this angle of attack, there is evidence of a severe flow breakdown which the theory cannot handle. The reduction in leading-edge sweepback angle from that of the previous

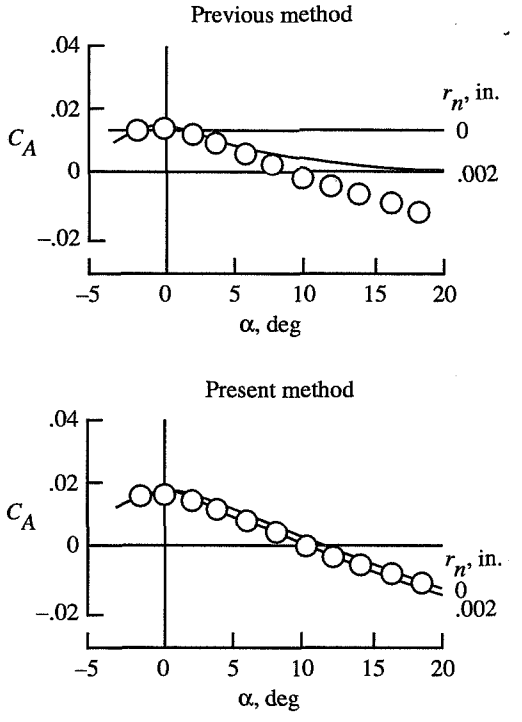

Sketch L

correlations may be responsible, at least in part, for the earlier and more severe breakaway of the experimental axial-force coefficient from the computer code prediction. For large sweep angles, drastic flow separation would be expected to begin near the wingtip at relatively small angles and progress inward as the angle of attack is increased. This would result in a thrust loss that is more gradual than that for small sweep angles where drastic flow separation would be expected to occur more abruptly. As noted earlier, axial-force breakaway can be very severe for two-dimensional airfoils (zero sweep angle) at low Mach numbers.

When leading- and trailing-edge flaps for the trapezoidal wing fighter are deflected to 20°, the results shown in figure 12(b) are obtained. Again, the present method predicts a somewhat greater amount of attainable thrust but fails to adequately predict the experimental values of achieved thrust. At a lift coefficient of about 0.6, where the deflected flaps provide a substantial drag reduction, both the present and the previous methods give a reasonable prediction of the performance. Again, the change in attainable thrust prediction with deflected flaps has less effect than that with undeflected flaps. Because of this smaller effect for wings with deflected flaps (or twisted and cambered wings), the remainder of the theoretical-experimental correlations will be restricted to flat or slightly cambered wings.

Data for a supersonic transport configuration from reference 21 are shown in figure 13. Comparisons of this data with the previous method were given in reference 6. The present method gives a better prediction of C_A and C_D. Experimental axial-force data for this wing with very high leading-edge sweep angles do not display the sharp upturn away from the computer code estimate shown in the previous example. For this wing at the specified test Mach number of 0.25, the normal Mach number is about 0.08 for the inboard panel and about 0.12 for the outboard panel. The reasonably good correlation of computer code results with the experimental data should help to allay some previously expressed concerns regarding the proper selection of limiting pressures for very low normal Mach numbers. Similar results, which are not included in this collection, were obtained for another supersonic transport configuration tested in a different facility.

Data obtained at a supersonic Mach number for a wing with three different airfoil sections are shown in figure 14. These data from reference 22 were used in correlations presented in reference 8. For all leading edges, which included the sharp leading edge (fig. 14(a)), the standard leading edge (fig. 14(b)), and the blunt leading edge (fig. 14(c)), little discernible difference is noted between the predictions given by the two methods. Both give results in good agreement with the experimental data. For the sharp leading edge, the previous method with an estimated leading-edge radius works surprisingly well. However, as noted previously, it is much more sensitive to the radius selection than the present method. Without the assumed radius, the previous method would give a C_A value of 0.01 independent of the angle of attack.

An experimental program designed to examine the effects of wing leading-edge radius and Reynolds number on wing performance was reported in reference 23. Some examples from that report, which show the effects of leading-edge radius, are shown in figure 15. For these comparisons, only the present version of the attainable thrust method was used. The configuration that was selected had a leading-edge sweep angle of 61.7° and an unswept trailing edge. The test Mach number was estimated to be 0.22. The Reynolds number for the data presented in figure 15 has a small range between 9.72×10^6 and 10.14×10^6. For the sharp leading edge (fig. 15(a)) a very small leading-edge radius of 0.002 in. was assumed as before. For the other sections, leading-edge radii specified in the report were used. In the three plots in figure 15, the leading-edge radius has a significant effect on performance, and the present attainable thrust method predicts this performance quite well. The only appreciable discrepancy between theory and experiment occurs for the sharp leading-edge airfoil section. As noted in discussions of the present method development, the method is expected to be least accurate for thin wings

with sharp leading edges and forward locations of maximum thickness. The wing section thickness ratio is only 0.02 at the wing-body juncture, and the location of maximum thickness η is as low as 0.12 for much of the wingspan.

Figure 16 shows data for the same configuration as in figure 15 with the small leading-edge radius (actually more accurately characterized as a standard leading-edge radius with $r_i \approx 0.27$) at three additional Reynolds numbers. At the lowest Reynolds number (fig. 16(a)), the attainable thrust is somewhat overestimated, and at the highest Reynolds number (fig. 16(c)), it is slightly underestimated. However, in general, both the axial force and the drag are predicted reasonably well at all three Reynolds number.

The data presented in figures 17 and 18 provide additional verification of the present attainable thrust prediction method and also illustrate a problem that is sometimes encountered in assessing wing drag-due-to-lift characteristics from wind tunnel data. Data for a 44° sweptback wing of aspect ratio 2 with a 3-percent-thick rounded nose section in Mach number 0.61 flow taken from reference 24 are compared with theoretical results in figure 17. In figure 17(a), for a Reynolds number of 1.9×10^6, rather peculiar behavior of the experimental C_A occurs in the angle-of-attack range from ±3°. This test model, which employed no artificial means of stabilizing the boundary layer, may have generated a flow with large laminar flow regions at and near 0° angle of attack. With increasing angle of attack, the flow apparently became predominantly turbulent. The assessment of drag-due-to-lift characteristics requires the establishment of a $C_{D,0}$ value reflecting the type of flow (laminar-turbulent transition) present at lifting conditions. The experimental C_D (and C_A) at $\alpha = 0°$ of about 0.0070 does not represent such a value. However, as shown in the C_A plot, an appropriate $C_{D,0}$ can be found by fitting the curve given by the computer code to experimental axial-force coefficients in the range where the slopes agree. The $C_{D,0}$ value of 0.0100 given by this process, when combined with the computer code drag-due-to-lift prediction, provides good correlation with the measured results up to about 12° angle of attack. However, a significant discrepancy in the pitching moment, which is more than that found for most of the other configurations, is shown.

Data for the 44° sweptback wing at a higher Reynolds number of 4.8×10^6 are shown in figure 17(b). Here, the application of the curve-fit technique also requires the establishment of a representative $C_{D,0}$ value. However, in this case, only a single C_A data point (that closest to $\alpha = 0°$) departs significantly from the theory curve. Again, the drag polar data are well predicted.

Figure 18 presents data for the same configuration as in figure 17 with the exception of the substitution of a sharp leading edge for the rounded leading edge. For the calculations a constant leading-edge radius of 0.002 in. was assumed. Only a small $C_{D,0}$ correction was required for these test data. Comparison of these results with those in figure 17 shows almost no penalty in either theoretical or experimental C_A and C_D associated with the sharper leading edge. A small loss in leading-edge thrust is offset by a lower $C_{D,0}$.

Sketch M helps in a discussion of the importance of a proper establishment of $C_{D,0}$ in assessing drag-due-to-lift characteristics. The data shown here are for the configuration analyzed in figure 17. The circles represent the experimental data, and the solid lines a possible fairing of that data. The drag at zero lift displays an increase with increasing Reynolds number rather than a decrease as would be expected. This is in marked contrast to the behavior of the drag of this same configuration at higher lift coefficients (e.g., $C_L = 0.4$). The drag at zero lift is likely influenced by flow changes (transition from laminar to turbulent) not experienced at higher lift coefficients. At higher Reynolds numbers where the boundary layer at both lift coefficients is likely to be predominately turbulent, the two curves would tend to be parallel. An assessment of the required $C_{D,0}$ correction for a given wing, as represented by the arrow in sketch M, can be determined by use of the C_A curve-fitting technique previously discussed.

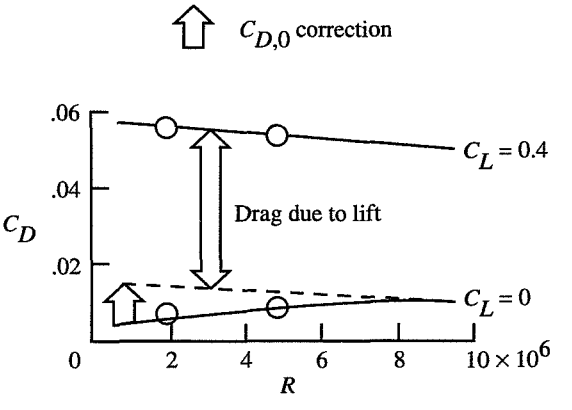

Sketch M

A review of all the correlations presented in figures 9–18 shows that, in general, the initial breakaway of axial force from the theoretical full-thrust curve is predicted quite well. However, for a wing with a 44° leading-edge sweep angle at a Mach number of 0.4, a more severe loss of thrust occurred beyond this point than that predicted by the present attainable thrust

method. For high-sweep angles ($\Lambda_{le} = 60°$ or more), the axial force is predicted with reasonable accuracy for angles of attack up to about 16° or 20°. Highly swept wings are expected to display a more gradual onset of the effects of drastic flow separation because the initial separation tends to occur near the wingtip and progress inward as the angle of attack is increased. This is in contrast to more moderately swept or unswept wing sections where the drastic separation can occur all at once.

Future Limiting Pressure Redefinition With Use of AERO2S Computer Code

As explained in the section of this paper entitled "Experimental Two-Dimensional Airfoil Analysis ($C_{p,\lim}$ Calibration)," the effects of Reynolds number and Mach number on attainable thrust are derived empirically by use of available two-dimensional airfoil experimental data. Thus, the accuracy of the whole system depends on the availability and accuracy of these experimental data. A new set of two-dimensional airfoil experiments tailored specifically for this problem would make a significant contribution to the technology. In addition, as indicated in a preliminary study included in the method development section, two-dimensional Navier-Stokes solutions may provide valuable additional information including extension of the capabilities of the experimental approach. In particular, better definition of limiting pressure coefficients is required at high Reynolds numbers for low Mach numbers. In the hope of encouraging such further activities, some suggestions for a revised calibration of the system are given.

The problem in calibrating the attainable thrust method is to find, by iteration, $C_{p,\lim}$ values that give axial-force coefficients fitting the experimental data as it breaks away from the theoretical full-thrust curve. To facilitate any future recalibration of the system, the AERO2S computer code has been modified to provide a two-dimensional airfoil solution. To use the computer code in the two-dimensional mode, set `JBYMAX = 1` and input data for two identical wing sections at the root and tip stations of a rectangular wing of any span. In this mode the computer code can be used to supply additional calibration data. This is accomplished by input of `xmcplt` values other than 1.0, which act as multipliers of the limiting pressure as now defined. When a chosen `xmcplt` value gives a ΔC_A curve matching the experimental data for a range of angles of attack near the breakaway point, the corresponding limiting pressure coefficient included in the output data is taken to be the value for the input Mach number and Reynolds number. A collection of such data for a large number of airfoils and test conditions then can be used to generate a revised curve-fit equation that might, but not necessarily, be similar in form to that presently used.

The part of the AERO2S and WINGDES computer codes that is to be changed to accommodate a new formulation of the limiting pressure coefficient definition can be found by conducting an automated search for `_cplt_`. Inclusion of the space before and after the name excludes other extraneous lines. In the AERO2S computer code, the `_cplt_` definition occurs twice, once for each surface.

All of the two-dimensional experimental data employed in the present analysis were for symmetrical sections. Airfoils with camber can also be used if necessary. For such airfoils, ordinate tables for a mean camber surface (halfway between lower and upper surface ordinates at a given chord station) are required. The computer code then provides an axial-force variation with angle of attack differing from the symmetrical section values, but the iteration process is no different. The goal is still to find $C_{p,\lim}$ values by iteration that match computer code and experimental axial-force data as the experimental data breaks away from the theoretical leading-edge full-thrust curve.

Concluding Remarks

A revised method (called the present method herein) for predicting attainable leading-edge thrust and its effect on airplane aerodynamic performance has been developed. The present method accommodates a greater range of airfoil shapes from very sharp to very blunt leading edges. It is also based on a wider range of Reynolds numbers than the range of the previous method. An additional aesthetic appeal of the present approach is a relationship between flow over the wing surface and the corresponding two-dimensional airfoil analysis that is more consistent with simple sweep theory concepts and accounts more accurately for the actual flow over the wing. The present method, when employed in the aerodynamic design and analysis computer codes WINGDES and AERO2S, provides results that generally give improved correlation with experimental wing-body axial-force data and reasonable estimates of the measured drag. Application of the present method for sharp leading-edge airfoil sections is simplified because the uncertainty concerning selection of an appropriate leading-edge radius to replace the nominal value of zero no longer exists. The present method can be expected to be most accurate for wings with standard airfoil sections and least accurate for nonstandard sections, particularly thin sections with sharp or nearly sharp leading edges and forward locations of maximum thickness.

Provisions have been made for a simplified recalibration of the empirical part of the present method when experimental two-dimensional airfoil data for a wider range of airfoil shapes or test conditions become available. Particularly, two-dimensional data are needed at high Reynolds numbers and low Mach numbers for low-speed flight conditions of large highly swept wings such as those employed on supersonic transport aircraft.

NASA Langley Research Center
Hampton, VA 23681-0001
November 30, 1995

Appendix A

Strategy for Thrust Factor Data Representation

The process used to collapse the large amount of two-dimensional attainable thrust factor data generated by use of the airfoil computer code to the relatively narrow bands shown in figure 5 is described. In addition, the development of an empirical equation to represent these bands and the dependence of the attainable thrust factor on the Mach number and airfoil geometric characteristic terms used in figure 5 is discussed.

For a given leading-edge radius index and Mach number, the collapse of data for the wide range of airfoil geometries shown in figure 3 is accomplished through use of the theoretical thrust parameter

$$P_{\mathrm{tt}} = c_{t,n}\beta_n \left[\frac{\left(\frac{\tau}{c}\right)_n \left(\frac{\eta}{0.5}\right)}{0.9} \right]^{e_1 - e_2}$$

and the attainable thrust parameter

$$P_{\mathrm{at}} = \frac{K_t}{1 + \left(\frac{\tau}{c}\right)_n^{1.2}}$$

Values of the exponents e_1 and e_2 are different for each radius index. The nominal value for the maximum thickness ratio is 0.09, and the nominal value for the location of maximum thickness is 0.5. The selected parameters collapse data for other thicknesses and locations of maximum thickness on the data band defined by the nominal values.

The attainable thrust parameter contains a section thickness term because the integrated attainable thrust coefficients given by the two-dimensional airfoil computer code show an almost linear increase with increasing thickness. Attainable thrust coefficients with no limiting (obtained from the $M_n = 0$ data, $C_{p,\mathrm{lim}} = -\infty$) give the maximum values. In sketch N, the maximum thrust factor K_t is shown as a function of the section thickness. The data in the sketch cover radius indices $r_{i,n} = 0$, 0.15, 0.30, 0.60, and 1.20, as well as locations of maximum thickness η of 0.1, 0.3, and 0.5. Most of the data cluster near a line given as maximum $K_t = 1 + (\tau/c)_n^{1.2}$. This line is defined primarily by the data for a standard leading-edge radius $r_{i,n} = 0.3$ and for a nominal value of the location of maximum thickness, $\eta = 0.5$. The data showing the greatest departure from this line are for the sharp leading edge $r_{i,n} = 0$ and the most forward location of maximum thickness $\eta = 0.1$. Because of the discrepancy shown here, and others noted

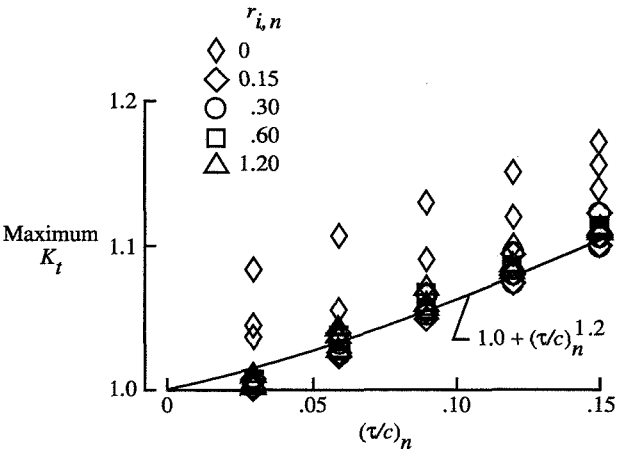

Sketch N

elsewhere in this paper, the attainable thrust prediction method is least accurate for airfoils with sharp leading edges and forward locations of maximum thickness. The attainable thrust parameter definition used here aids in the collapse of data for the range of section thickness from 0.03 to 0.15.

A sample of the strategy used to accomplish the reduction of the data to narrow bands is explained with the aid of sketches O and P. Here the object was to superimpose data for other thickness ratios on data for the nominal value of 0.09. Sketch O shows two-dimensional airfoil computer code results at a Mach number of 0.5 for an airfoil with a leading-edge radius index of 0.3 (standard) and a maximum thickness location of 0.5. The attainable thrust parameter is shown as a function of the theoretical thrust $c_{t,n}\beta_n$. To simplify the sketch, data are shown for only three thickness ratios.

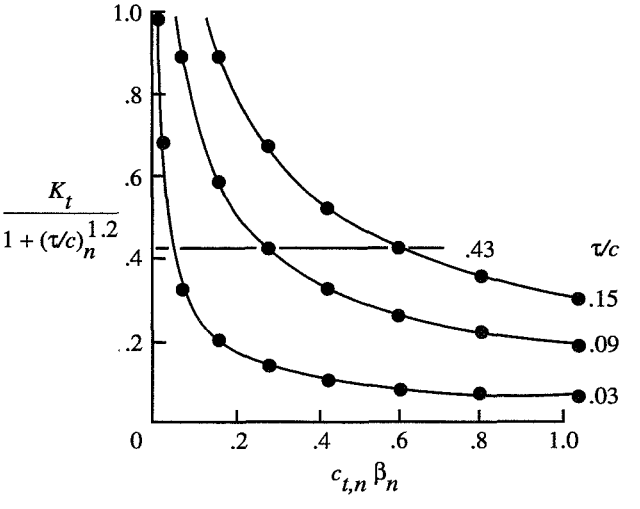

Sketch O

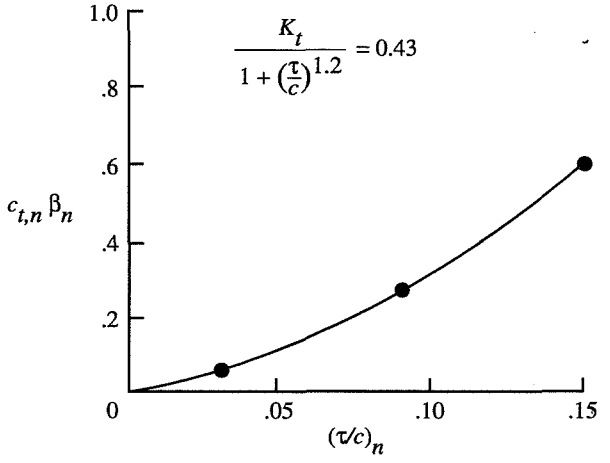

Sketch P

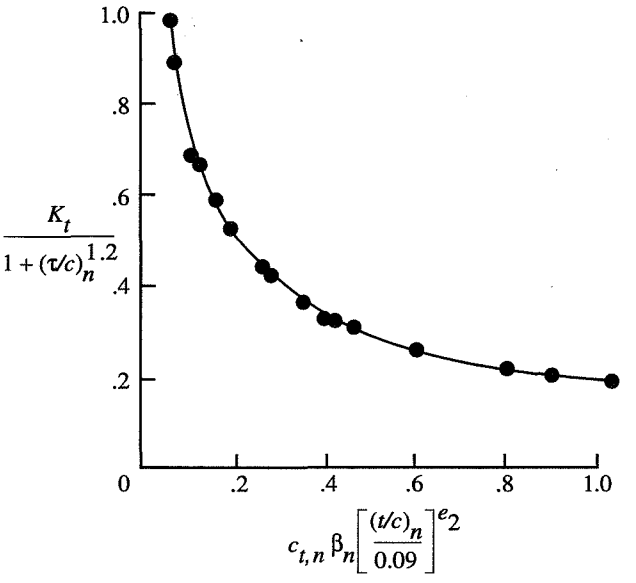

Sketch Q

The purpose of the exercise is to find an exponent e_2 for the theoretical thrust parameter that superimposes the data for thicknesses other than 0.09 on the 0.09 curve. The form of the transformation is taken to be

$$(c_{t,n}\beta_n)_{\left(\frac{\tau}{c}\right)_n}\left[\frac{\left(\frac{\tau}{c}\right)_n}{0.09}\right]^{e_2} = (c_{t,n}\beta_n)_{\left(\frac{\tau}{c}\right)_n=0.9}$$

so that

$$e_2 = \frac{\log(c_{t,n}\beta_n)_{\left(\frac{\tau}{c}\right)_n=0.09} - \log(c_{t,n}\beta_n)_{\left(\frac{\tau}{c}\right)_n}}{\log\left[\frac{\left(\frac{\tau}{c}\right)_n}{0.09}\right]}$$

The exponent e_2 is found from an examination of cross-plotted data such as that displayed in sketch P. Emphasis is placed on attainable thrust parameters in the middle of the range. For the example shown in sketch O, a thrust factor of 0.43 was chosen. For $(\tau/c)_n = 0.03$, the corresponding $c_{t,n}\beta_n$ is approximately 0.048, which requires an exponent of -1.57 to provide superposition. For $(\tau/c)_n = 0.15$, the corresponding $c_{t,n}\beta_n$ is approximately 0.60, which requires an exponent of -1.55. The selected exponent is taken as an average from a number of such evaluations for other thickness ratios and a range of thrust factors. When the chosen value of $e_2 = -1.60$ is used, the separate curves of sketch O are reduced to essentially the single curve shown in sketch Q.

A similar process was used to collapse the data for the other locations of maximum thickness onto the $\eta = 0.5$ curves. The collapsing process for maximum thickness and location of maximum thickness in combination resulted in the data organization shown in figure 5. For a given radius index and Mach number, data for a range of thickness and a range of maximum thickness location now have only a small amount of scatter about values for the nominal thickness $(\tau/c)_n = 0.09$ and the nominal maximum thickness location $\eta = 0.5$. An ideal solution for this collapsing process would also provide for superposition of the data for other Mach numbers on the $M_n = 0.5$ data in each of the plots in figure 5 and, in addition, would allow all data for the different radius indices to be superimposed on the $r_{i,n} = 0.3$ data. Such a solution could not be found. Instead, a means of devising a single equation to provide a curve fit of the data in figure 5 was employed.

The problem of relating the attainable thrust parameter to changes in Mach number and leading-edge radius as shown in figure 5 was handled by application of an equation of the form

$$P_{at} = k(P_{tt})^{e_3}$$

to the data bands through selection of the constant k and the exponent e_3. When two points on the desired curve are specified, the exponent e_3 may be determined from the expression

$$e_3 = \frac{\log(P_{at})_1 - \log(P_{at})_2}{\log(P_{tt})_1 - \log(P_{tt})_2}$$

The two points were chosen to represent the curve in the region of greatest interest, generally, near the P_{at}

midrange. For example, with $r_{i,n} = 0.3$ (fig. 5(c)), the curve for $M_n = 0.5$ is plotted to pass through the points

$$[(P_{at})_1 = 0.60, (P_{tt})_1 = 0.15]$$

and

$$[(P_{at})_2 = 0.30, (P_{tt})_2 = 0.48]$$

to give an exponent $e_3 \approx -0.60$ and a constant $k \approx 0.20$. The exponent was found to have little dependence on the Mach number. Therefore, although k depends on both the Mach number M_n and the radius index $r_{i,n}$, e_3 depends only on the radius index.

When the preceding process was carried out for each of the five Mach numbers for each of the five leading-edge radius indices, the following equations provided a reasonable representation of the constant and exponents:

$$k = \left\{0.14[1.0 - (1.0 - \sqrt{r_{i,n}})M_n^5] + 0.11\sqrt{r_{i,n}}\right\} \times \left(\frac{1 - M_n}{M_n}\right)^{0.48(1+r_{i,n}^{0.3})}$$

$$e_1 = 0.4r_{i,n}^{0.16} - 0.7$$

$$e_2 = 1.6r_{i,n}^{0.10} - 3.0$$

$$e_3 = -0.32r_{i,n}^{0.10} - 0.3$$

The faired curves shown in figure 5 were defined by use of these constants and exponents in equation (1).

Appendix B

Navier-Stokes Solutions for Two-Dimensional Airfoils

An essential part of the attainable thrust prediction method is the determination of effective limiting pressure coefficients and their dependence on local Mach number and Reynolds number. As described previously, this is accomplished through the use of wind tunnel data for two-dimensional airfoil sections. However, recognize that wind tunnel test results are subject to some limitations. The results are dependent on the precision of the measuring devices, on model accuracy (including surface smoothness), and on wind tunnel flow quality, which can vary from test to test and from facility to facility. Furthermore, and perhaps more importantly, the information provided by currently available data does not cover a matrix of test conditions (Mach number and Reynolds number) as broad ranged and as closely spaced as desired. In particular, some uncertainty exists with regard to the dependence of limiting pressures on Mach number for low Reynolds numbers. Also, a broader range of Reynolds numbers is required to provide a more confident extrapolation to flight conditions.

To address some of these concerns, an exploratory investigation of the use of a Navier-Stokes equation-solving computer code to provide a substitute for experimental data was performed. First, to validate the computer code for application to this problem, computer code solutions were compared with representative experimental data. Then, computer code results were used to provide some limited samples of the use of Navier-Stokes solutions to supplement or replace experimental data.

The Navier-Stokes computer code CFL3D employed in this study is described in reference 19. The governing equations used in the two-dimensional version of this computer code are the two-dimensional, Reynolds-number-averaged Navier-Stokes equations written in conservative form and expressed in a body-fitted coordinate system. These equations are solved by an implicit, finite-volume, upwind spatially factored algorithm. More information about this computational method and its accuracy is contained in reference 19. Turbulent viscosity was simulated with the transport equation of Spalart-Allmaras. (See ref. 25.)

A 2-D grid was constructed for each of the following airfoils: NACA 0006, NACA 0009, NACA 0012, NACA 64-010 with 257 and 81 grid points in the streamwise and normal directions, respectively. Each grid was sufficiently clustered normal to the body surface to resolve the viscous boundary layer. The grids were also clustered at the airfoil nose and trailing edge.

Computations were performed on the CRAY-2S at NASA Langley Research Center with the use of multiblock iteration to accelerate convergence. A converged solution for a typical case was obtained after approximately 1500 iterations.

Sample comparisons of Navier-Stokes computer code results with wind tunnel experimental data are shown in figure B1. In general, these comparisons demonstrate the capability of the Navier-Stokes method to predict the flow characteristics and forces for two-dimensional airfoils over a range of free-stream conditions. As with any computational analysis, the method used in this study is subject to some limitations and uncertainties. The solution is limited by the numerical accuracy of the computer code; CFL3D is accurate in time to the second order and in space to the third order. Discretization of the geometry results in loss of resolution, which can further affect solution accuracy. Proper modeling of turbulent flow presents another potential problem. The transition point of the boundary layer from laminar to turbulent is not known, and how well the Spalart-Allmaras turbulence model performs in regions of separated flow is uncertain.

On completion of the limited verification exercise, the Navier-Stokes computer code was used to provide supplementary information to better define the complicated dependence of $C_{p,\lim}$ on Mach number at low speeds. For this purpose the NACA 0009 airfoil was evaluated for Mach numbers of 0.05, 0.10, 0.16, 0.20, 0.30, and 0.50 at a Reynolds number of 9×10^6. The limiting pressure for the computer code data was defined by use of the same iteration process that was applied to the wind tunnel data. An example of a plot that was used is shown in sketch R. A curve generated by use of these

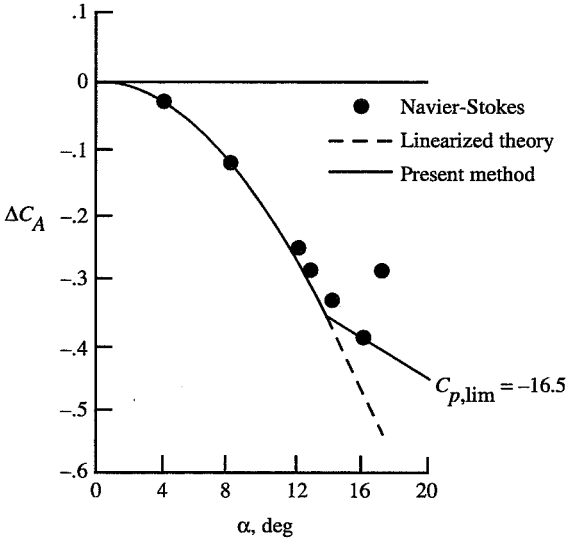

Sketch R

data is superimposed on the plot in figure 7(d), which presents data for wind tunnel test results at the same Reynolds number.

Navier-Stokes results were also used to provide supplementary information on the dependence of the limiting pressure on Reynolds number. For this purpose the NACA 0009 airfoil was evaluated for additional Reynolds numbers of 1×10^6, 100×10^6, and 1000×10^6 at a Mach number of 0.16. Limiting pressure coefficients obtained from these data are shown in sketch K.

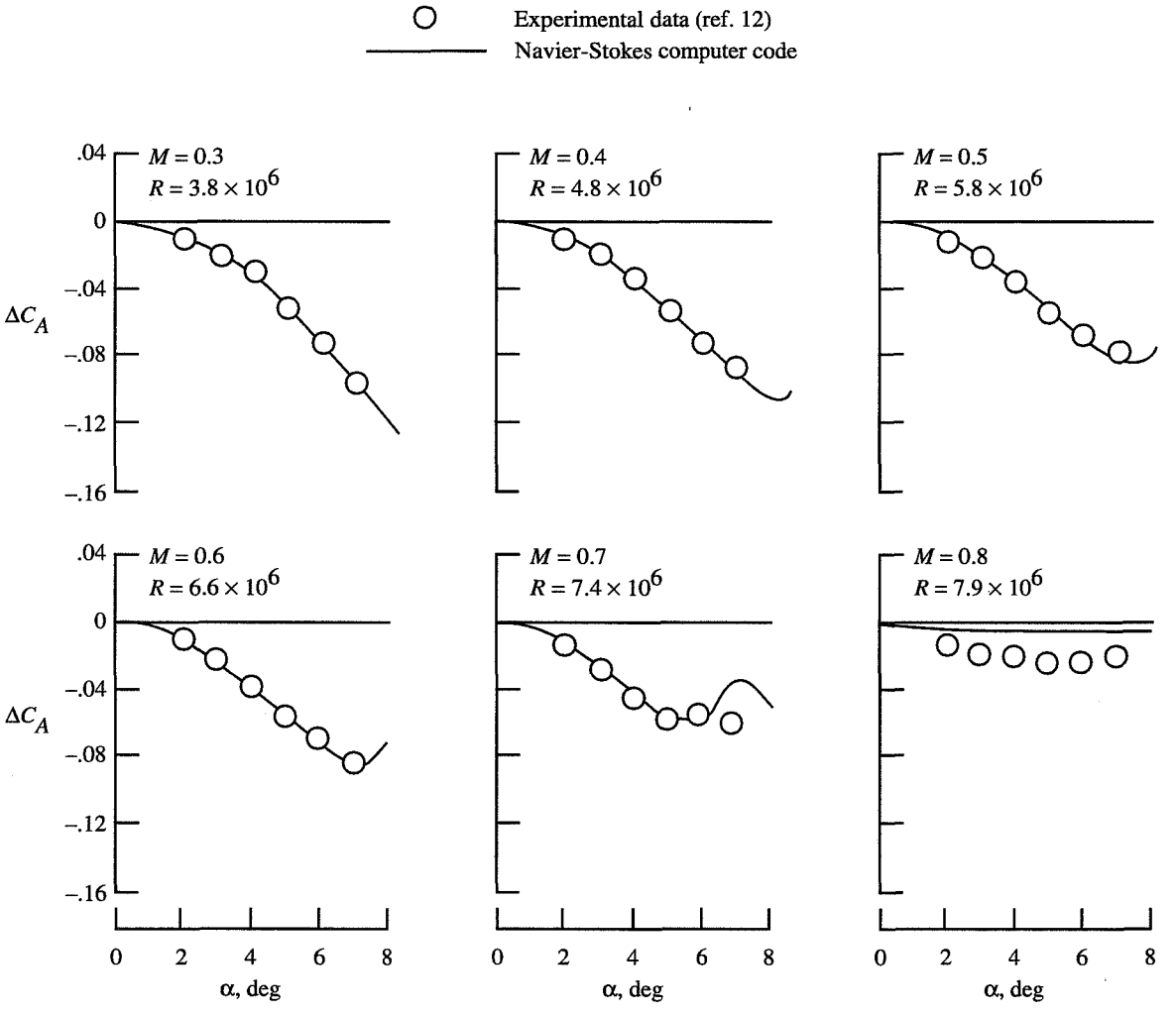

(a) NACA 64-010 airfoil.

Figure B1. Experimental and Navier-Stokes computer code (CFL3D) data for two-dimensional airfoils.

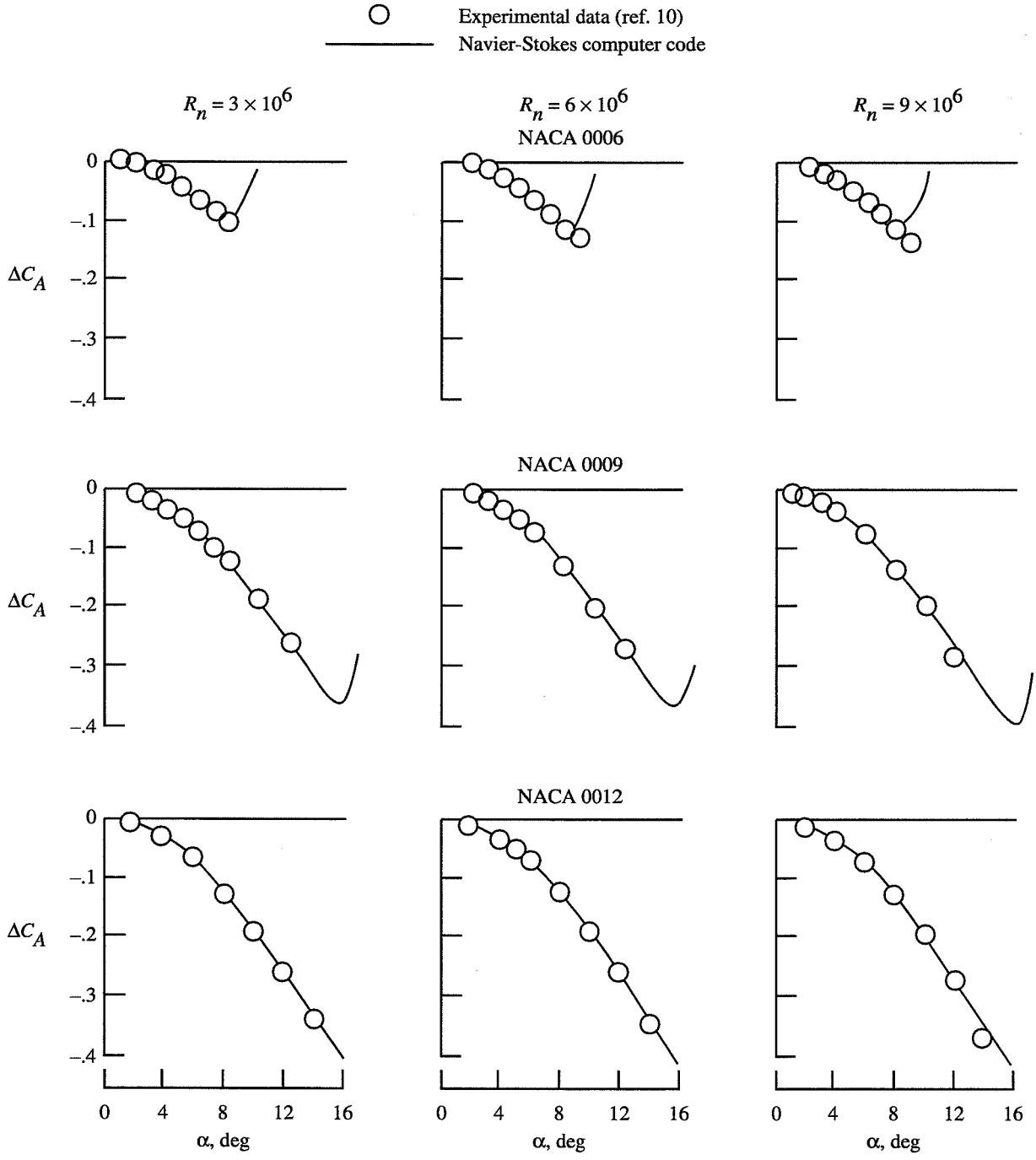

(b) NACA 0006, NACA 0009, and NACA 0012 airfoils; $M = 0.16$.

Figure B1. Concluded.

References

1. Carlson, Harry W.; Mack, Robert J.; and Barger, Raymond L.: *Estimation of Attainable Leading-Edge Thrust for Wings at Subsonic and Supersonic Speeds.* NASA TP-1500, 1979.

2. Carlson, Harry W.; and Walkley, Kenneth B.: *A Computer Program for Wing Subsonic Aerodynamic Performance Estimates Including Attainable Thrust and Vortex Lift Effects.* NASA CR-3515, 1982.

3. Carlson, Harry W.; and Walkley, Kenneth B.: *An Aerodynamic Analysis Computer Program and Design Notes for Low Speed Wing Flap Systems.* NASA CR-3675, 1983.

4. Carlson, Harry W.; and Walkley, Kenneth B.: *Numerical Methods and a Computer Program for Subsonic and Supersonic Aerodynamic Design and Analysis of Wings With Attainable Thrust Considerations.* NASA CR-3808, 1984.

5. Carlson, Harry W.; and Darden, Christine M.: *Applicability of Linearized-Theory Attached-Flow Methods to Design and Analysis of Flap Systems at Low Speeds for Thin Swept Wings With Sharp Leading Edges.* NASA TP-2653, 1987.

6. Carlson, Harry W.; and Darden, Christine M.: *Validation of a Pair of Computer Codes for Estimation and Optimization of Subsonic Aerodynamic Performance of Simple Hinged-Flap Systems for Thin Swept Wings.* NASA TP-2828, 1988.

7. Carlson, Harry W.; Darden, Christine M.; and Mann, Michael J.: *Validation of a Computer Code for Analysis of Subsonic Aerodynamic Performance of Wings With Leading- and Trailing-Edge Flaps With a Canard or Horizontal-Tail Surface and an Application to Optimization.* NASA TP-2961, 1990.

8. Carlson, Harry W.; and Mann, Michael J.: *Survey and Analysis of Research on Supersonic Drag-Due-to-Lift Minimization With Recommendations for Wing Design.* NASA TP-3202, 1992.

9. Pinkerton, Robert M.; and Greenberg, Harry: *Aerodynamic Characteristics of a Large Number of Airfoils Tested in the Variable-Density Wind Tunnel.* NACA Rep. 628, 1938.

10. Abbott, Ira H.; and Von Doenhoff, Albert E.: *Theory of Wing Sections.* Dover Publ., Inc., 1959.

11. Stephens, W. A.; Goradia, S. H.; and Braden, J. A.: *Mathematical Model for Two-Dimensional Multi-Component Airfoils in Viscous Flow.* Lockheed-Georgia Co., 1971.

12. Loftin, Laurence K., Jr.: *Aerodynamic Characteristics of the NACA 64-010 and 0010-1.10 40/1.051 Airfoil Sections at Mach Numbers From 0.30 to 0.85 and Reynolds Numbers From* 4.0×10^6 *to* 8.0×10^6. NACA TN 3244, 1954.

13. Daley, Bernard N.; and Dick, Richard S.: *Effect of Thickness, Camber, and Thickness Distribution on Airfoil Characteristics at Mach Numbers up to 1.0.* NACA TN 3607, 1956. (Supersedes NACA RM L52G31a.)

14. McCullough, G. B.: *Effect of Reynolds Number on the Stalling Characteristics and Pressure Distributions of Four Moderately Thin Airfoil Sections.* NACA TN 3524, 1955.

15. Jacobs, Eastman N.; Ward, Kenneth E.; and Pinkerton, Robert M.: *The Characteristics of 78 Related Airfoil Sections From Tests in the Variable-Density Wind Tunnel.* NACA Rep. 460, 1933.

16. Jacobs, Eastman N.; and Sherman, Albert (appendix by Ira H. Abbott): *Airfoil Section Characteristics as Affected by Variations of the Reynolds Number.* NACA Rep. 586, 1937.

17. Loftin, Laurence K., Jr.; and Von Doenhoff, Albert E.: *Exploratory Investigation at High and Low Subsonic Mach Numbers of Two Experimental 6-Percent-Thick Airfoil Sections Designed To Have High Maximum Lift Coefficients.* NACA RM L51F06, 1951.

18. Ladson, Charles L.; and Hill, Acquilla S.: *High Reynolds Number Transonic Tests of an NACA 0012 Airfoil in the Langley 0.3-Meter Transonic Cryogenic Tunnel.* NASA TM-100527, 1987.

19. Thomas, James L.; and Newsome, Richard W.: Navier-Stokes Computations of Lee-Side Flows Over Delta Wings. AIAA-86-1049, May 1986.

20. Nicholas, W. U.; and Naville, G. L.: *An Evaluation of the Relative Merit of Wing-Canard, Wing-Tail, and Tailless Arrangements for Advanced Fighter Applications.* FZA-547, Fort Worth Div., General Dynamics, Apr. 19, 1984.

21. Coe, Paul L., Jr.; Kjelgaard, Scott O.; and Gentry, Garl L., Jr.: *Low-Speed Aerodynamic Characteristics of a Highly Swept, Untwisted, Uncambered Arrow Wing.* NASA TP-2176, 1983.

22. Wood, Richard M.; and Miller, David S.: *Experimental Investigation of Leading-Edge Thrust at Supersonic Speeds.* NASA TP-2204, 1983.

23. Henderson, William P.: *Effects of Wing Leading-Edge Radius and Reynolds Number on Longitudinal Aerodynamic Characteristics of Highly Swept Wing-Body Configurations at Subsonic Speeds.* NASA TN D-8361, 1976.

24. Hall, Charles F.: *Lift, Drag, and Pitching Moment of Low-Aspect-Ratio Wings at Subsonic and Supersonic Speeds.* NACA RM A53A30, 1953.

25. Spalart, P. R.; and Allmaras, S. R.: A One-Equation Turbulence Model for Aerodynamic Flows. AIAA-92-0439, Jan. 1992.

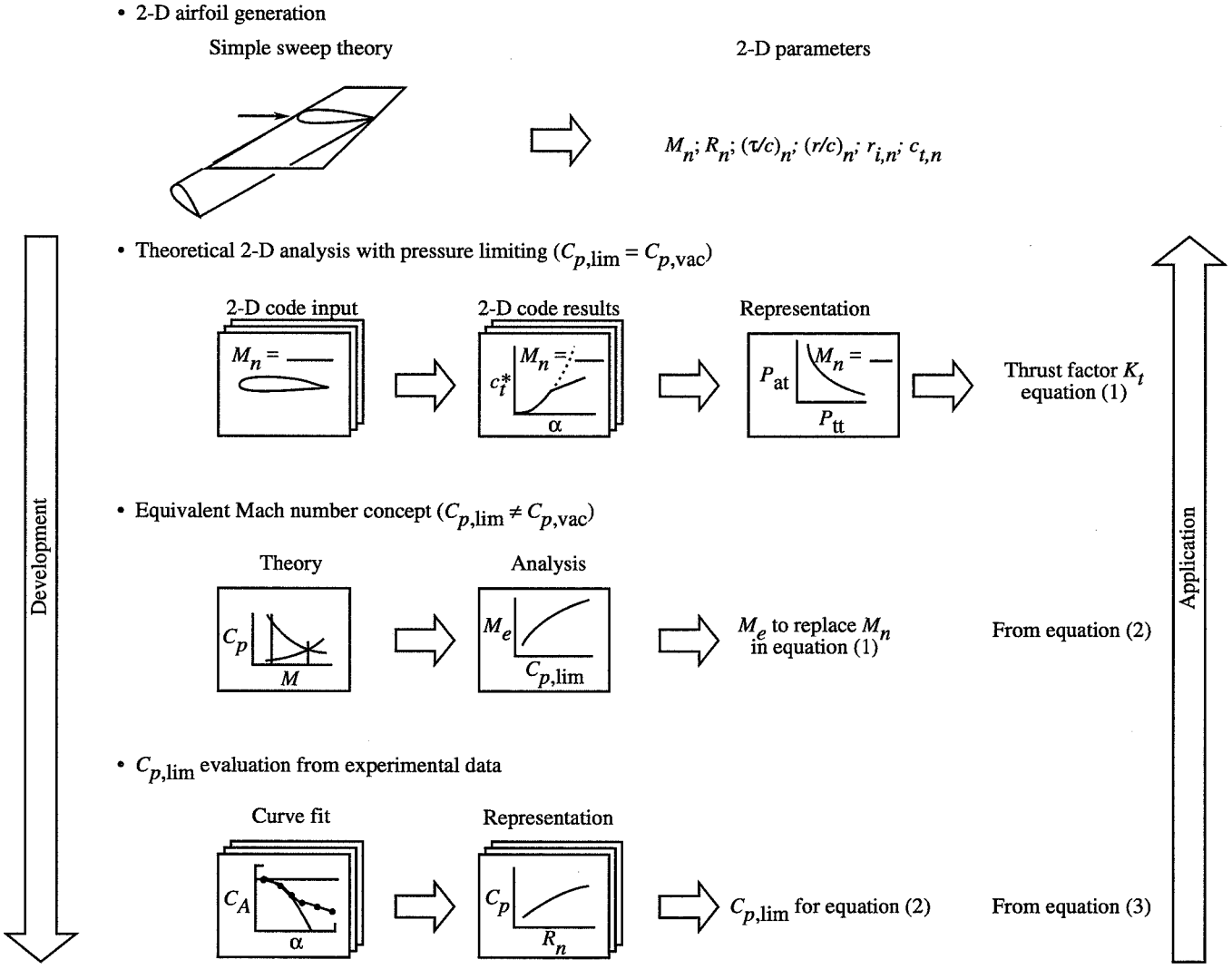

Figure 1. Attainable thrust prediction method development.

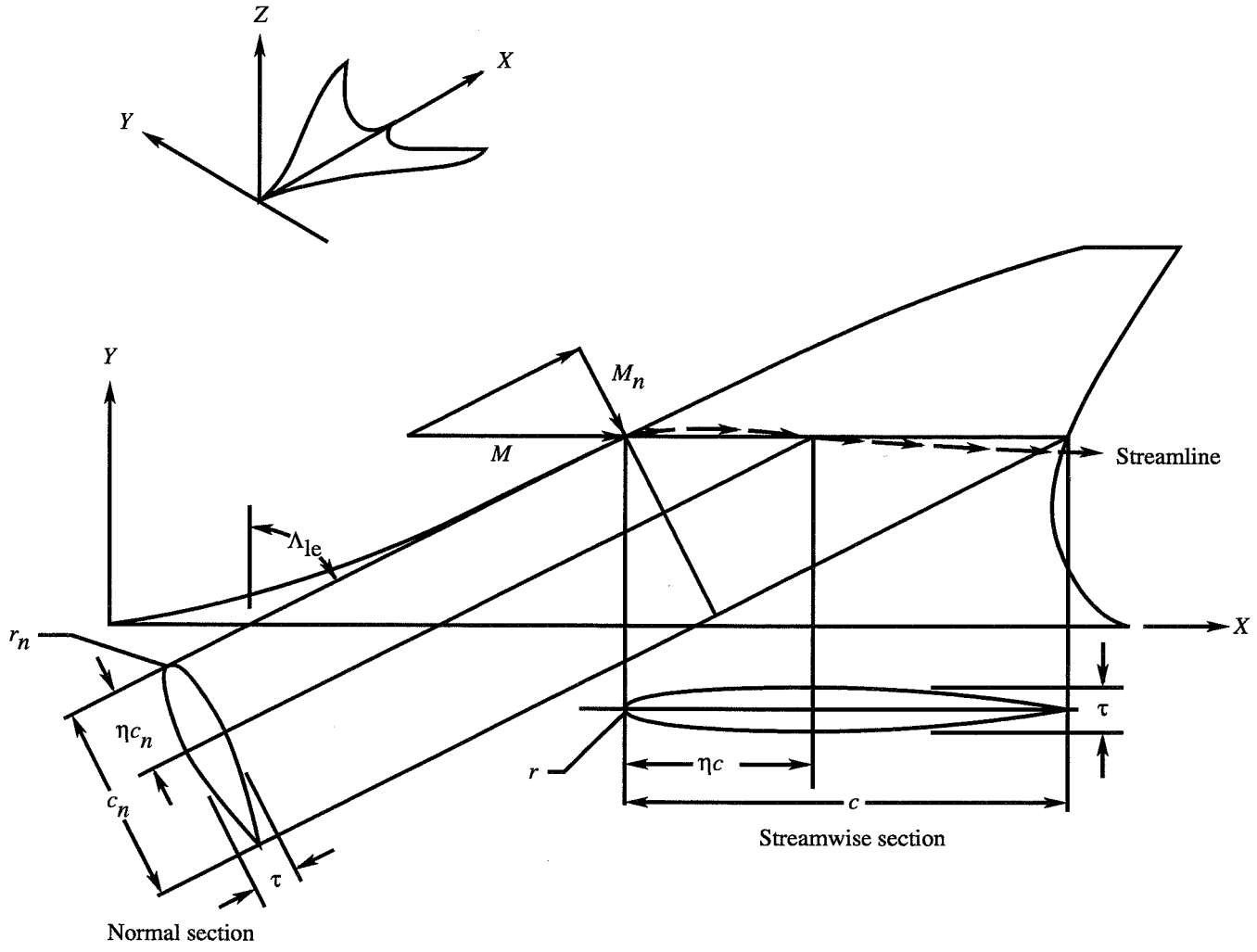

Figure 2. Relationship between streamwise and normal wing sections.

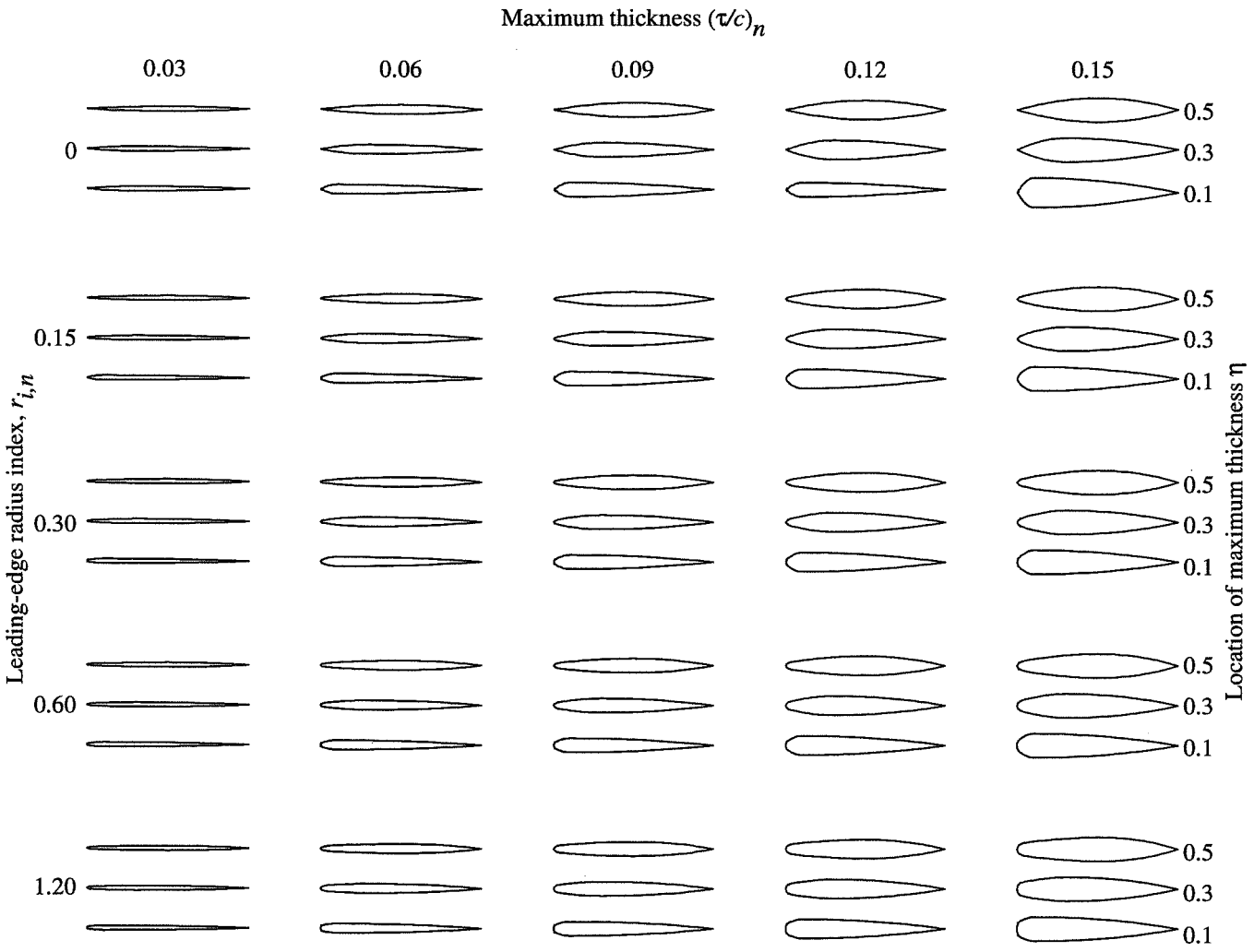

Figure 3. Two-dimensional airfoils used in study.

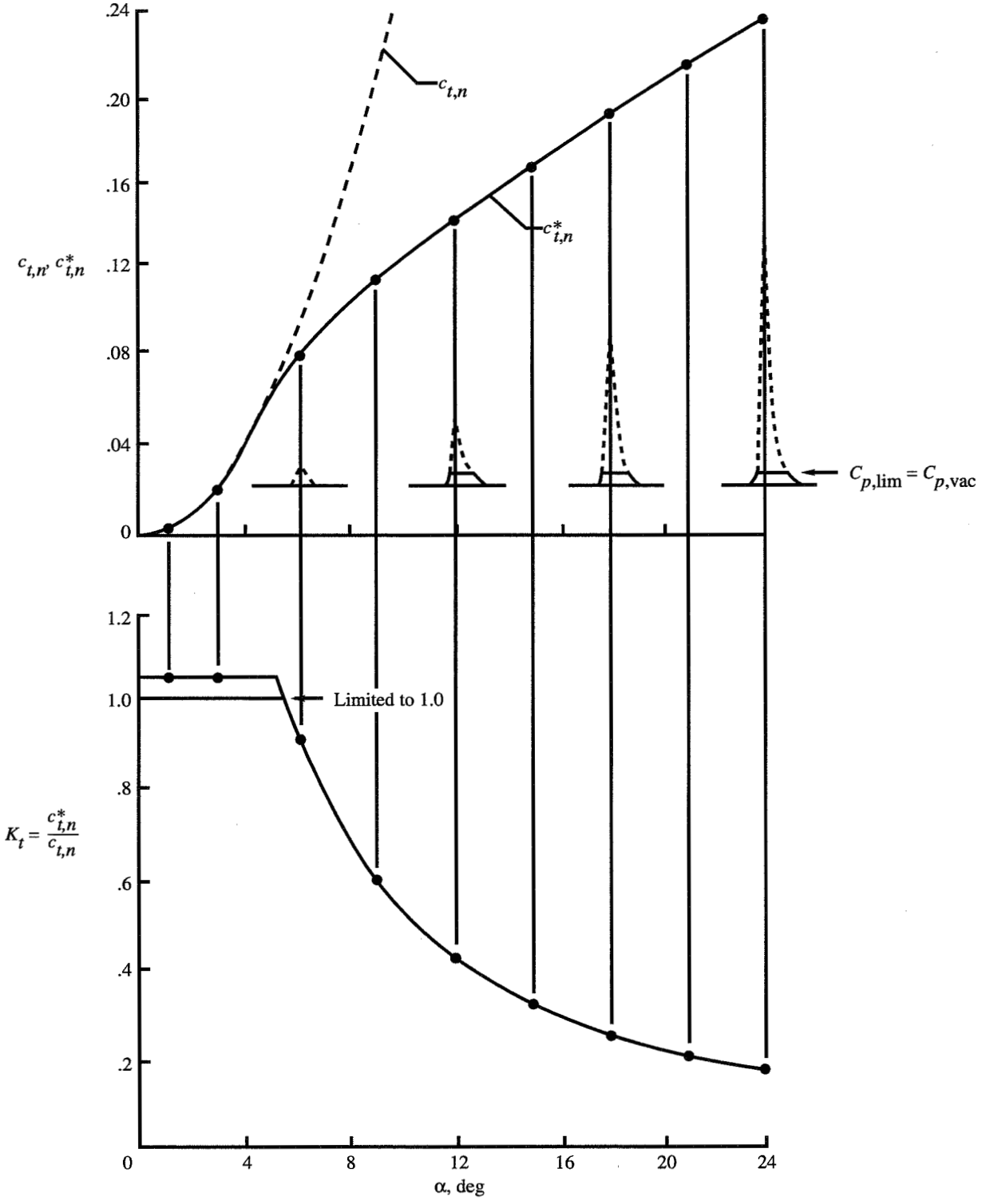

Figure 4. Example of thrust factor variation with angle of attack. $(\tau/c)_n = 0.09$; $\eta_n = 0.5$; $r_{i,n} = 0.3$; $M_n = 0.5$.

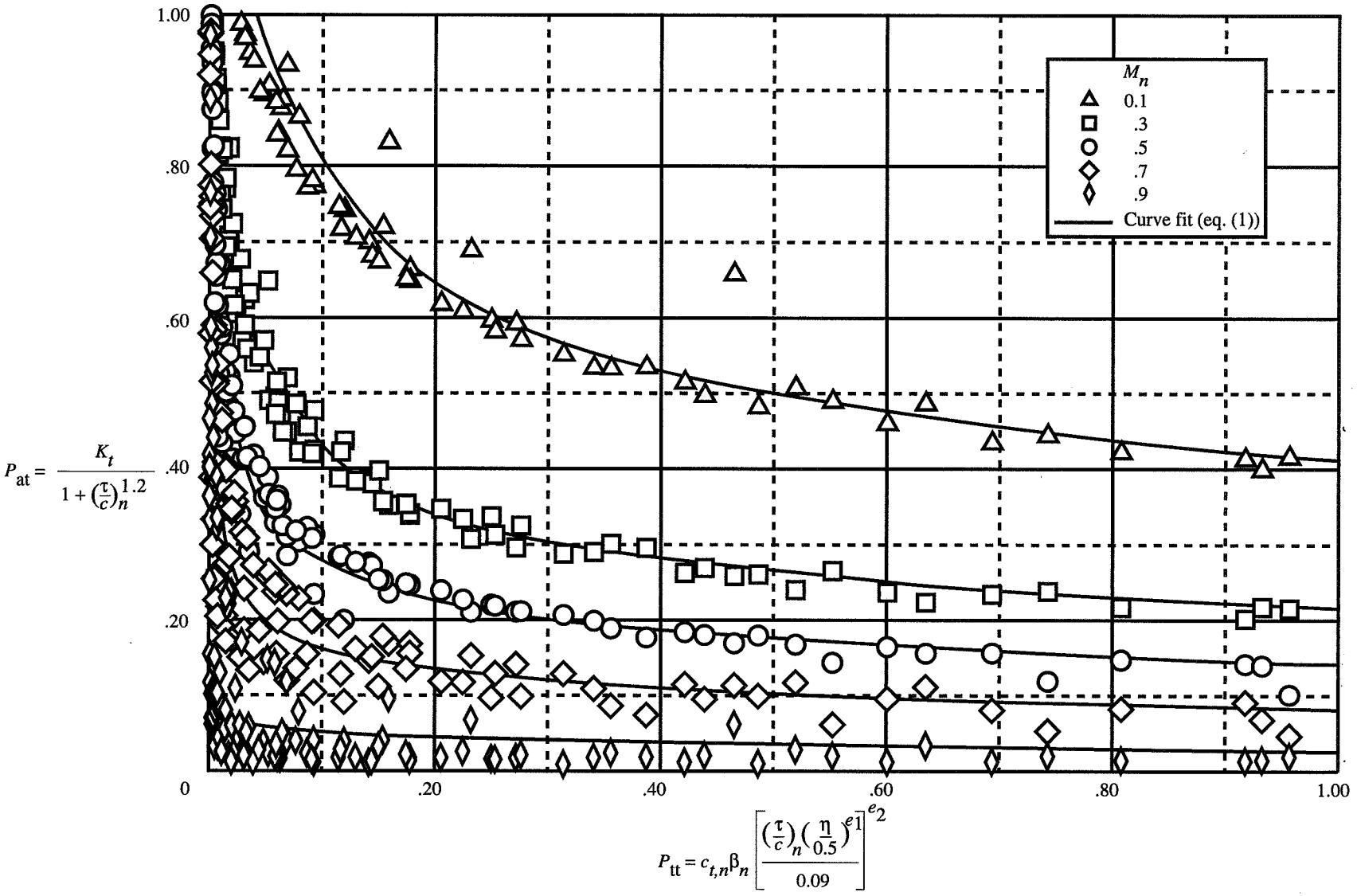

(a) Sharp leading edge; $r_{i,n} = 0$.

Figure 5. Attainable thrust factor.

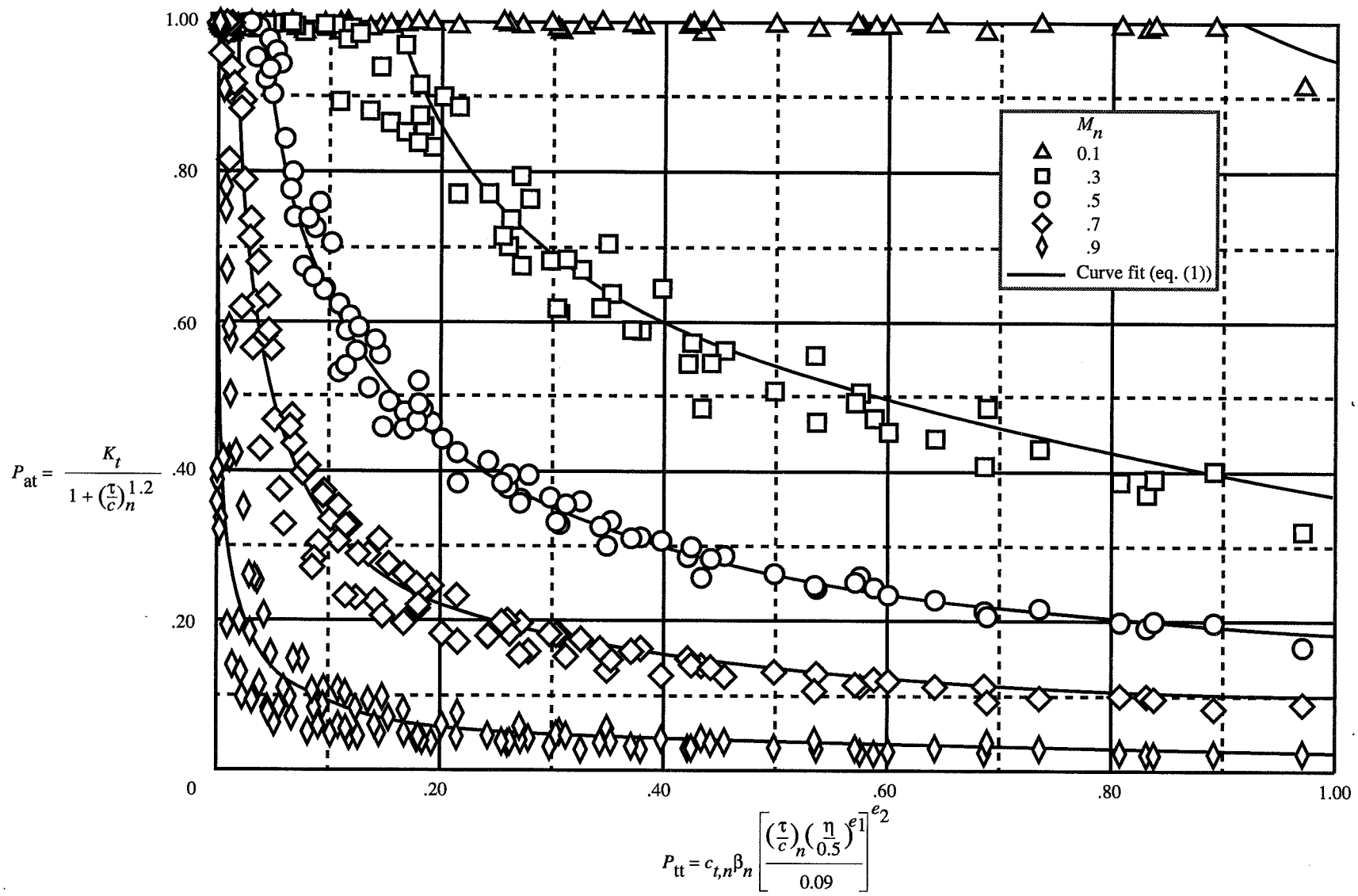

(b) Semisharp leading edge; $r_{i,n} = 0.15$.

Figure 5. Continued.

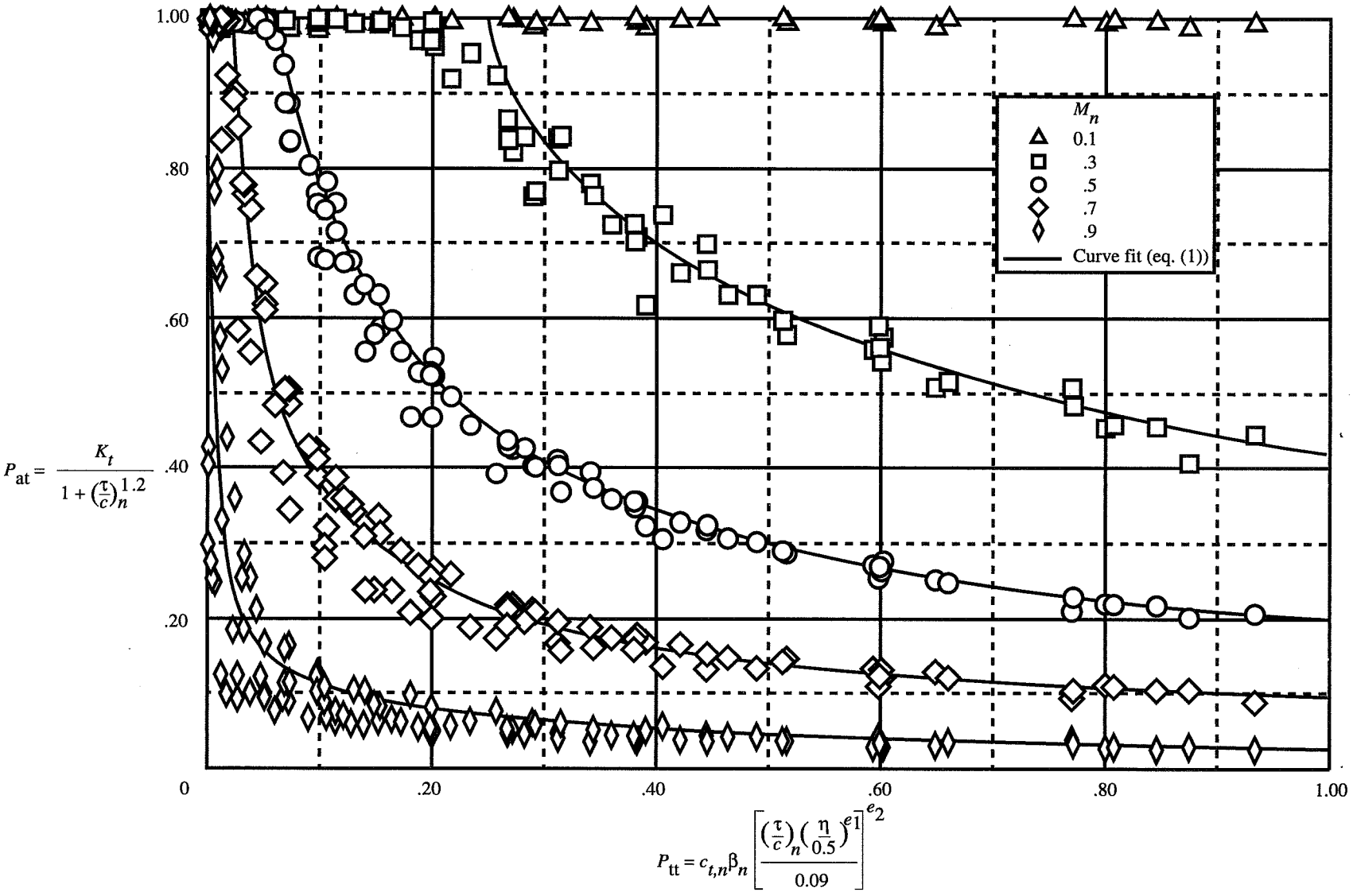

(c) Standard leading edge; $r_{i,n} = 0.3$.

Figure 5. Continued.

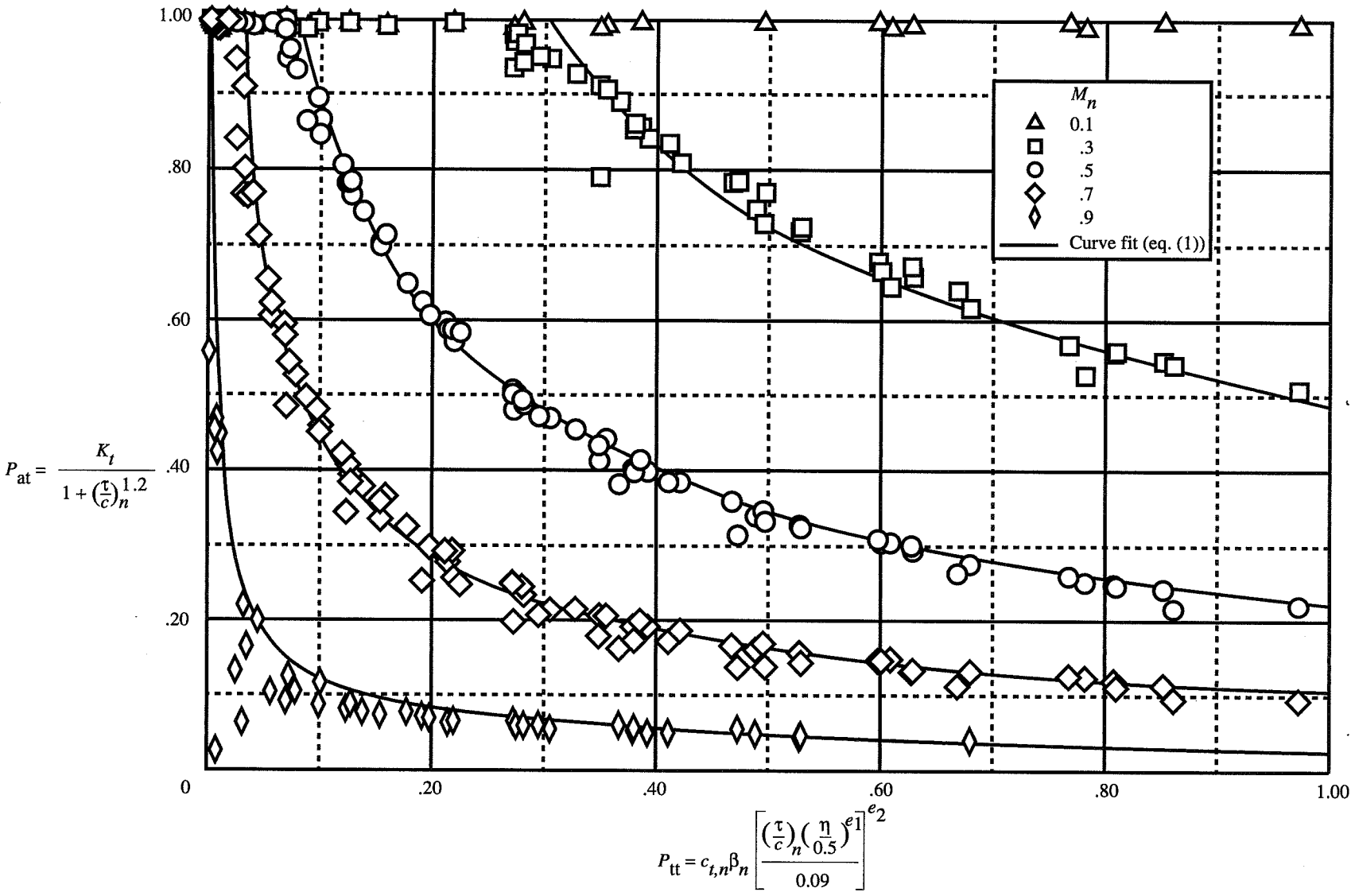

(d) Semiblunt leading edge; $r_{i,n} = 0.6$.

Figure 5. Continued.

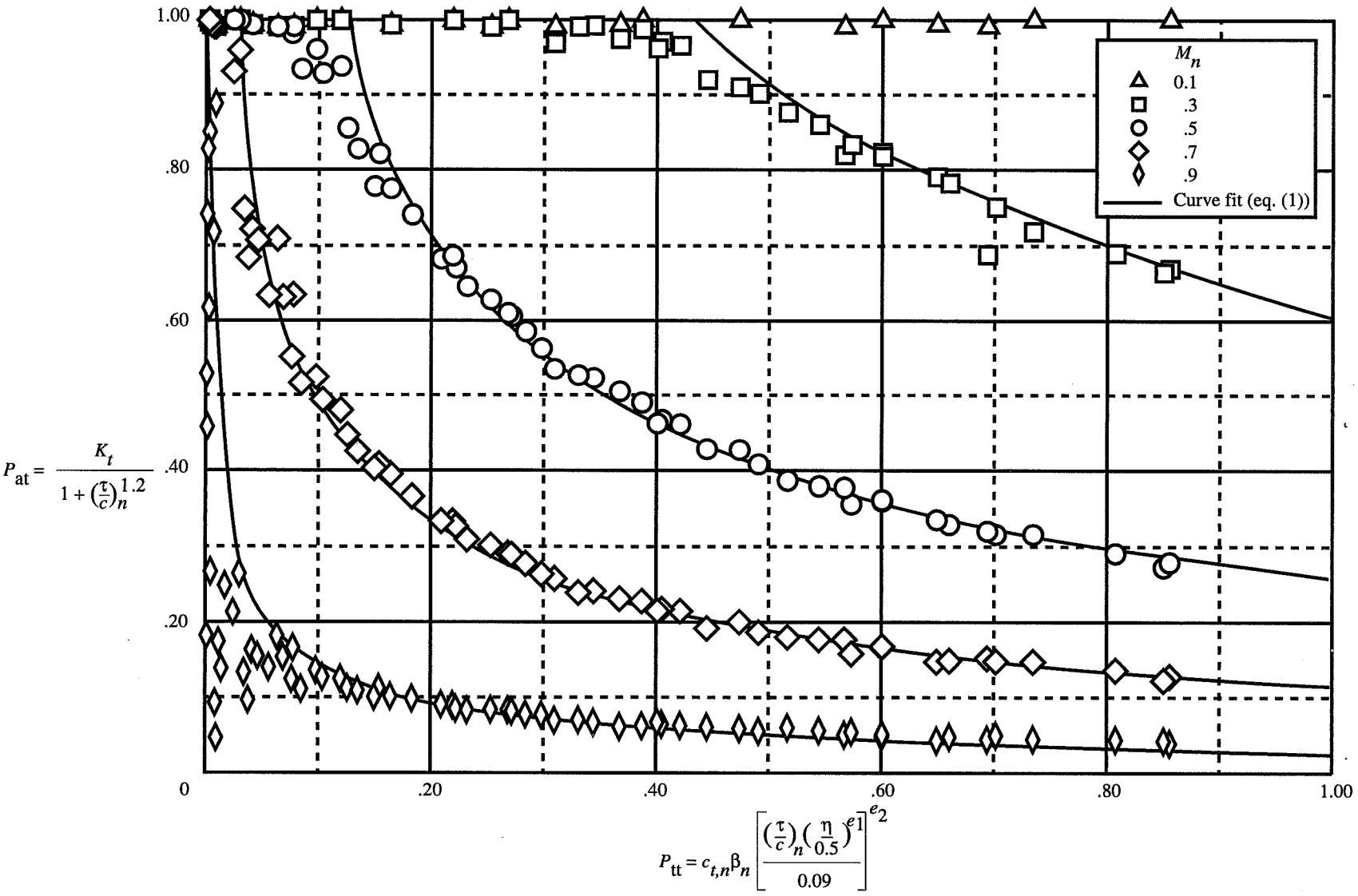

(e) Blunt leading edge; $r_{i,n} = 1.2$.

Figure 5. Concluded.

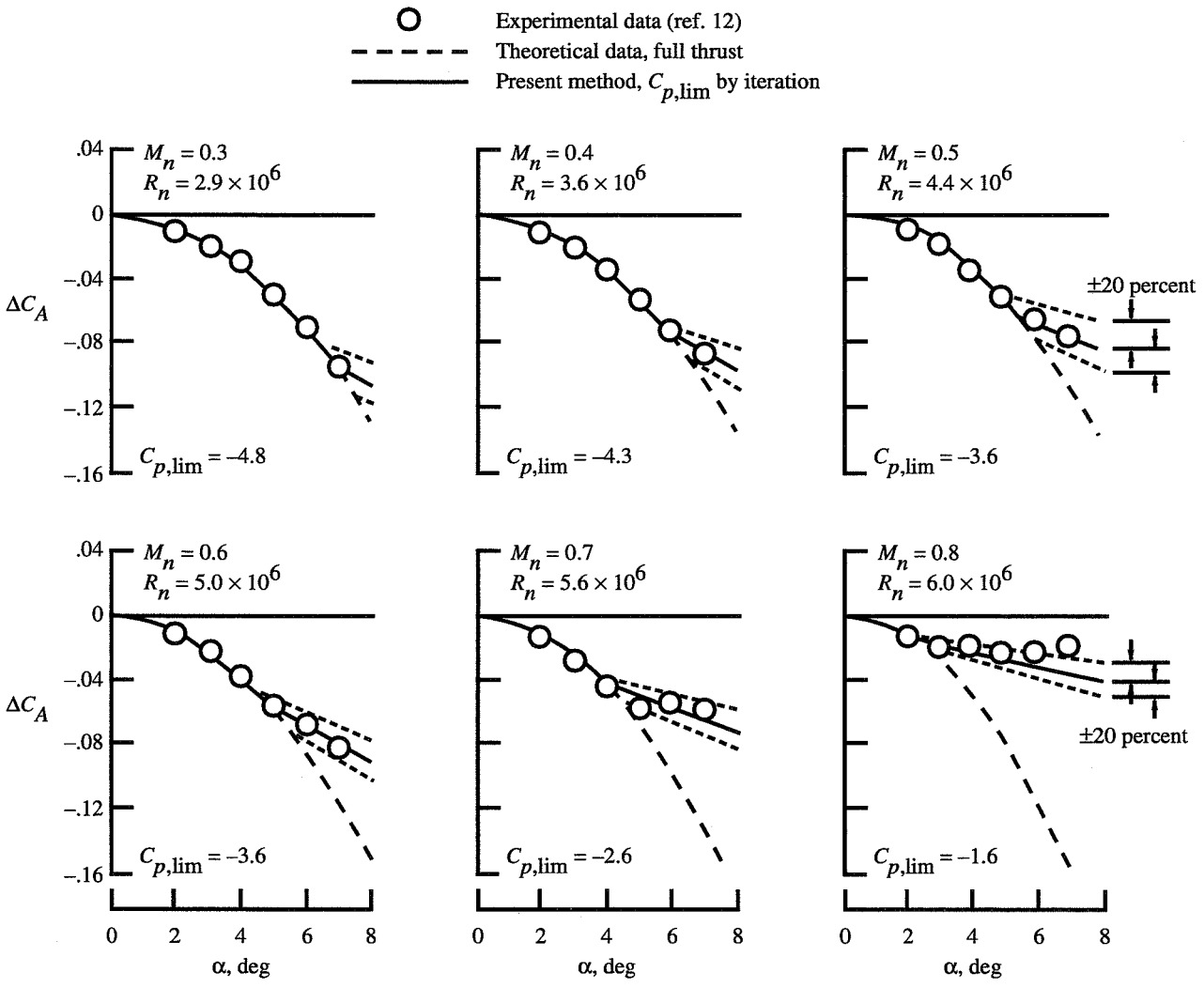

(a) NACA 64-010 airfoil.

Figure 6. Example of two-dimensional experimental data to define limiting pressures.

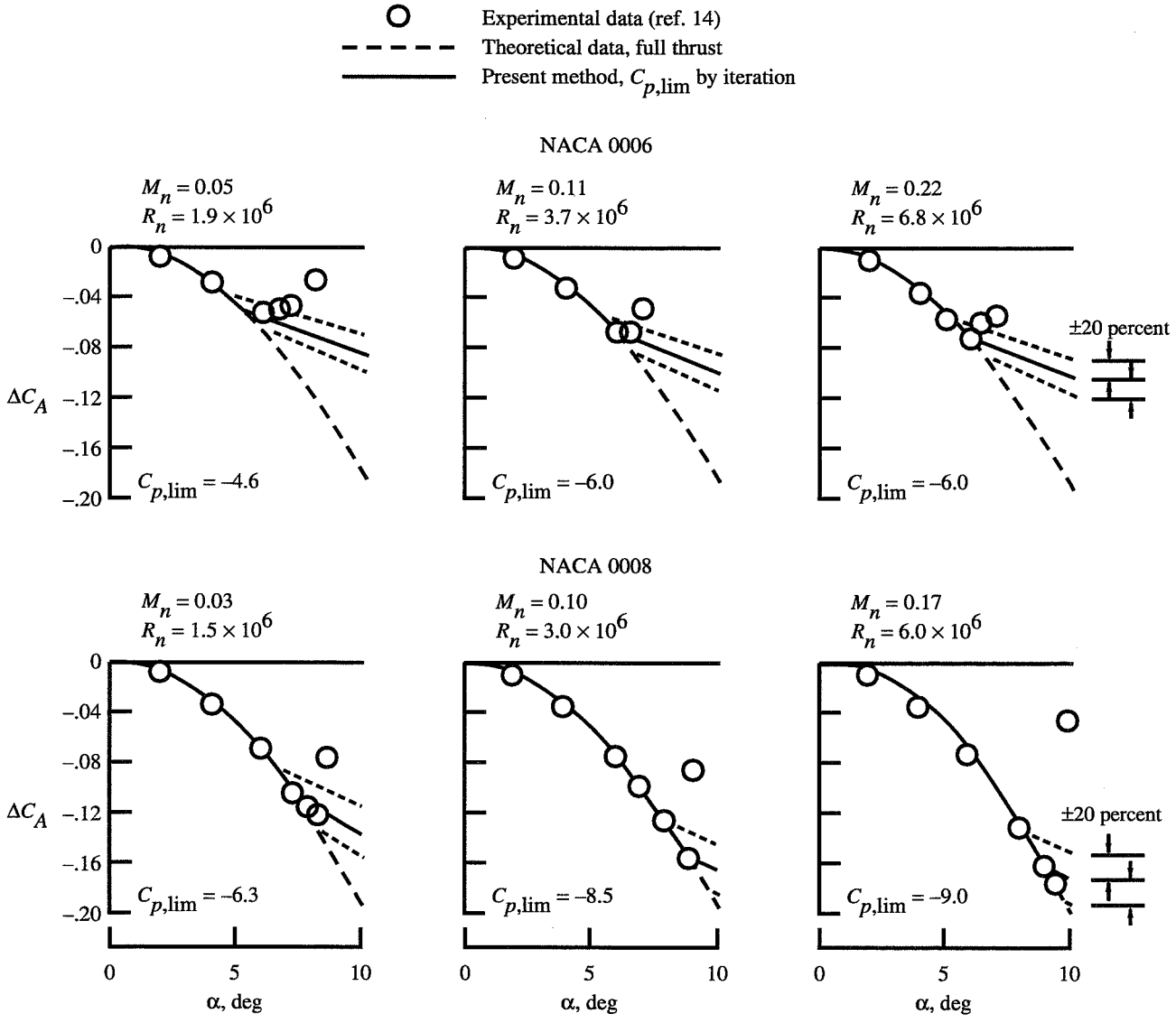

(b) NACA 0006 and NACA 0008 airfoils.

Figure 6. Continued.

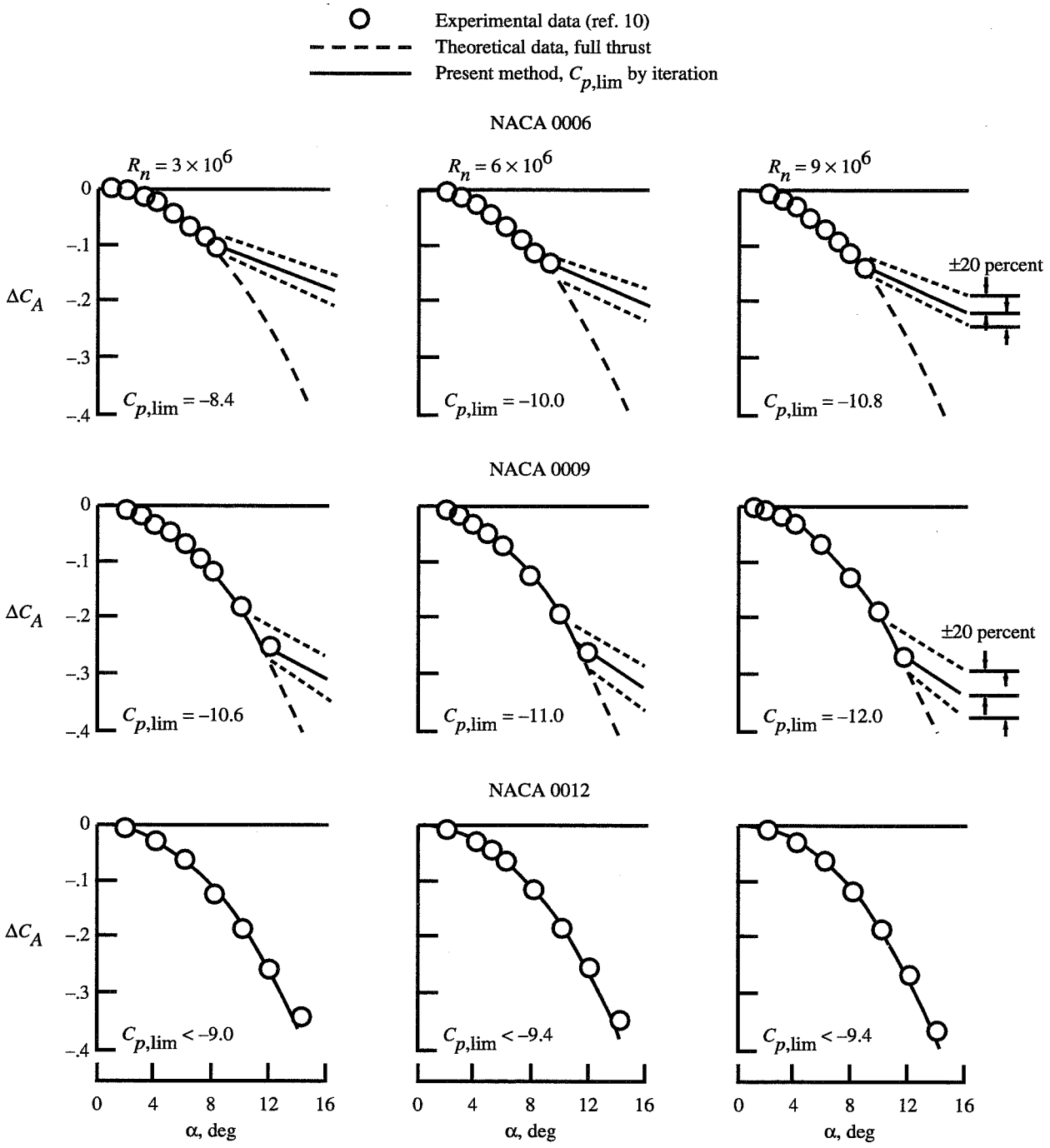

(c) NACA 0006, NACA 0009, and NACA 0012 airfoils; $M = 0.16$.

Figure 6. Concluded.

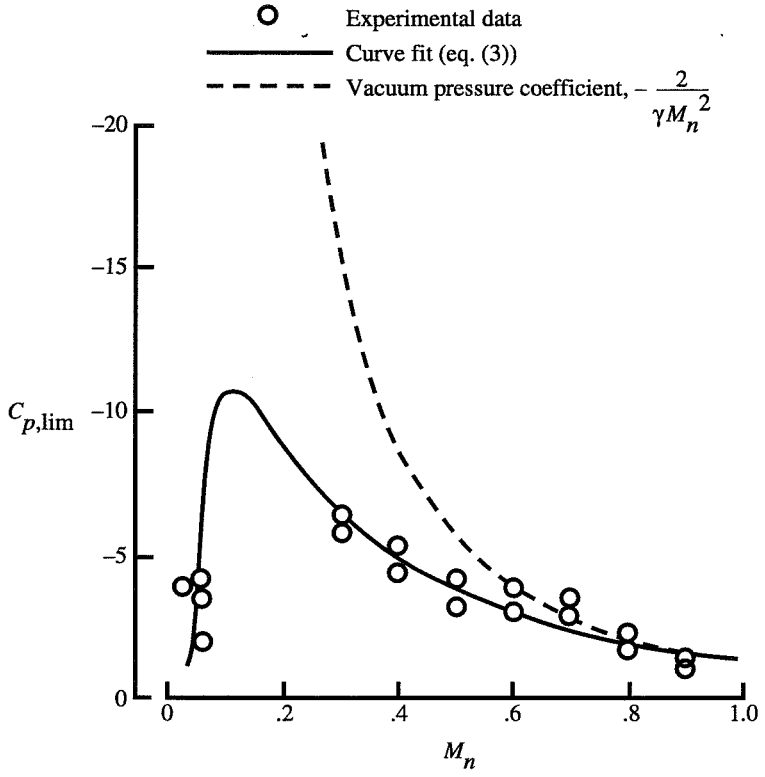

(a) $R_n = 1 \times 10^6$.

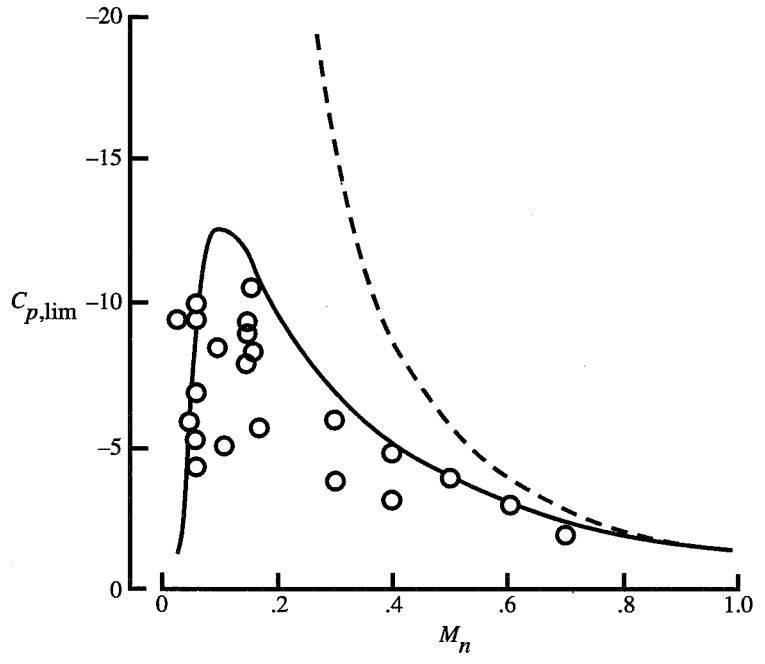

(b) $R_n = 3 \times 10^6$.

Figure 7. Limiting pressure coefficient definition from two-dimensional experimental data.

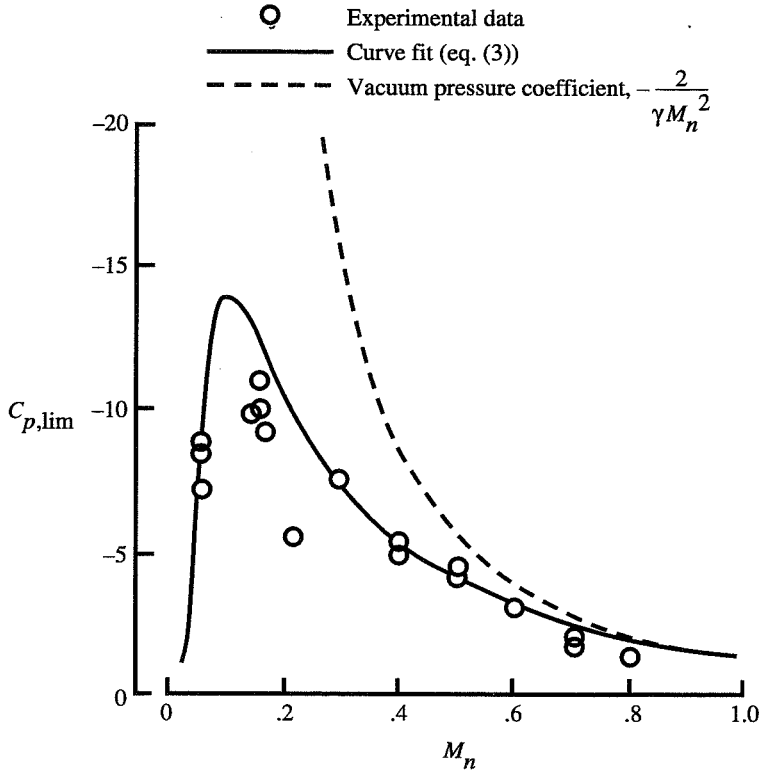

(c) $R_n = 6 \times 10^6$.

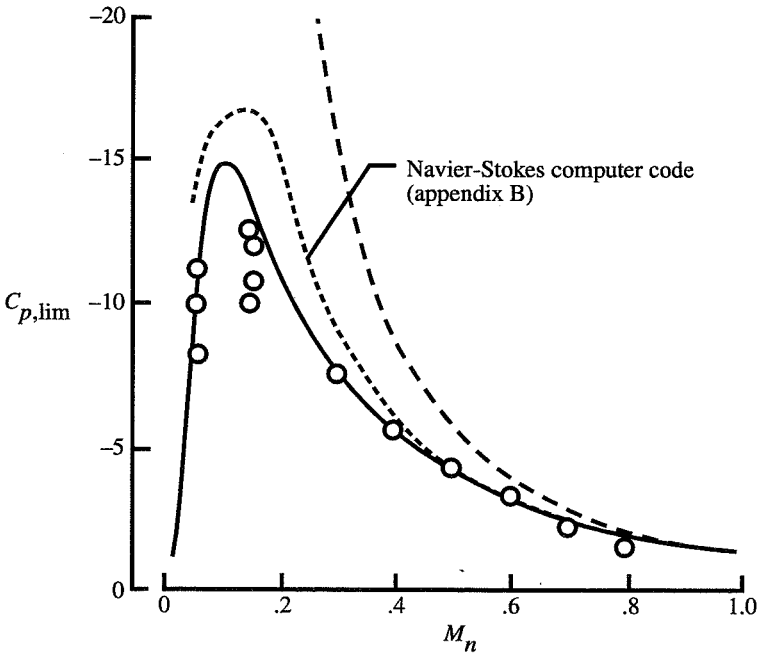

(d) $R_n = 9 \times 10^6$.

Figure 7. Continued.

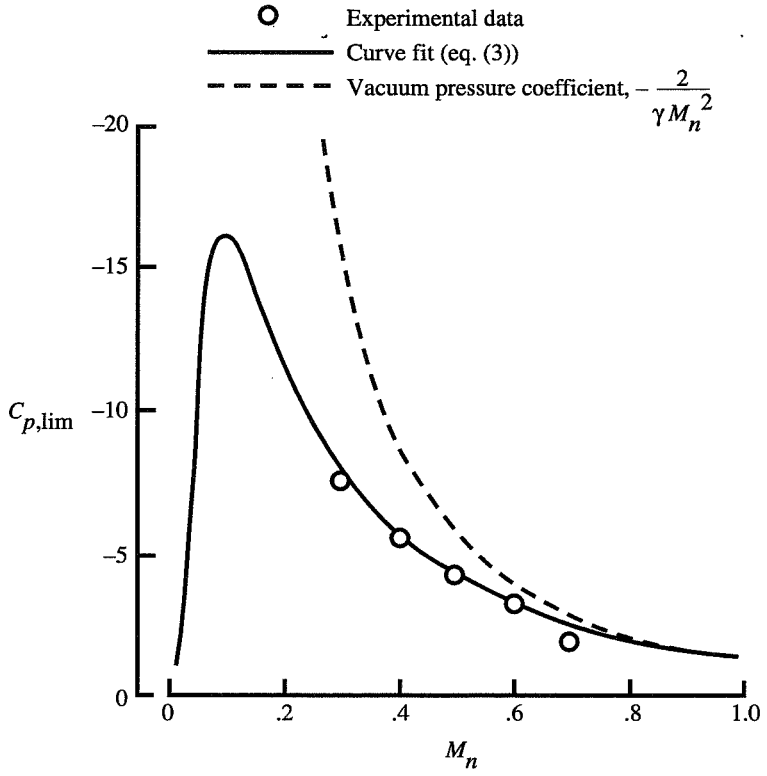

(e) $R_n = 15 \times 10^6$.

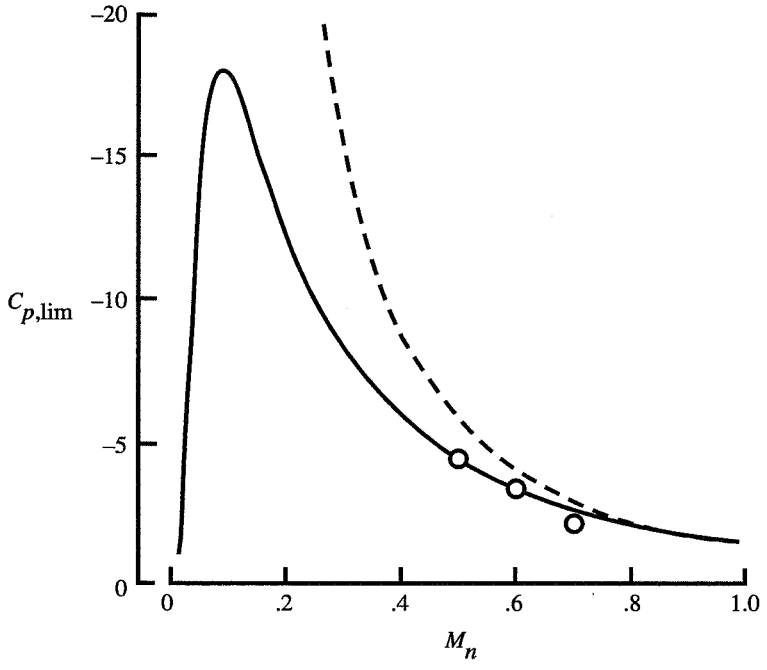

(f) $R_n = 30 \times 10^6$.

Figure 7. Concluded.

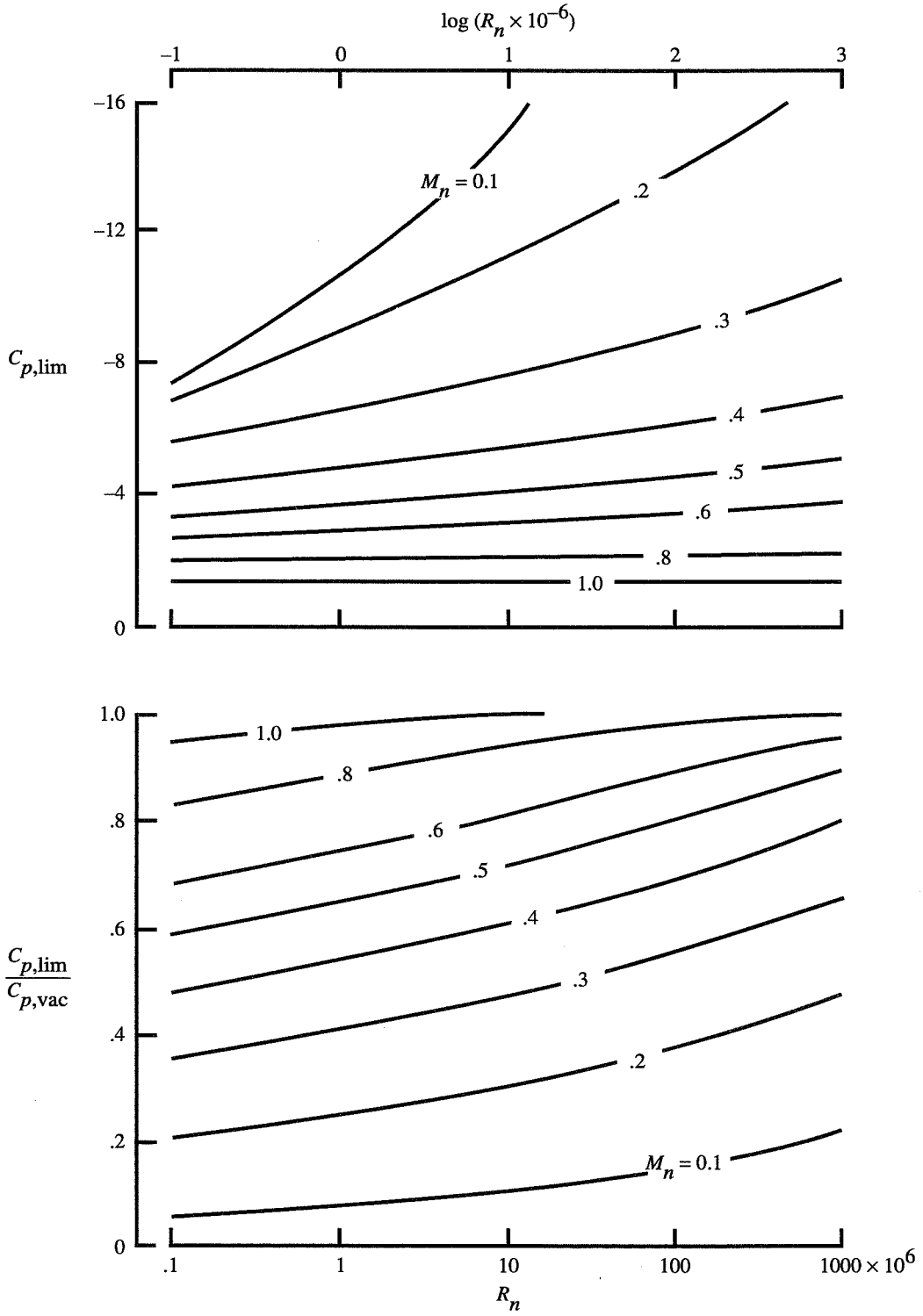

Figure 8. Variation of limiting pressure coefficient with Reynolds number.

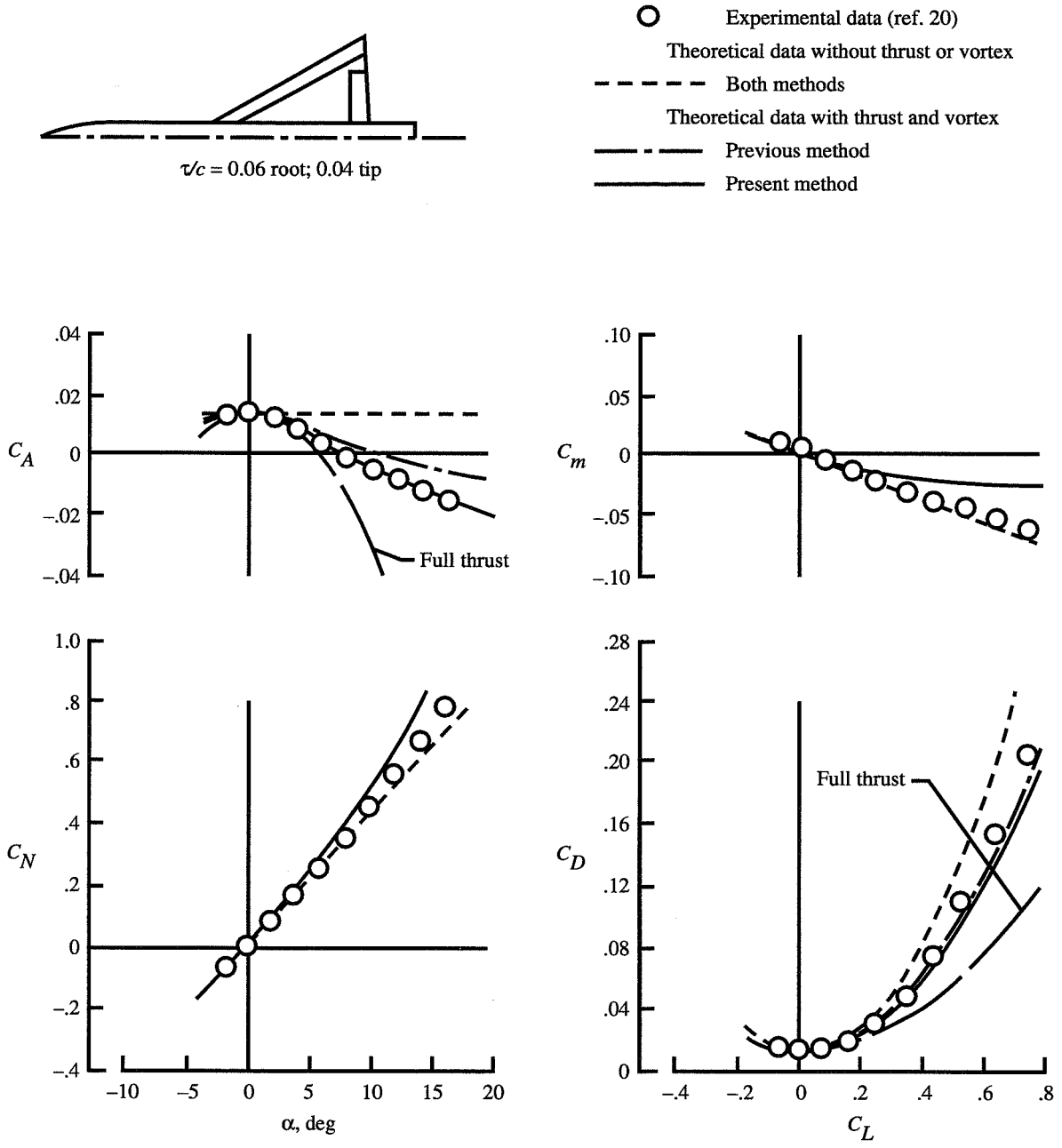

(a) $\delta_{L,n} = 0°$; $\delta_{T,n} = 0°$.

Figure 9. Theoretical and experimental data for 60° swept delta wing fighter with rounded leading-edge NACA 64A00X airfoil. $M = 0.4$; $R = 2.5 \times 10^6$.

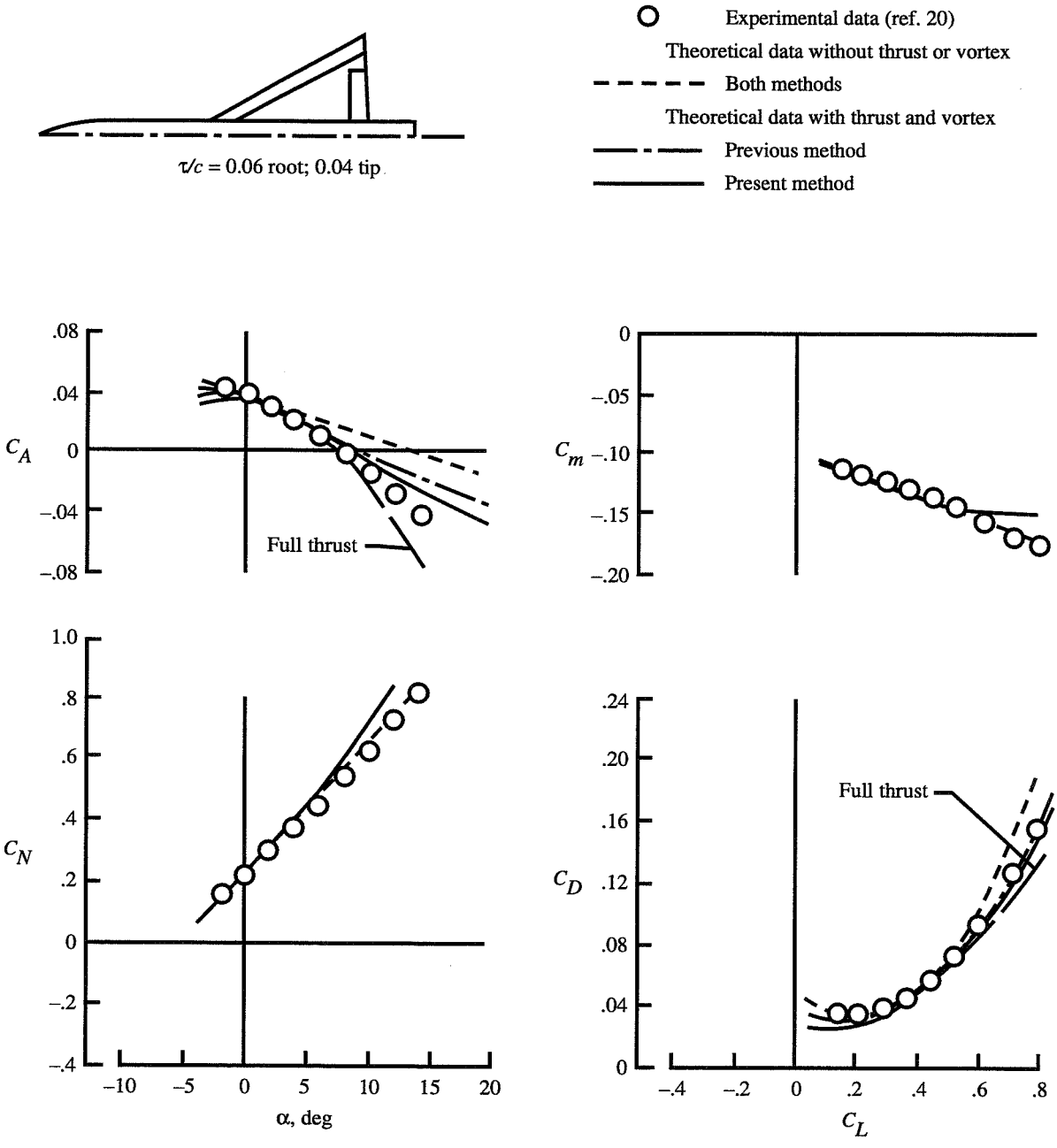

(b) $\delta_{L,n} = 20°$; $\delta_{T,n} = 20°$.

Figure 9. Concluded.

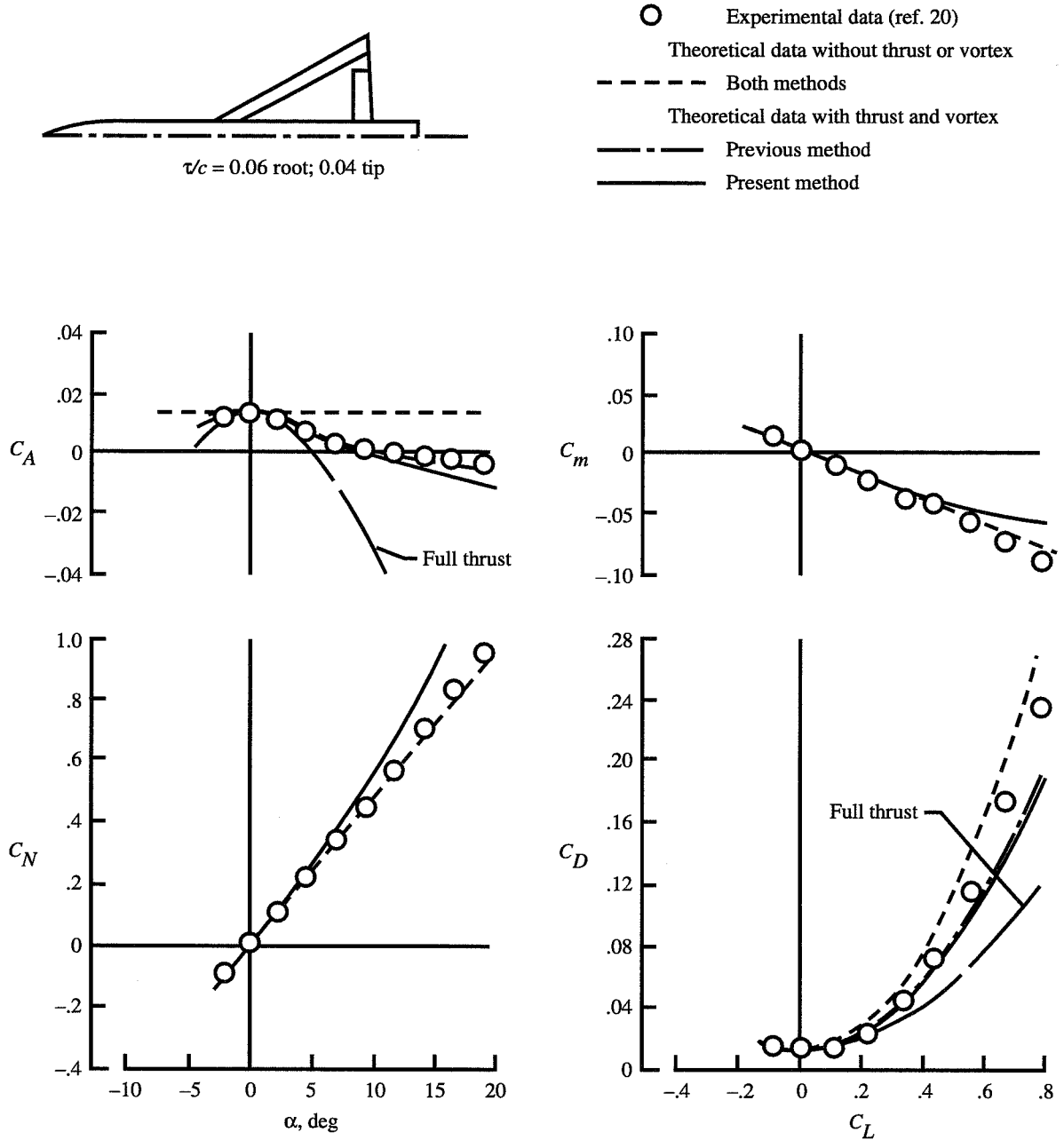

Figure 10. Theoretical and experimental data for 60° swept delta wing fighter with rounded leading-edge NACA 64A00X airfoil. $M = 0.8$; $R = 4.1 \times 10^6$.

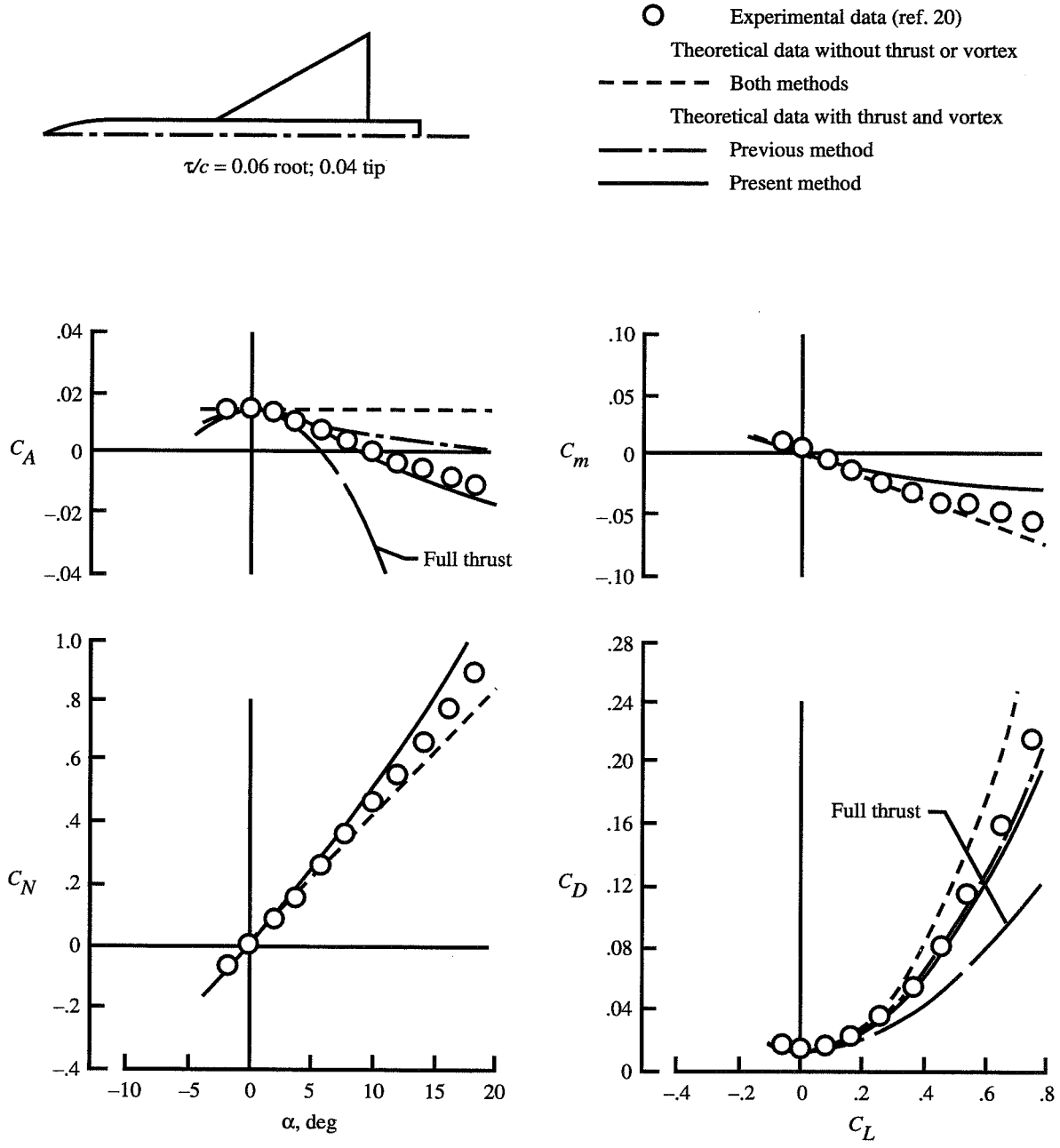

Figure 11. Theoretical and experimental data for 60° swept delta wing fighter with sharp leading-edge airfoil. $M = 0.4$; $R = 2.5 \times 10^6$.

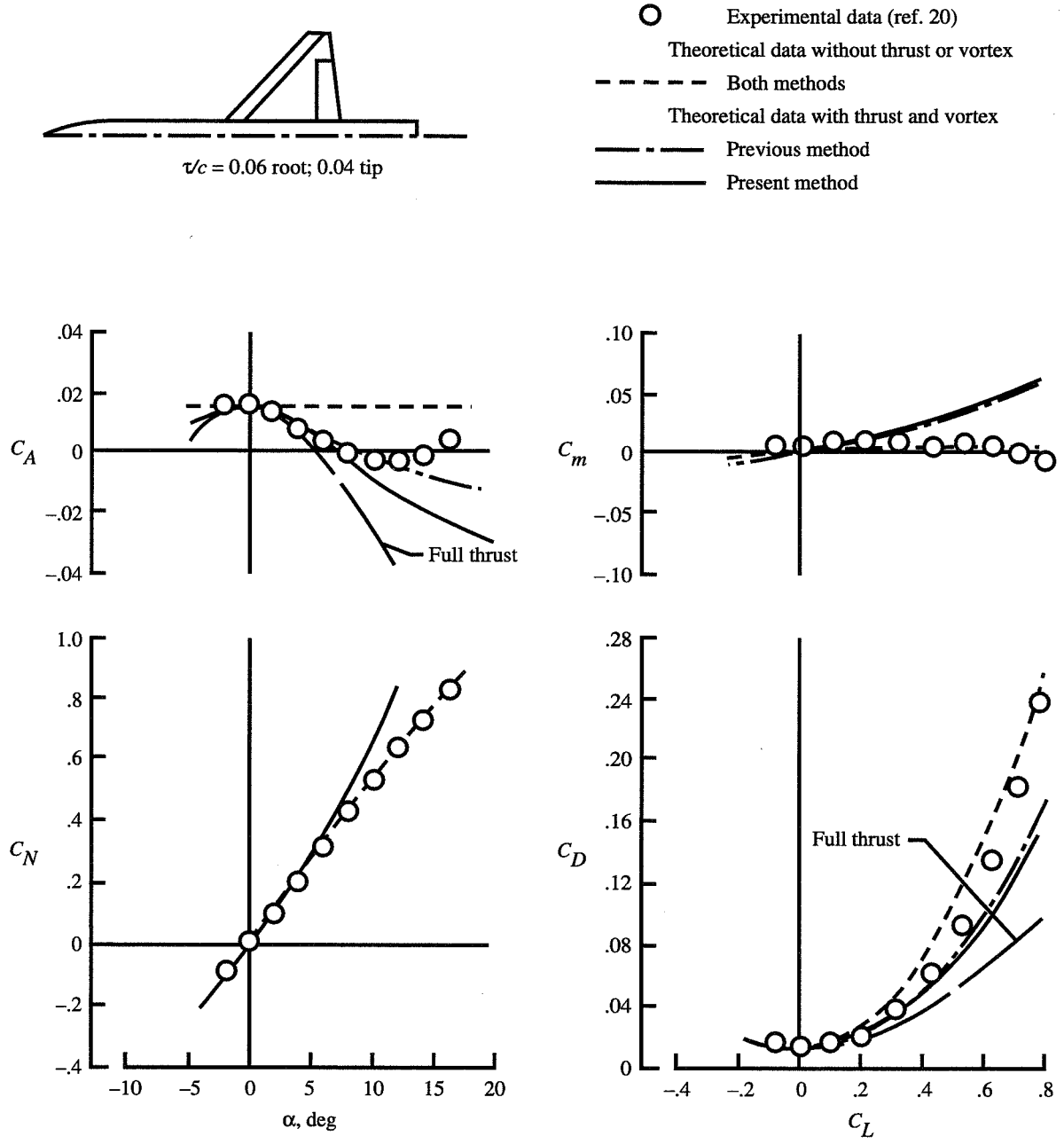

(a) $\delta_{L,n} = 0°$; $\delta_{T,n} = 0°$.

Figure 12. Theoretical and experimental data for 44° swept trapezoidal wing fighter with NACA 64A00X airfoil. $M = 0.4$; $R = 1.9 \times 10^6$.

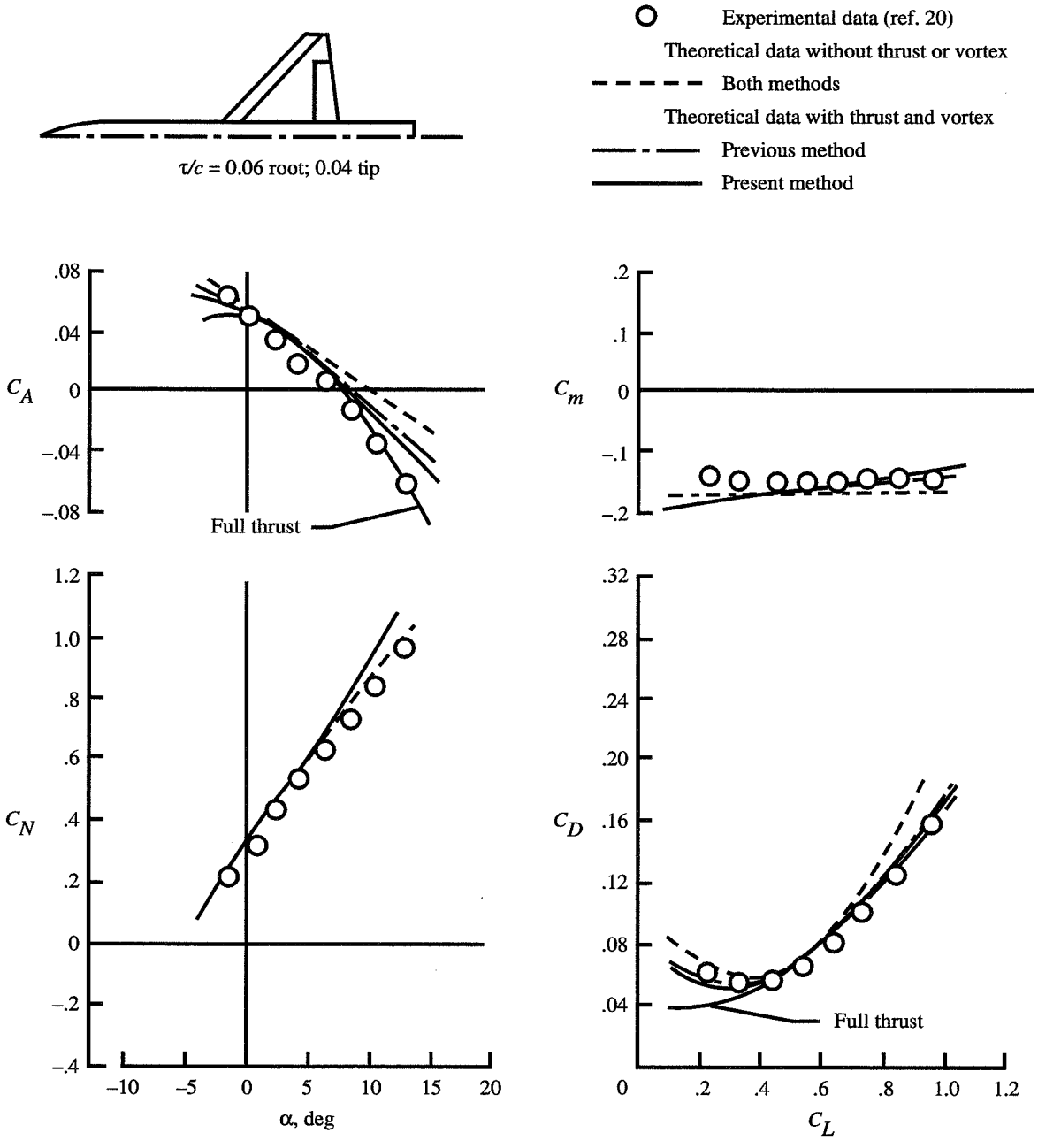

(b) $\delta_{L,n} = 20°$; $\delta_{T,n} = 20°$.

Figure 12. Concluded.

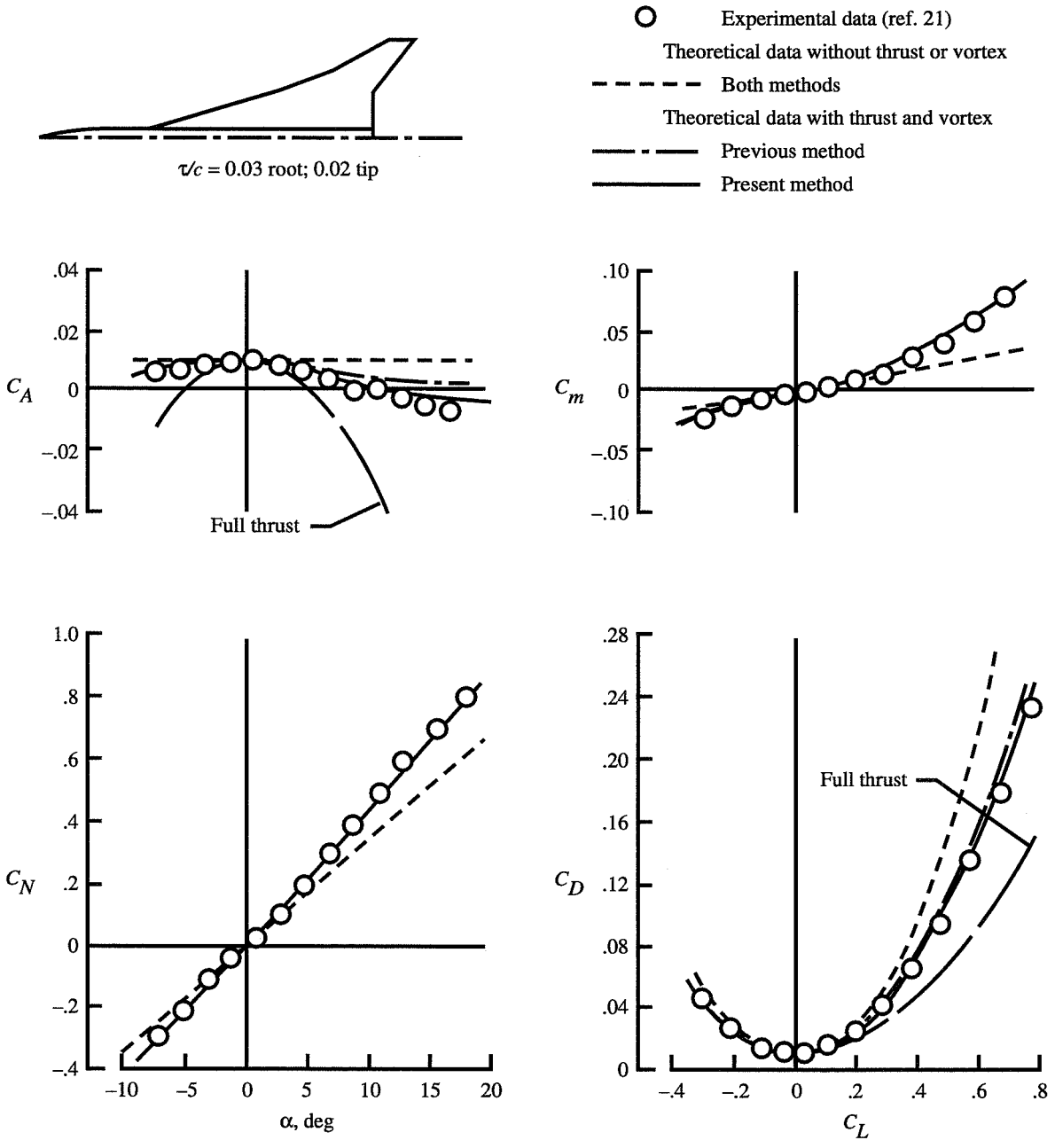

Figure 13. Theoretical and experimental data for generic arrow wing supersonic transport. $M = 0.25$; $R = 4.8 \times 10^6$.

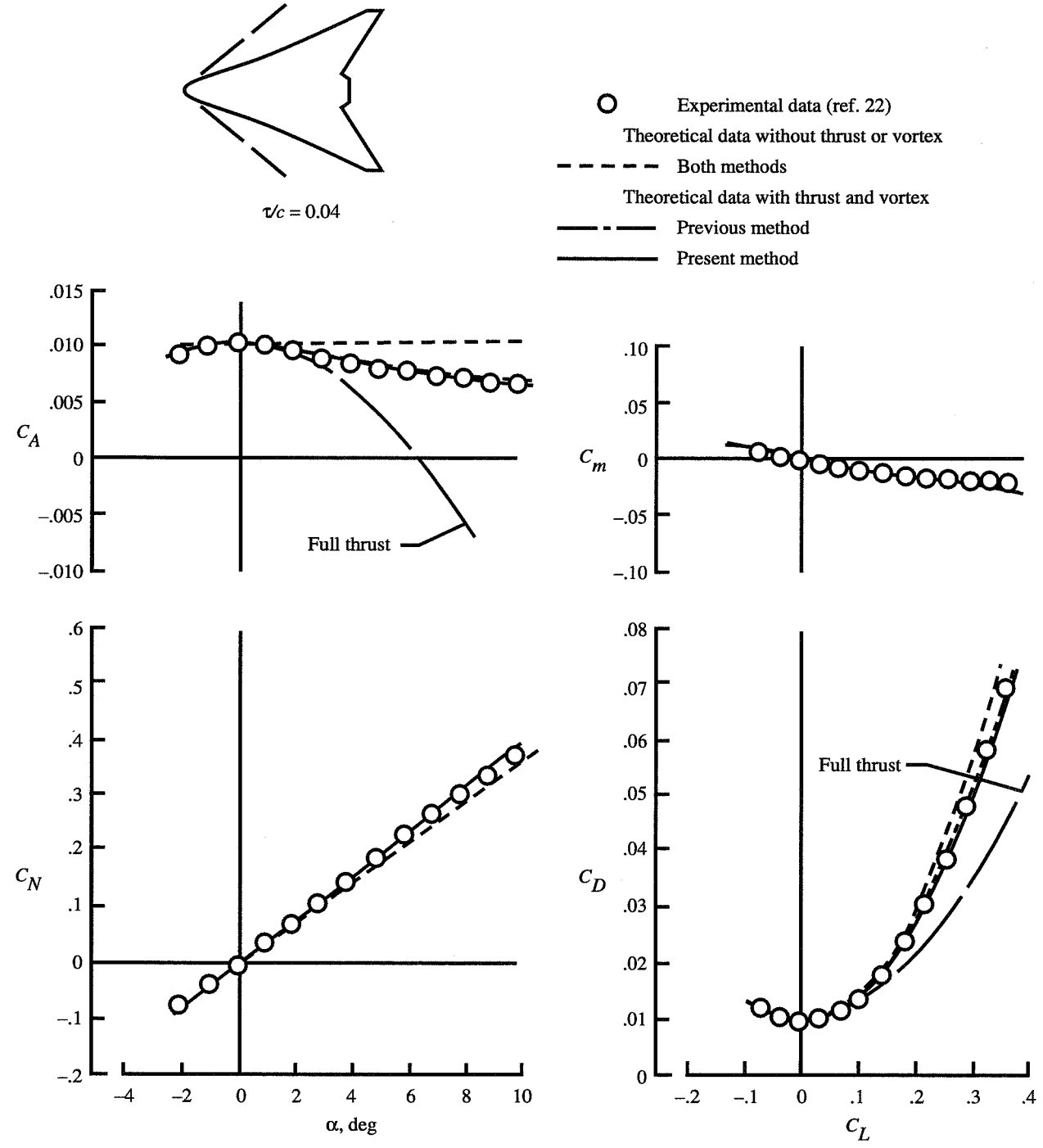

(a) Sharp leading edge.

Figure 14. Theoretical and experimental data for flat modified arrow wing-body combination with various wing sections. $M = 1.6$; $R = 2.6 \times 10^6$.

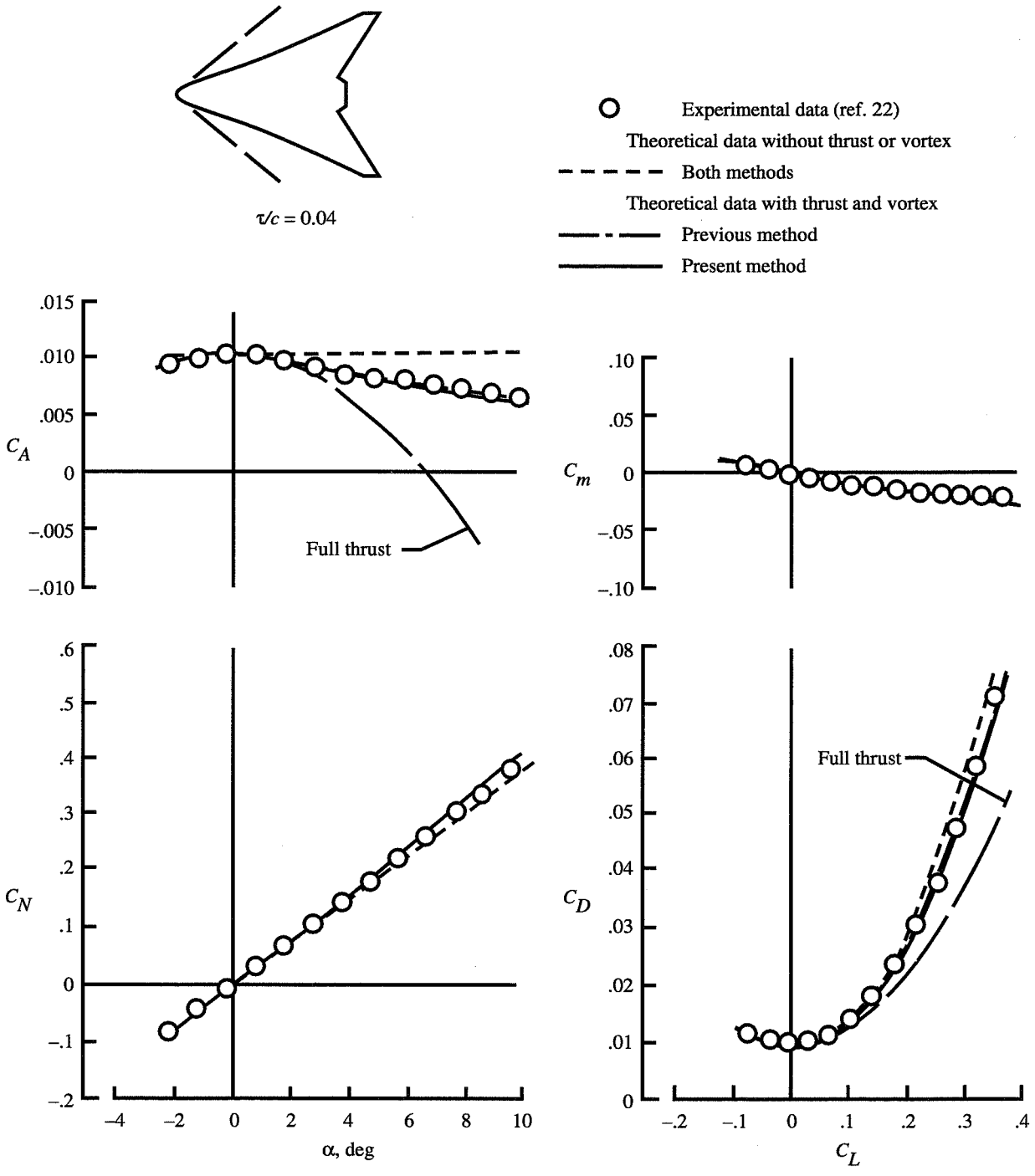

(b) Standard leading edge.

Figure 14. Continued.

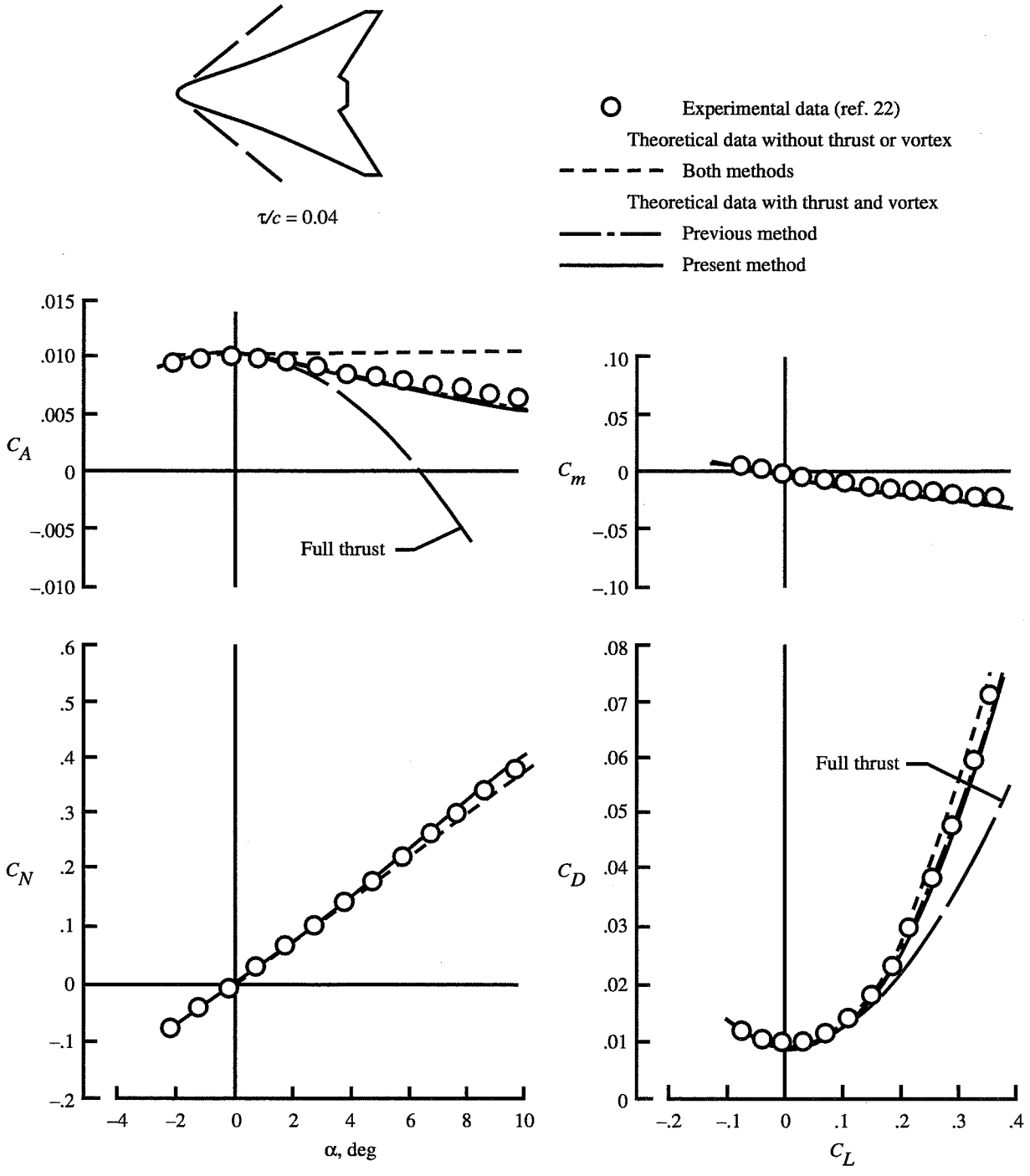

(c) Blunt leading edge.

Figure 14. Concluded.

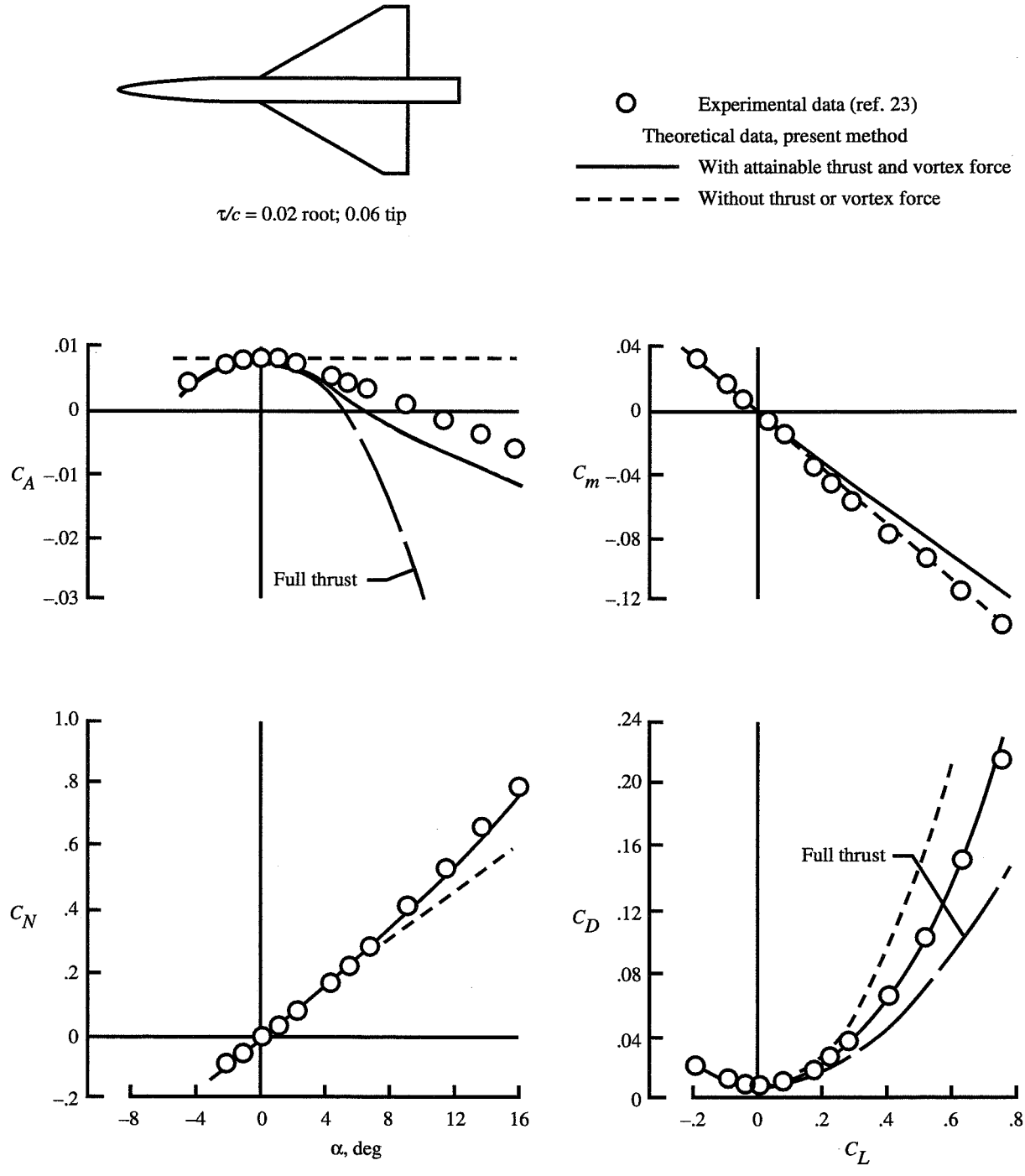

(a) Sharp leading edge.

Figure 15. Theoretical and experimental data for 61.7° swept delta wing body combination with various wing sections. $M = 0.22$; $R \approx 10 \times 10^6$.

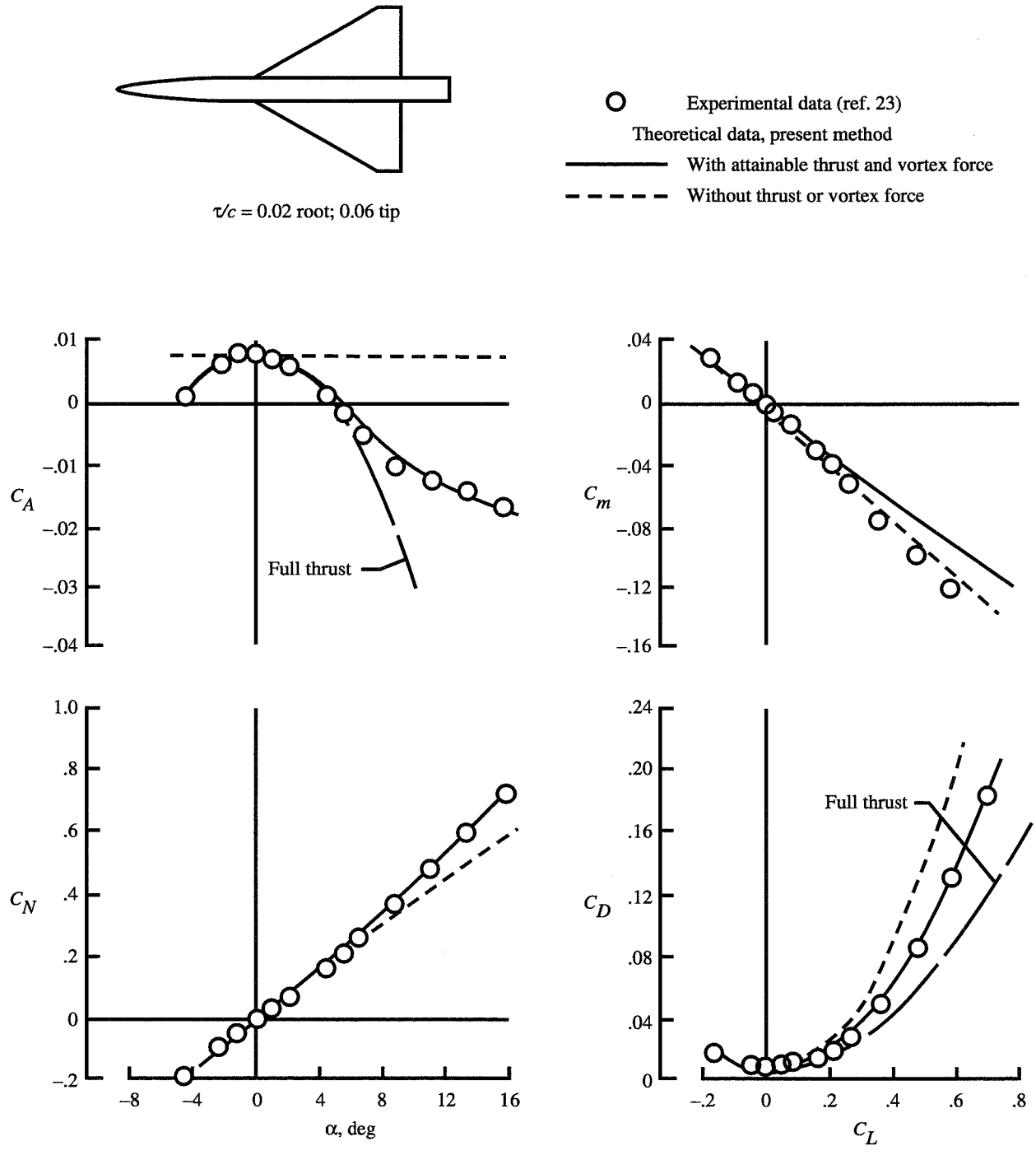

(b) Small leading-edge radius.

Figure 15. Continued.

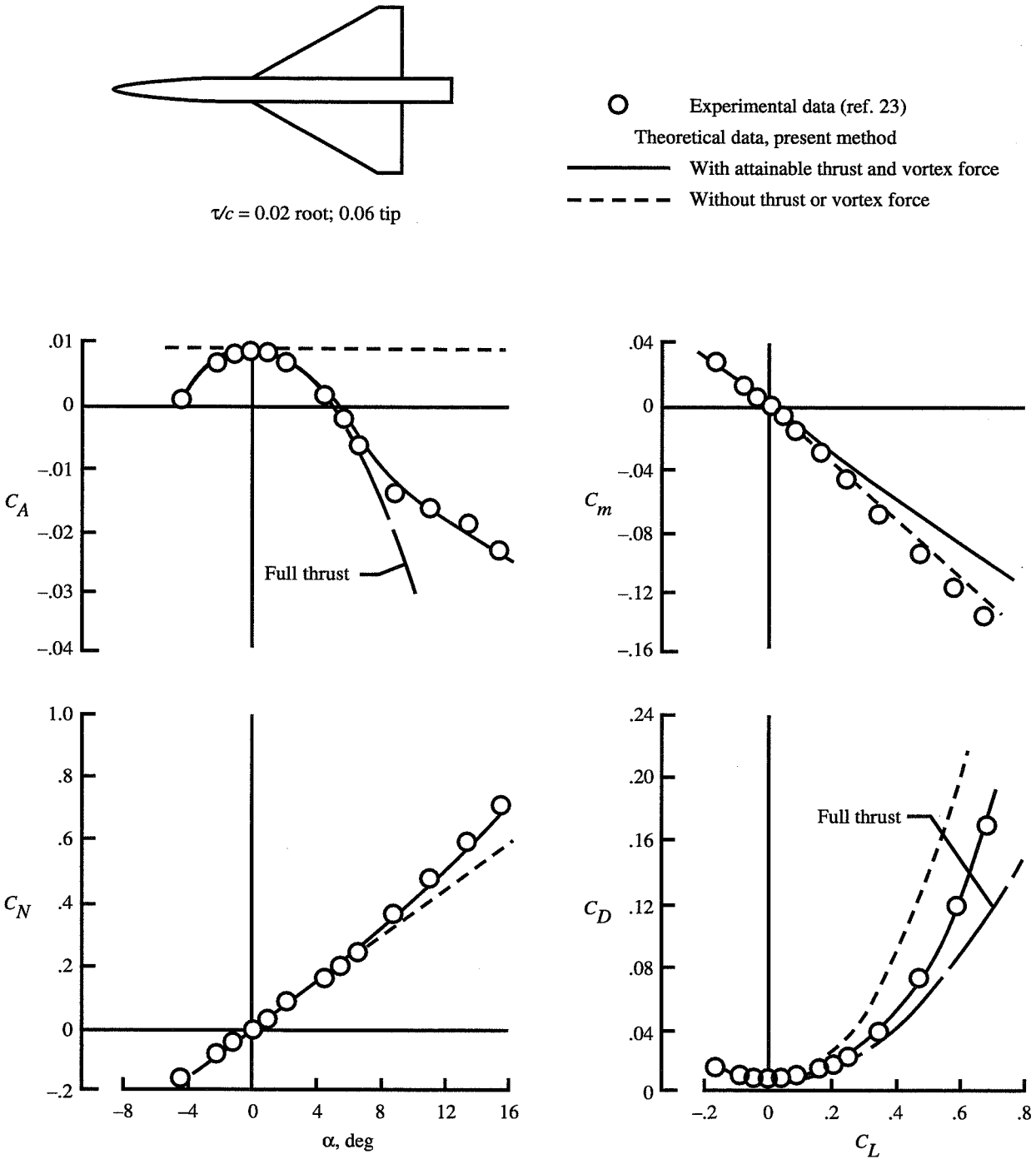

(c) Large leading-edge radius.

Figure 15. Concluded.

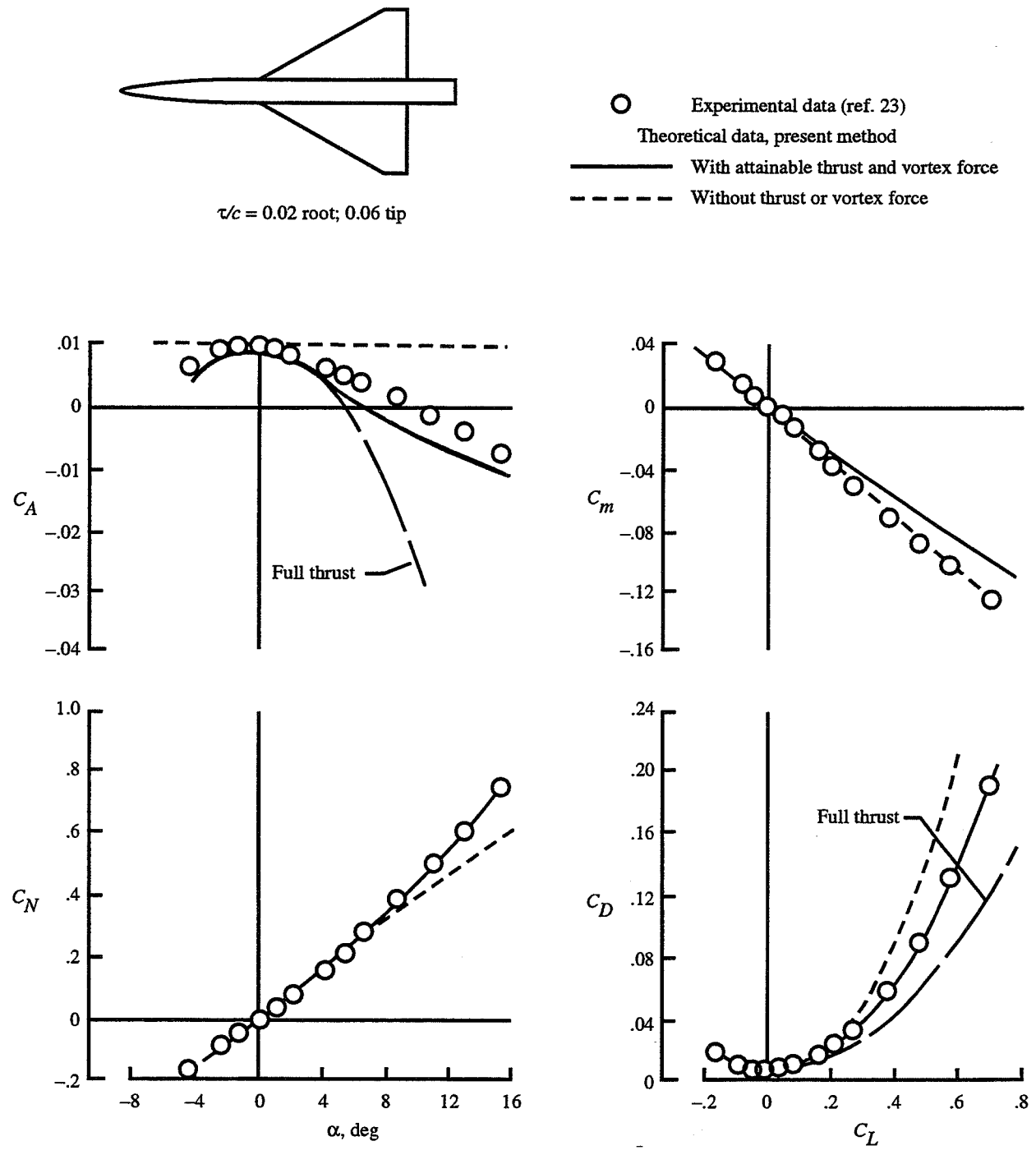

(a) $R = 2.4 \times 10^6$.

Figure 16. Theoretical and experimental data for 61.7° swept delta wing body combination at several additional Reynolds numbers. Small leading-edge radius; $M = 0.22$.

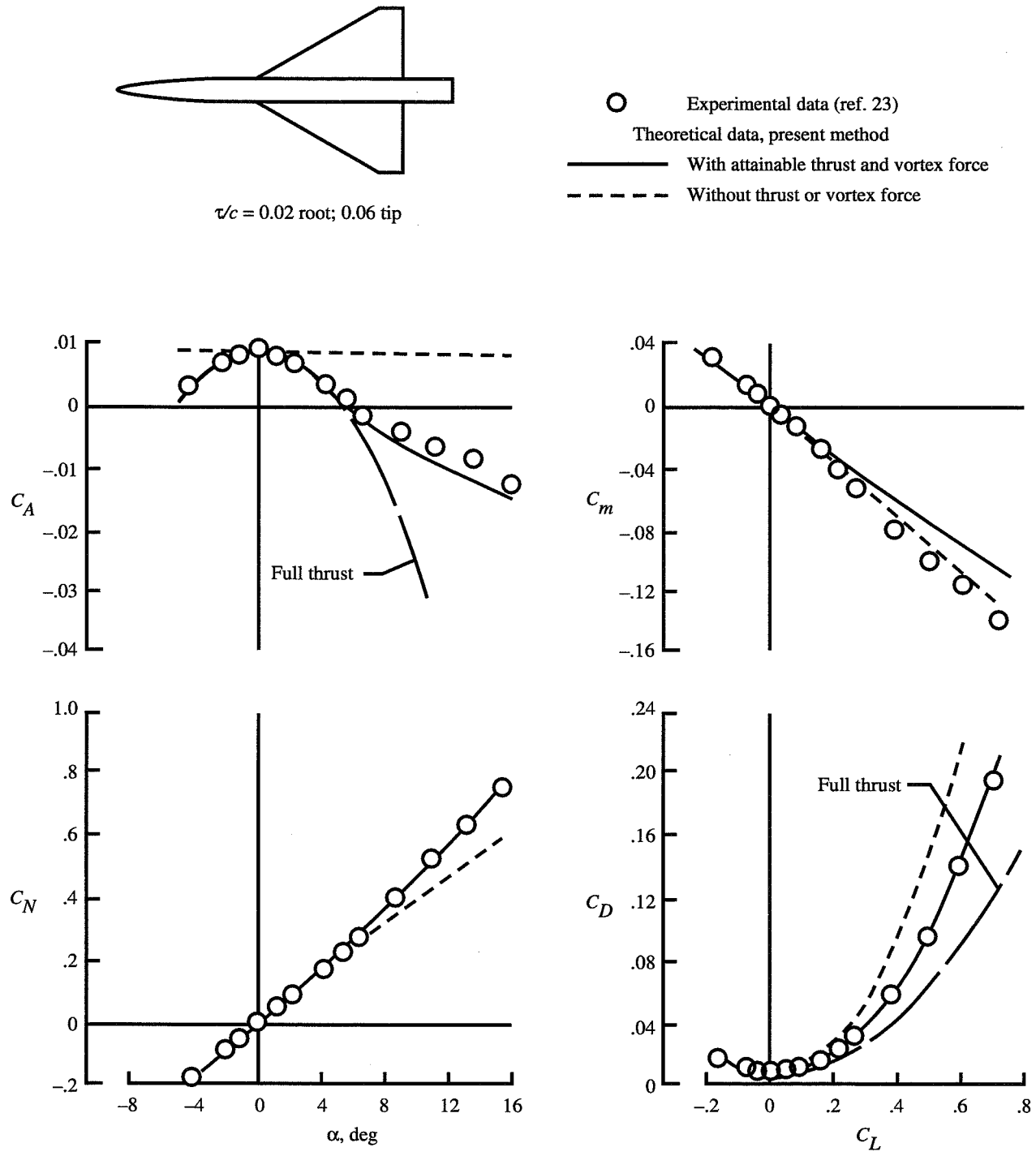

(b) $R = 6.3 \times 10^6$.

Figure 16. Continued.

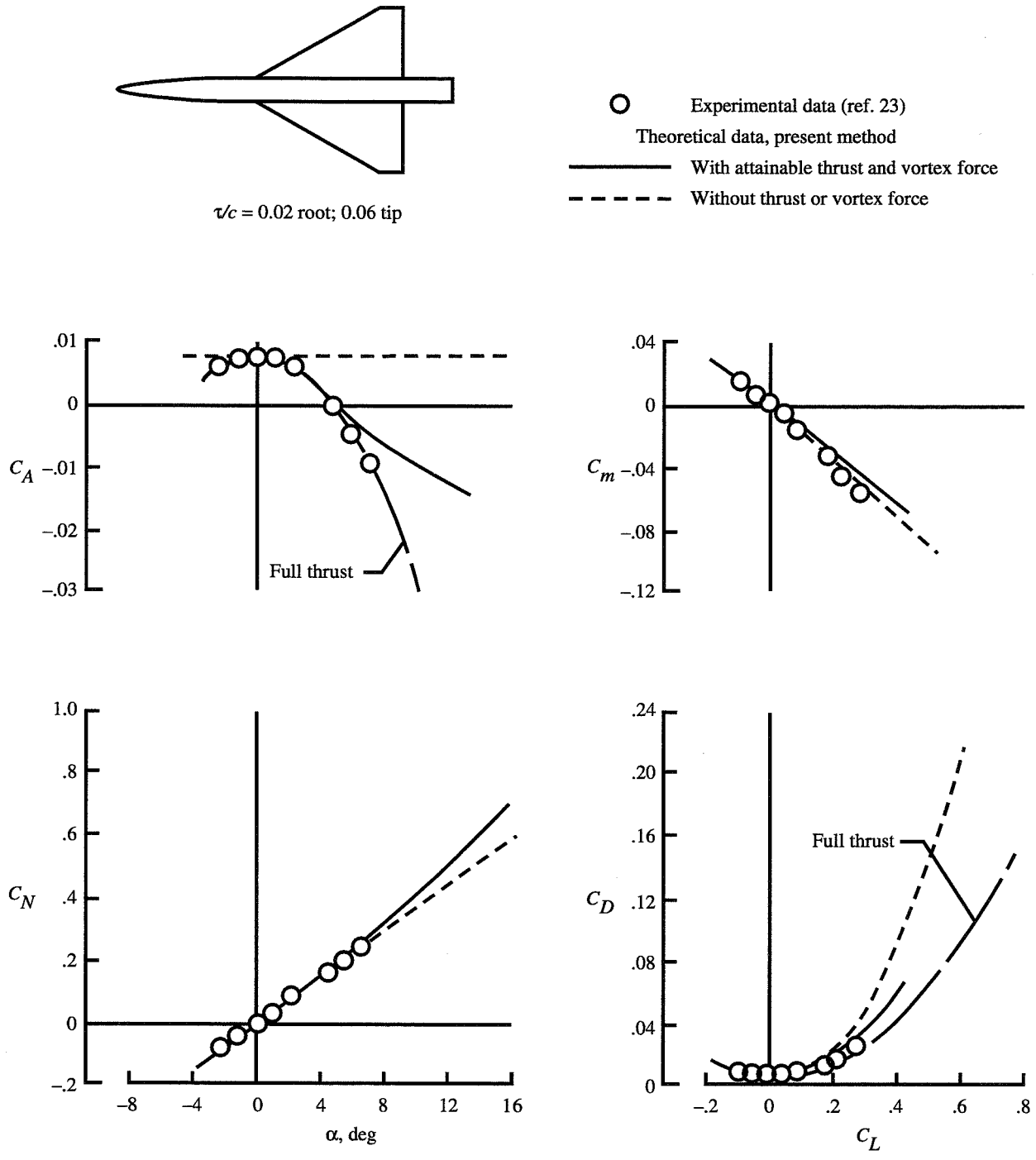

(c) $R = 15.4 \times 10^6$.

Figure 16. Concluded.

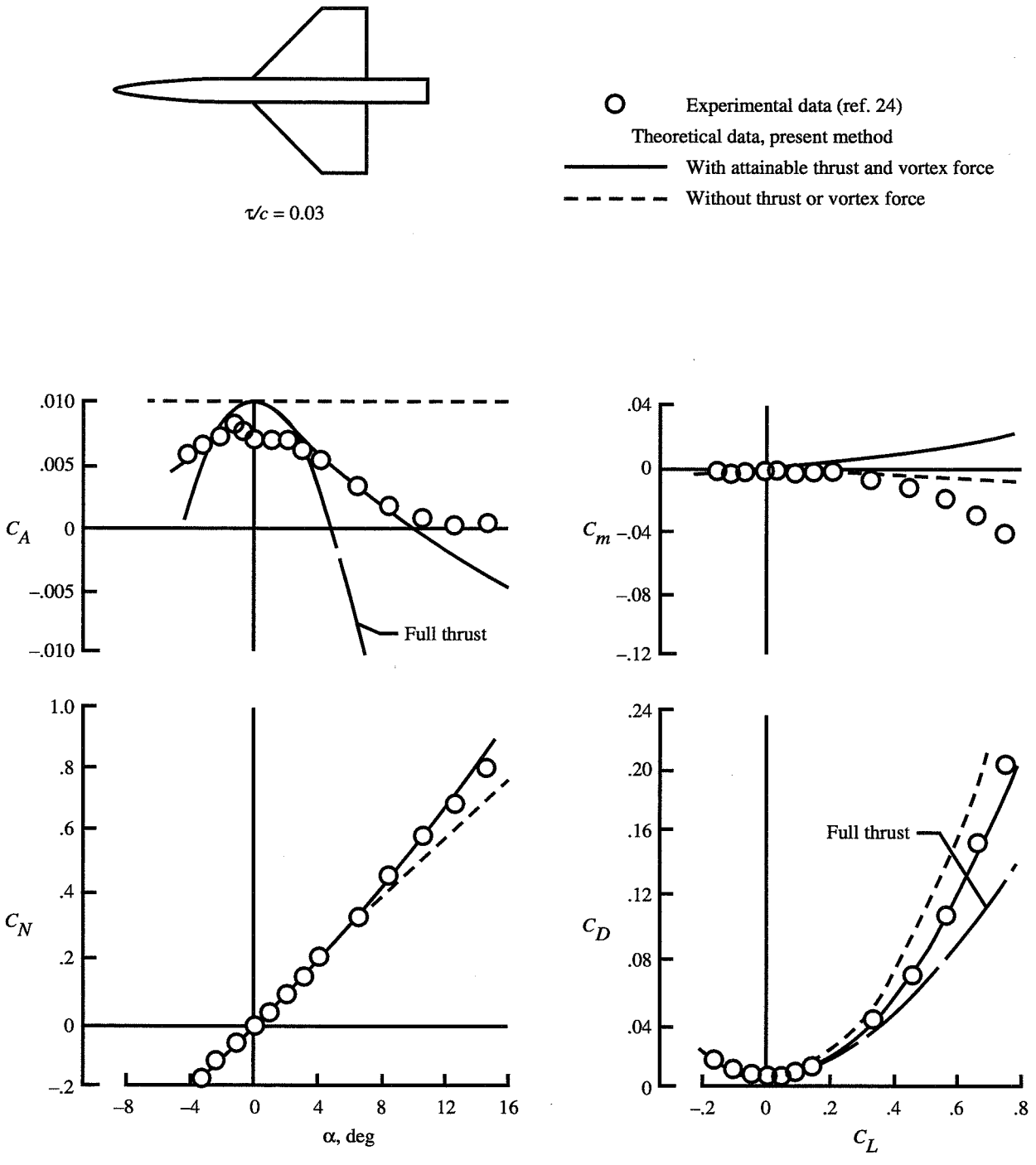

(a) $R = 1.9 \times 10^6$.

Figure 17. Theoretical and experimental data for 45° swept trapezoidal wing body combination. Moderate leading-edge radius; $M = 0.61$.

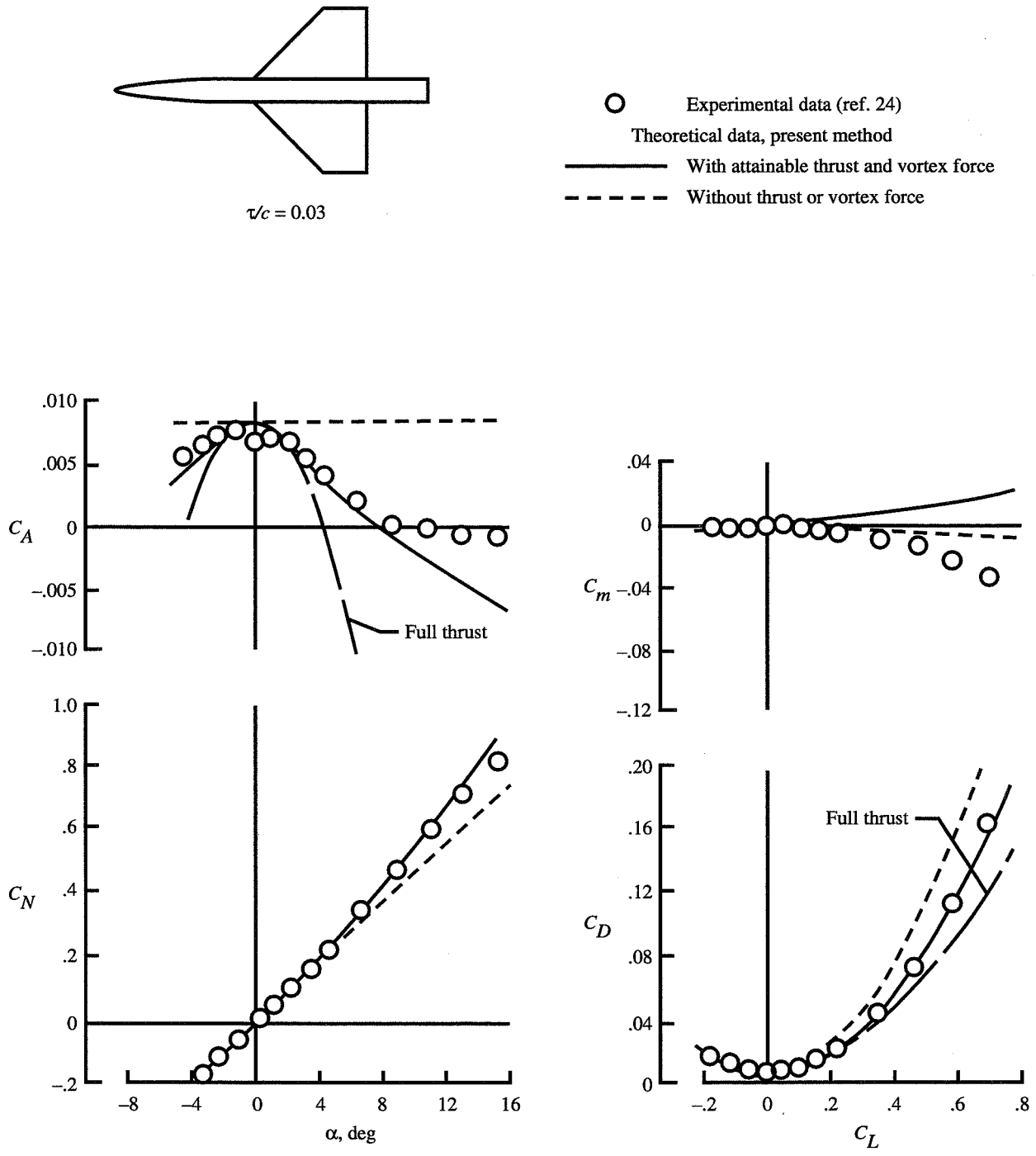

(b) $R = 4.8 \times 10^6$.

Figure 17. Concluded.

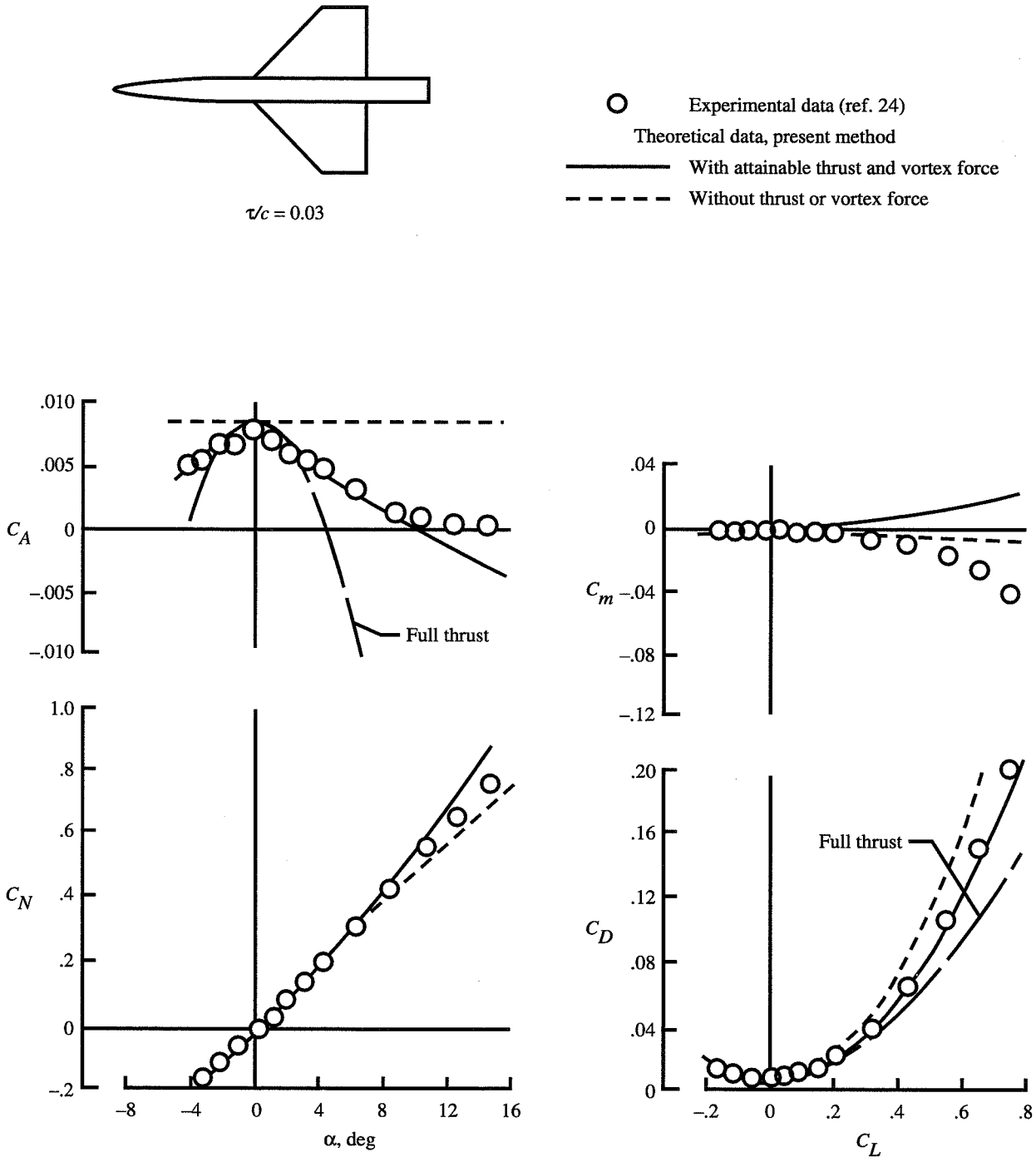

(a) $R = 1.9 \times 10^6$.

Figure 18. Theoretical and experimental data for 45° swept trapezoidal wing body combination. Sharp leading edge; $M = 0.61$.

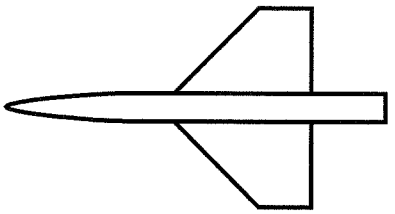

$\tau/c = 0.03$

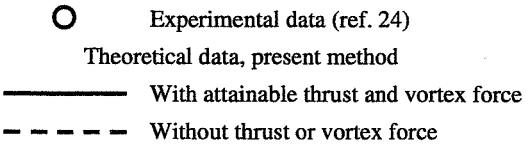

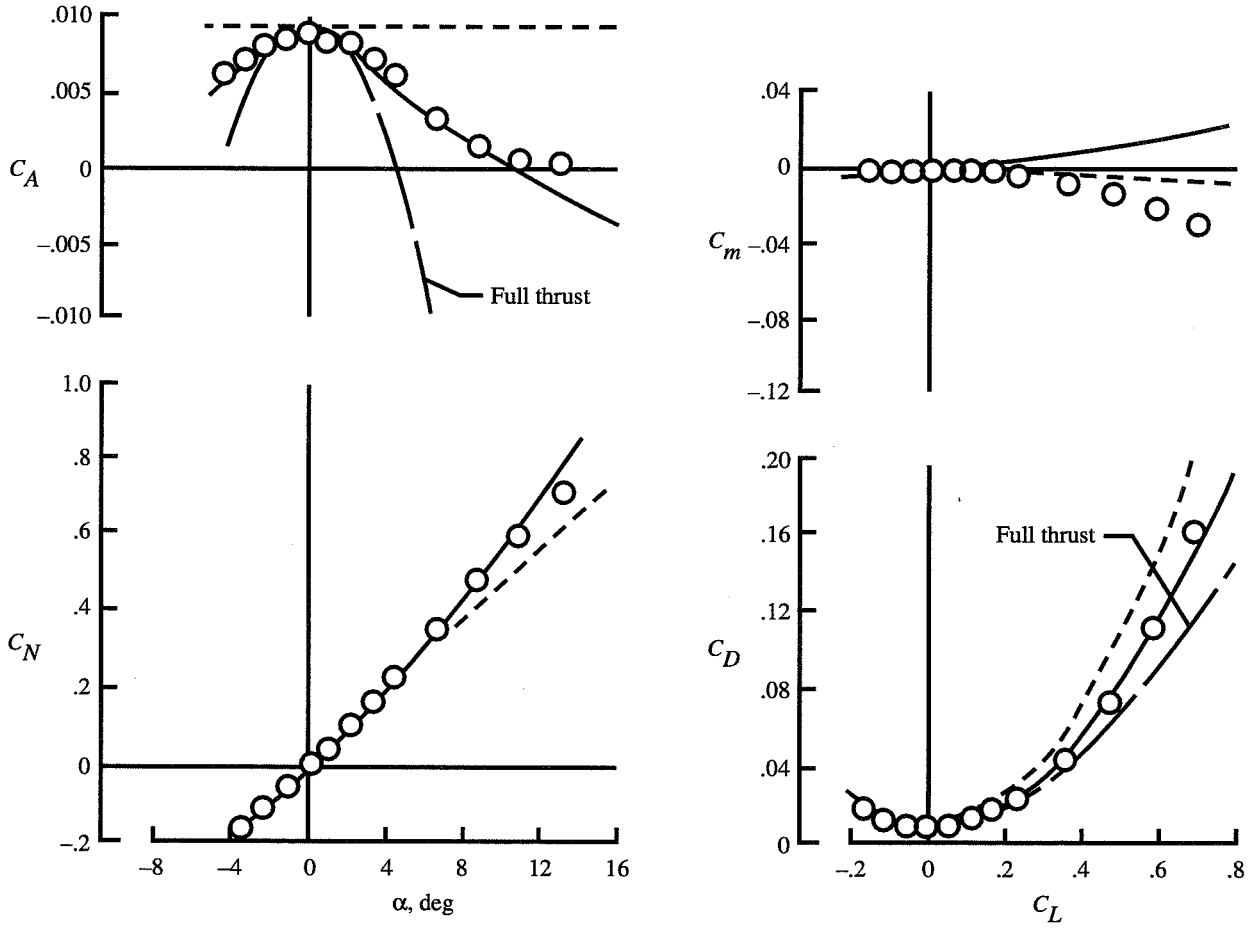

(b) $R = 4.8 \times 10^6$.

Figure 18. Concluded.

REPORT DOCUMENTATION PAGE

Form Approved
OMB No. 0704-0188

1. AGENCY USE ONLY *(Leave blank)*	2. REPORT DATE	3. REPORT TYPE AND DATES COVERED
	April 1996	Technical Paper

4. TITLE AND SUBTITLE
Improved Method for Prediction of Attainable Wing Leading-Edge Thrust

5. FUNDING NUMBERS
WU 505-68-70-02

6. AUTHOR(S)
Harry W. Carlson, Marcus O. McElroy, Wendy B. Lessard,
and L. Arnold McCullers

7. PERFORMING ORGANIZATION NAME(S) AND ADDRESS(ES)
NASA Langley Research Center
Hampton, VA 23681-0001

8. PERFORMING ORGANIZATION REPORT NUMBER
L-17440

9. SPONSORING/MONITORING AGENCY NAME(S) AND ADDRESS(ES)
National Aeronautics and Space Administration
Washington, DC 20546-0001

10. SPONSORING/MONITORING AGENCY REPORT NUMBER
NASA TP-3557

11. SUPPLEMENTARY NOTES
Carlson: Lockheed Engineering & Sciences Company, Hampton, VA; McElroy and Lessard: Langley Research Center, Hampton, VA; McCullers: ViGYAN, Inc., Hampton, VA.

12a. DISTRIBUTION/AVAILABILITY STATEMENT
Unclassified–Unlimited
Subject Category 02
Availability: NASA CASI (301) 621-0390

12b. DISTRIBUTION CODE

13. ABSTRACT *(Maximum 200 words)*
Prediction of the loss of wing leading-edge thrust and the accompanying increase in drag due to lift, when flow is not completely attached, presents a difficult but commonly encountered problem. A method (called the previous method) for the prediction of attainable leading-edge thrust and the resultant effect on airplane aerodynamic performance has been in use for more than a decade. Recently, the method has been revised to enhance its applicability to current airplane design and evaluation problems. The improved method (called the present method) provides for a greater range of airfoil shapes from very sharp to very blunt leading edges. It is also based on a wider range of Reynolds numbers than was available for the previous method. The present method, when employed in computer codes for aerodynamic analysis, generally results in improved correlation with experimental wing-body axial-force data and provides reasonable estimates of the measured drag.

14. SUBJECT TERMS	15. NUMBER OF PAGES
Aerodynamics; Linearized theory; Numerical methods; Attainable thrust	63
	16. PRICE CODE: A04

17. SECURITY CLASSIFICATION OF REPORT	18. SECURITY CLASSIFICATION OF THIS PAGE	19. SECURITY CLASSIFICATION OF ABSTRACT	20. LIMITATION OF ABSTRACT
Unclassified	Unclassified	Unclassified	